INTERLAMINAR FRACTURE OF UNIDIRECTIONAL REINFORCED COMPOSITES WITH TOUGHNENED RESIN SYSTEMS

by

AARON SLAGER

Presented to the Faculty of the Graduate School of

The University of Texas at Arlington in Partial Fulfillment

of the Requirements

for the Degree of

MASTER OF SCIENCE IN MATERIALS SCIENCE AND ENGINEERING

THE UNIVERSITY OF TEXAS AT ARLINGTON

May 2007

ACKNOWLEDGEMENTS

I would like to express my sincere gratitude to my co-workers who were able gain funding this research project and who also aided in designing and manufacturing test specimens. I would also like to thank my graduate Committee for their help with my thesis, especially Dr. Chan for his expertise and Dr. Meletis for allowing me to finish my graduate work in an unorthodox fashion. Finally and most of all, I am forever grateful of my family and the teachers throughout my educational career.

April 12, 2007

ABSTRACT

INTERLAMINAR FRACTURE OF UNIDIRECTIONAL REINFORCED COMPOSITES WITH TOUGHNENED RESIN SYSTEMS

Publication No. _____

Aaron Slager, M.S.

The University of Texas at Arlington, 2007

Supervising Professor: Dr. Meletis

Several undisclosed fiberglass and carbon fiber laminates with toughened resin systems were tested and examined. Experiments were conducted to determine Modes I and II interlaminar fracture toughness for each of the nine laminates with varying types of processing forms such as roving, tape, and slit tape of glass and carbon fibers. Fractography was then used to correlate the fracture toughness results with the unique characteristics and failure mechanisms.

Overall, fiberglass laminates had larger interlaminar fracture toughness for both Modes I and II over the carbon laminates. This was also confirmed by the significant

amount of the fractured surface area and complex fracture features of the fiberglass laminates.

Mode I fiberglass specimens had a large amount of fiber bridging, whereas carbon specimens had relatively very little. Of the fiberglass specimens, fiber bridging occurred more prevalently in the roving material than tape. However, the onset of fracture toughness was very similar for the roving and tape fiberglass resin systems.

For the glass and carbon fiber laminates with the same resin systems, an increase in fracture toughness was observed for fiberglass due to a higher strain and a lower modulus and stiffness.

TABLE OF CONTENTS

LIST OF ILLISTRATIONS

LIST OF TABLES

CHAPTER 1

INTRODUCTION AND LITERATURE REVIEW

1.1 Introduction

Failure analysis of composites becomes very important to determine the nature of loading of a structural component. Of the three types of failure, interlaminar, intralaminar, and translaminar, the most common is interlaminar because of the varying Poisson ratios of different ply orientations. An interlaminar crack is most commonly called a delamination. The loading conditions also vary for each of the three types of composite failure, which include tension (Mode I), shear (Mode II), tearing (Mode III), or a combination of the three. Failure analysis examines the physical evidence left behind from a fracture or crack face that have characteristic features that change with loading, type of fiber or resin material, structural configuration, environment, as well as several other factors.

The most effective way to examine the characteristic fracture features that are produced from different loading conditions is to fabricate test specimens and load them in a controlled manner. From these test specimens, the characteristic fracture features can then be documented with a known crack direction.

1.2 Literature Review

The fracture toughness of a laminate can vary greatly, depending upon the resin system used, its curing temperature and agent, curing process, and the conditions the

laminate has been exposed to and the amount of moisture absorption. The first resin systems utilized were extremely brittle until rigid and rubbery compounds were introduced into the resin systems that dramatically increased fracture toughness. Glass transition temperatures generally range 150-300°F with the lower curing resin systems exhibiting greater toughness at room temperature. Better bonding agents were also used to increase the cohesive strength between the fiber and resin.

Pure epoxy resins are used because of their low cure shrinkage, excellent adhesion to both metallic and non-metallic surfaces, low moisture absorption (0.01-0.2% in 24 hours), high strength in reinforced laminate form, and superior chemical and corrosion resistance. The main drawback of epoxy resin is their poor fracture toughness, where typical fracture energy (G_{Ic}) ranged 0.45-1.70 in-lbs/in^2 [1].

Particulate toughened epoxies increase the fracture toughness of the laminate while reducing costs, improving heat transfer and electrical conductivity, controlling the coefficient of thermal expansion, specific gravity, strength, and stiffness [1]. Moloney et al. [2] have shown that (1) increasing the filler volume fraction increases the composite modulus and toughness (2) increasing particle size decreases the composite strength (3) increasing the filler strength and modulus increases the composite modulus, strength, and fracture toughness (K_{Ic}) (4) K_{Ic} of the composite is insensitive to the type of filler and its particle size (5) improved particle-matrix adhesion does not improve K_{Ic} appreciably (6) good bonding is essential for good strength and (7) high strength and high fracture energy (G_{Ic}) are mutually exclusive.

Rubber-modified epoxies have a dramatic effect on the laminate properties such as a reduction in stiffness, lower glass transition temperature, reduction in yield strength,

increases the coefficient of thermal expansion, and most significantly increases the fracture resistance. This was first shown by McGarry et al. that improvements in toughness could be achieved by adding certain liquid rubbers to the epoxy formulations. The maximum fracture energy of rubber-modified epoxy is approximately 30 times that of the pure epoxy [3]. However, the same increase is not obtained when the modified resin is used as an adhesive or as a matrix in composites because of the dependence of fracture energy on epoxy film thickness [1]. When the epoxy film becomes too thick, the full toughening effect is not observed.

Interlaminar fracture toughness of unidirectional reinforced composites vary as little as 0.40 and 0.97 in-lbs/in^2 for Modes I and II, respectively, for HMS-3501-6 [4] and as high as 8.34 and 15.4 in-lbs/in^2 for Modes I and II, respectively, for AS4/PEEK [5]. Within one resin system, such as AS4/PEEK, several references can differ in fracture toughness results with a lower value of 4.43 and 6.86 in-lbs/in^2 for Modes I and II, respectively [6] for a lower matrix volume composite as well as other factors.

1.3 Fracture Mechanics Approach

The study of fracture mechanics assumes a small crack-like flaw is present in a structure that can not be detected using conventional non-destructive methods. For the case of composites, a small delamination or crack is to be assumed. The fracture mechanics approach for delaminations is based on the assessment of the propagation of an existing delamination and the amount of energy that is required for it to propagate. The fracture toughness of a material is normally measured by critical strain energy release, G_c, or the critical stress intensity factor, K_c. For composites, the stress field at the

crack tip process zone can be very complex with the varying number of plies and fiber orientations, thus justifying the use of strain energy release rate.

As of recently, there has been much debate for recommended Mode II testing methods since no testing standard has been widely accepted. Mode I interlaminar fracture toughness testing for fiber-reinforced polymer matrix composites shall be performed per ASTM D 5528.

1.4 Objective and Outline of this Thesis

The objective for this thesis was to measure the interlaminar fracture toughness of unidirectional reinforced composites with toughened resin systems for Modes I and II. A total of nine coupons composed of six different fibers and five different toughened resin systems were tested for each Mode. Fractography shall then be used to correlate the fracture toughness with identified and documented characteristic fracture features for both types of loading.

Beyond the literature review of Chapter 1, a detailed description of test coupon fabrication methods for roving, tape, and slit tape materials as well as the respective ply stacking sequences are presented in Chapter 2. Other information found in Chapter 2 would be the complete test procedures for both Modes I and II testing, a summary of the overall observations during testing, and calculations required to determine fracture toughness.

Fractography of all tested coupons were to be completed for analyzing the fracture mechanisms associated with both tests and to document the unique fracture or crack features. The small photography library and failure analysis of each material are presented in Chapter 3.

Chapter 4 presents all testing results and a correlation between the fracture toughness and fracture surface morphology of different ply forms with varying fibers and resin systems. Other factors affecting observed results are also discussed. Finally, a conclusion is drawn in Chapter 5.

CHAPTER 2

EXPERIMENTAL STUDY

A major weakness of structural composite laminates has been the development of interlaminar delaminations. Intralaminar and translaminar failure do not occur as often under designed operating conditions. Many test procedures have now been devised to measure the interlaminar fracture toughness during static and cyclic loading conditions. The knowledge gained from these new tests help engineers develop design allowables, durability analysis, and failure criterion for composite damage tolerance.

2.1 Description of the Test Program

Several undisclosed test specimens were fabricated at Bell Helicopter Textron Inc. for the Double Cantilever Beam (DCB) and End-Notch Flexure (ENF) tests to determine the interlaminar fracture toughness of Modes I and II, respectively. All specimens were tested in a properly calibrated Materials Testing Services (MTS) machine at room temperature and in dry conditions. Mode I test specimens were designed in accordance with ASTM D 5528. However, there is currently no widely accepted standard for Mode II test specimens. The undisclosed fiberglass and carbon fiber laminates with toughened resin systems tested are listed in Table 2.1. Only one glass fiber and five different carbon fibers were used in the tested laminates.

Table 2.1: Material designation for undisclosed fiber and toughened resin systems tested.

Material	Fiber	Resin System
A	Glass Tape	Epoxy1
B	Glass Roving	Epoxy1
C	Glass Tape	Epoxy2
D	Glass Roving	Epoxy2
E	Carbon1 Tape	Epoxy3
F	Carbon2 Tape	Epoxy1
G	Carbon4 Tape	Epoxy4
H	Carbon5 Tape	Epoxy5
I	Carbon3 Slit Tape	Epoxy2

2.2 Double Cantilever Beam (DCB) Test

DCB specimens test the interlaminar fracture toughness of a laminate subjected to a force in tension (Mode I). Since the debonding process in metals is similar to that of laminated composites, Wilkins, et al. [7] developed a straight-sided specimen as used in ASTM D 5528. The Mode I test set-up is shown in Figure 2.1.

The specimen is a rectangular, uniform thickness, unidirectional laminated composite with a non-adhesive insert at its mid-plane that serves as the delamination initiator. During the test, controlled opening displacement or cross-head movement is to be recorded as well as load and delamination length using a MTS 880 2-1 machine with grips mounted on a 550 lbs (2,450 N) load cell. The specimen is loaded to start a natural delamination from the non-adhesive insert. The complete test procedure is given in Section 2.2.2.

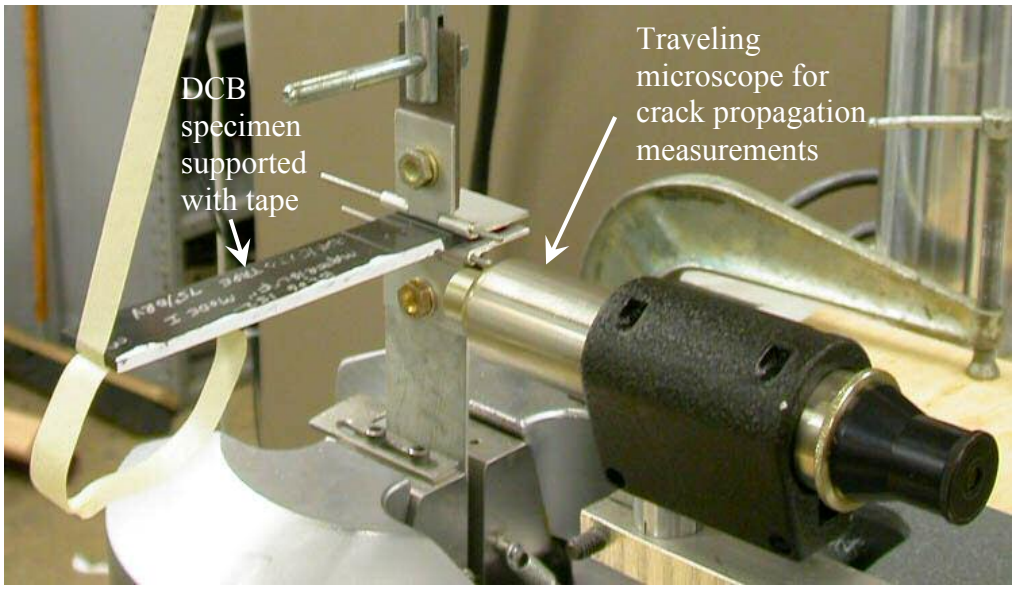

Figure 2.1: DCB test set-up for testing Mode I specimens.

2.2.1 DCB Fabrication

Roving, tape and slit tape were the three types of test panel fabrication studied. All tape coupons were cut from 13 x 13 inch (33 x 33 cm) cured panels after the individual plies were cut from a much larger roll of flat unidirectional prepreg from the manufacturer and placed in the respective sequence as shown in Table 2.2. A 0.0005 inch (0.013 mm) thick polytetrafluoroethylene (PTFE) insert ([T]) was centrally located as shown in Figure 2.2. Sectioning through the panel was determined by ultrasonic inspection to 1) ensure no rejectable voids were present prior to coupon processing and 2) locate the centerline of the centrally located PTFE tape. After the panel was sectioned in half, piano hinge halves (MS20001-6) were bonded to the crack initiation end of the specimen using AF163-2K film adhesive. Each specimen was then sectioned from the panel and finally machined to approximately 6.0 inches (15 cm) in length and 1.000 ±0.002 inch (25.40 ±0.05 mm) in width and a PTFE insert length of 2.0 inches (51 mm). Cured resin content was not determined for each panel, but the given values in Table 2.3 are approximate values based upon the supplier's batch buy-off requirements.

Table 2.2: Panel fabrication information.

Material	Lay-up	Measured Thickness (inch)
A - Glass Tape, Epoxy1	$[0_{16}/T/0_{16}]$	0.286-0.293
B - Glass Roving, Epoxy1	$[0_{12}/T/0_{12}]$	0.321-0.323
C - Glass Tape, Epoxy2	$[0_{12}/T/0_{12}]$	0.291-0.295
D - Glass Roving, Epoxy2	$[0_{16}/T/0_{16}]$	0.329-0.332
E - Carbon1 Tape, Epoxy3	$[0_{9}/T/0_{9}]$	0.129-0.131
F - Carbon2 Tape, Epoxy1	$[0_{9}/T/0_{9}]$	0.145-0.149
G - Carbon4 Tape, Epoxy4	$[0_{9}/T/0_{9}]$	0.131-0.135
H - Carbon5 Tape, Epoxy5	$[0_{9}/T/0_{9}]$	0.132-0.138
I - Carbon3 Slit Tape, Epoxy2	$[0_{9}/T/0_{9}]$	0.137-0.142

Table 2.3: Approximate cured resin content values for all materials.

Material	Cured Resin Content (wt%)
A - Glass Tape, Epoxy1	28
B - Glass Roving, Epoxy1	27
C - Glass Tape, Epoxy2	34
D - Glass Roving, Epoxy2	32
E - Carbon1 Tape, Epoxy3	35
F - Carbon2 Tape, Epoxy1	34
G - Carbon4 Tape, Epoxy4	30
H - Carbon5 Tape, Epoxy5	30
I - Carbon3 Slit Tape, Epoxy2	35

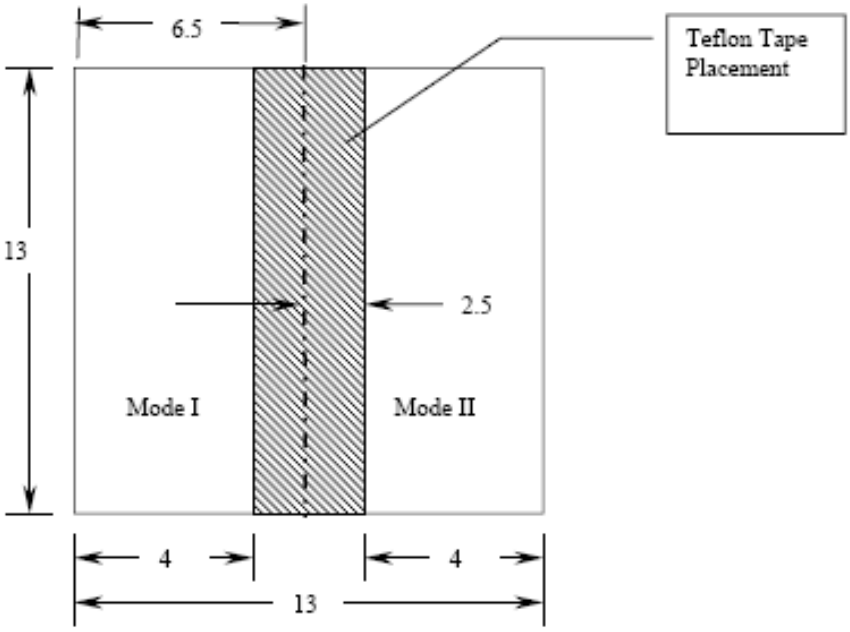

Figure 2.2: Panel configuration for Modes I and II test coupons. The panels were sectioned near the center to separate the two types of test specimens for further manufacture.

Roving and slit tape panels were fabricated using a 3 foot (91 cm) diameter drum and winding the 0.125 inch (3.18 mm) material with a tow spacing of 0.200 inch (5.08 mm) per tow (see Figure 2.3). The wound material was then cut and stacked per the lay-up sequence in Table 2.1. Inconsistent tow spacing can cause variance in fiber volume content among other mechanical properties. All roving material have a 12K tow (12,000 filaments per tow) that is comprised of twisted unidirectional fibers. Slit tape is the flat unidirectional fiber tape that has been slit into narrow tows.

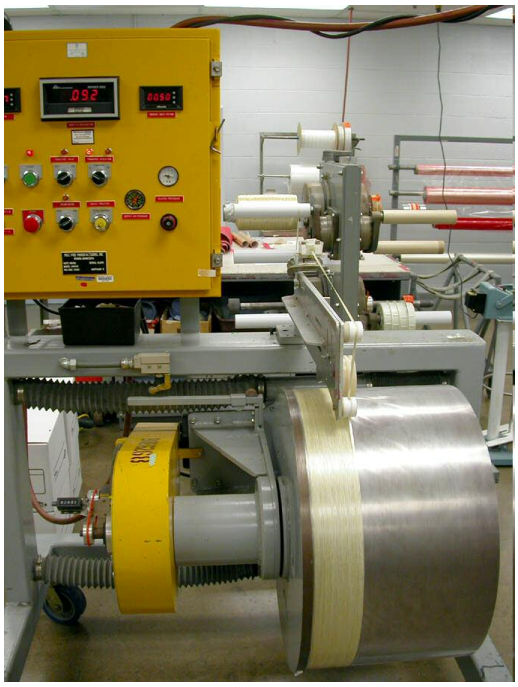

Figure 2.3: Manufacture of roving and slit tape panels.

2.2.2 Test Procedure

1. Measure and record the width and thickness of each specimen to the nearest 0.002 inch (0.05 mm) at the midpoint and at 1.0 inch (25 mm) from the either end.
2. Coat one edge just ahead of the insert with a thin layer of water-based typewriter correction fluid, or equivalent, to aid in the visual detection of delamination onset. Mark the first 0.2 inch (5 mm) from the insert on either edge with thin vertical lines every 0.04 in. (1.0 mm). Mark the remaining 0.8 inch (20 mm) with thin vertical lines every 0.2 inch (5 mm).
3. Mount the load hinges on the specimen in the grips of the loading machine, making sure that the specimen is aligned and centered.
4. The end of the specimen opposite the grips should be supported before loading. The supported end may rise off the support as load is applied.

5. Set an optical traveling microscope in a position to observe the motion of the delamination front as it grows along one edge. The microscope must have a magnification no greater than 70X and be capable of pinpointing the delamination front with the accuracy of at least ±0.02 inch (±0.5 mm).
6. As load is applied, measure the delamination length, a, on one side of the specimen. The initial delamination length, a_0, is the distance from the load line to the end of the insert.
7. The loading shall be stopped once the delamination has grown 0.1 to 0.2 inch (3 to 5 mm). Remark the crack tip after unloading. This ensures a natural crack has been formed.
8. Reload the specimen at a constant cross-head rate of 0.1 inch/minute (2.5 mm/minute).
9. Record the load, cross-head displacement, and delamination growth.
10. During loading, record the point at which the visual onset of delamination movement was observed.

2.2.3 Interpretation of Test Results

From the DCB test, a resistance-type fracture develops and the recorded data is used to calculate G_{Ic} during delamination growth. The resistance curve (R curve) can show varying behaviors at the onset of the delamination, and as such, three definitions for an initiation value of G_{Ic} have been pursued further and are described below (see Figure 2.4). All G_{Ic} values were determined using the 5% offset/maximum load technique.

1. Deviation from Linearity (NL) – An onset of delamination value of G_{Ic} from the load and displacement curve at the point of deviation from linearity. This

assumes that the delamination starts to grow from the insert in the interior of the specimen and represents a lower bound value for G_{Ic}.

2. Visual Observation (VIS) – A visual onset value for G_{Ic} as recorded corresponding to the load and displacement from the first point at which the delamination is visually observed from the insert.
3. 5% Offset/Maximum Load (5%/Max) – A value of G_{Ic} calculated by determining the intersection of the load-displacement curve and a line drawn from the origin and offset by a 5% increase in compliance of the linear portion of the R curve.

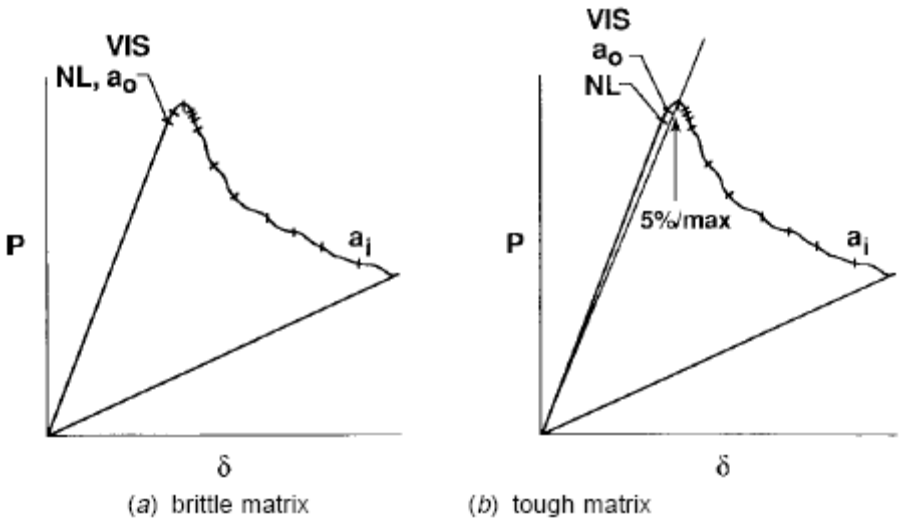

Figure 2.4: Load vs. displacement trace from a typical DCB test used to calculate the onset of delamination growth.

2.2.4 Observation and Calculation

Post-examination of the test specimens did not reveal any permanent bending deformation of the two separate specimen halves or major deviations of the delamination from the mid-plane of the laminate.

For the glass fiber and respective resin systems, a steady increase in G_{Ic} with crack growth was apparent. This is due to fiber bridging, which occurs between two 0°

unidirectional plies and becomes resistance for a delamination to grow [8-10]. Since most delaminations that are found in structural laminates between dissimilar fiber orientations, fiber bridging does not occur and is considered an artifact of unidirectional DCB test specimens. Fiber bridging was observed in a couple of the carbon/epoxy laminates (Materials F and G); otherwise G_{Ic} remained relatively constant with increasing crack length. Some carbon/epoxy laminates experienced crack jumps after propagating 3-4 inches (8-10 cm) in length. This shows unstable crack advancement and data past that length should be ignored.

Figure 2.5 shows an example of a load vs. cross-head displacement curve recorded by the MTS 880 2-1 machine. For almost all specimens, an approximate 10-15% higher load was observed at the onset of crack growth as compared to the immediate load required to propagate the crack. This was contributed to a resin-rich area at the end of the PTFE insert, which was the reason for starting a natural crack. Linear elastic behavior was observed at the onset of released strain energy.

Fiberglass specimens did not show unstable crack growth like carbon fiber specimens. From Figure 2.5, the carbon example showed two steps at cross-head displacements of 0.39 and 0.51 inch (10.2 and 13.0 mm), which corresponded to crack lengths of 3.2 and 3.7 inches (81 and 94 mm), respectively. This stopping and restarting of the crack was observed in several carbon specimens after varying crack lengths. Thus, carbon fiber specimens showed unstable energy release rates, G_{Ic}, with larger crack lengths.

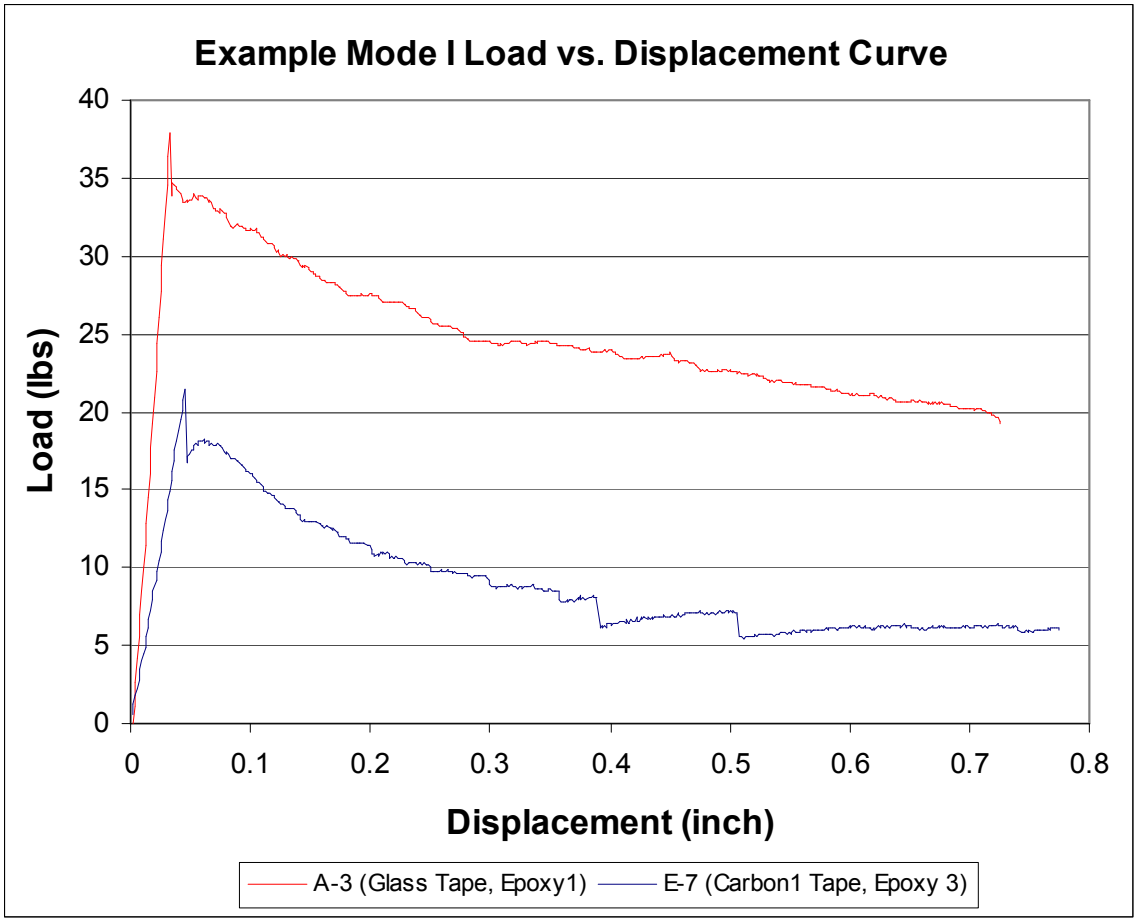

Figure 2.5: Load vs. cross-head displacement example curves of Mode I glass and carbon tape specimens.

The *Modified Beam Theory (MBT) Method* was used to obtain the strain energy release rate for a perfectly built-in DCB, which is given as,

$$G_{Ic} = \frac{3P\delta}{2ba} \qquad (1)$$

where P is the load, δ is the load point displacement, b is the specimen width, and a is the delamination length.

The MBT method will overestimate G_{Ic} due to the fact that the DCB specimen in not perfectly built-in and rotation may occur at the delamination front. To compensate for a rotation is to assume that the DCB has a slightly longer delamination, $a + |\Delta|$, where Δ may be determined experimentally by generating a least squares plot of the cubic root

of compliance, $C^{1/3}$, as a function of delamination length (see Figure 2.6). Compliance, C, is the ratio of the load point displacement to the applied load, δ/P.

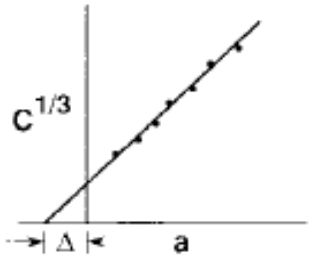

Figure 2.6: Determining rotation compensation for the Modified Beam Theory Method.

2.3 End-Notched Flexure (ENF) Test

ENF specimens test the interlaminar fracture toughness of a laminate subjected to a shear force (Mode II). There is currently no widely accepted standard for Mode II test specimens. ASTM D 790 was used as a guideline for the three-point flexural tests. The Mode II test set-up is shown in Figure 2.7.

The specimens were made from the same panels as the Mode I specimens, which were a rectangular, uniform thickness, unidirectional laminated composite with a non-adhesive insert at its mid-plane that serves as a delamination initiator. The test consisted of a compliance baseline with varying crack lengths (*Compliance Calibration Method* explained in 2.3.3) before the ultimate load to initiate a shear crack. The specimen is wedged open to start a natural delamination from the non-adhesive insert. A MTS 880 3-3 machine with a 20,000 lbs (89 KN) load cell was used for monitoring loads. The complete test procedure is given in Section 2.3.2.

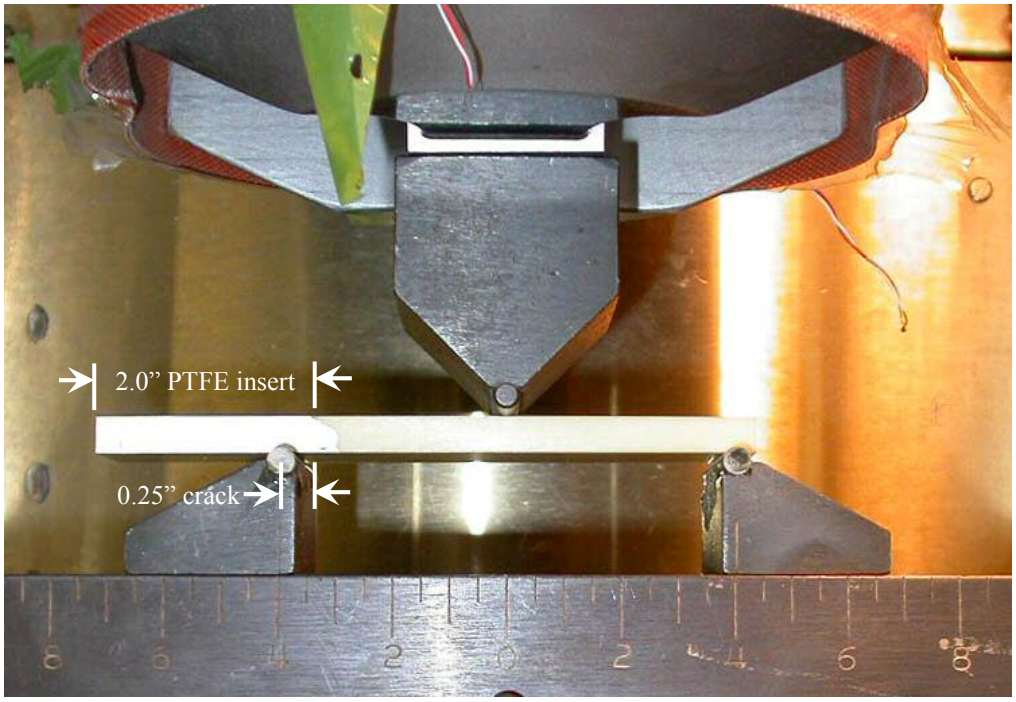

Figure 2.7: Three-point bend test for Mode II test specimens. Compliance baseline was performed with this specimen’s response being tested for a 0.25 inch crack. Complete explanation is given in 2.3.3.

2.3.1 DCB Fabrication

The Mode II specimens were fabricated from the same panels as the Mode I specimens (see Section 2.2.1). Roving, tape and slit tape were the three types of test panel fabrication studied. All tape coupons were cut from 13 x 13 inch (33 x 33 cm) cured panels after the individual plies were cut from a much larger roll of flat unidirectional prepreg from the manufacturer and placed in the respective sequence as shown in Table 2.2. The 0.0005 inch (0.013 mm) thick polytetrafluoroethylene (PTFE) insert ([T]) was centrally located as shown in Figure 2.2. Sectioning through the panel was determined by ultrasonic inspection to 1) ensure no rejectable voids were present prior to coupon processing and 2) locate the centerline of the centrally located PTFE tape. After the panel was sectioned in half, the piano hinge halves (MS20001-6) were bonded to the crack initiation end of the specimen using AF163-2K film adhesive. Each

specimen was then sectioned from the panel and finally machined to approximately 6.0 inches (15 cm) in length and 1.000 ±0.002 inch (25.40 ±0.05 mm) in width and a PTFE insert length of 2.0 inches (51 mm).

2.3.2 Test Procedure

1. Measure and record the width and thickness of each specimen to the nearest 0.002 inch (0.05 mm) at the midpoint and at 1.0 inch (25 mm) from either end.
2. Find the compliance baseline by moving the test specimen so that the 2.0 inch (51 mm) PTFE insert is only 0.50 inch (12.7 mm) past a support to simulate a 0.50 inch (12.7 mm) long crack.
3. Load the specimen to approximately half the load required for shearing to occur at a cross-head rate of 0.05 inch/minute (1.3 mm/minute).
4. Record the load and displacement values continuously.
5. Perform Steps 2-4, increasing the crack length every 0.25 inch (6.4 mm) to a final crack length of 1.75 inches (44.4 mm).
6. Wedge open the crack 0.1 to 0.2 inch (3 to 5 mm) past the end of the PTFE insert for a natural crack initiator.
7. Relocate the test specimen so that the crack is 1.0 inch (25 mm) from a support, was half the distance from a support and load pin.
8. Record and load the specimen until shearing occurs. Unload the specimen.

2.3.3 Observation and Calculation

Post-examination of the test specimens did not reveal any permanent bending deformation of the two separate specimen halves or major deviations of the delamination from the mid-plane of the laminate.

Since there was a span of 4.0 inches (10.2 cm) for all Mode II three-point bend tests with a 1.0 inch (25 mm) pre-existing crack, the resultant shear crack propagated approximately 1.0 inches (25 mm) to the center of the specimen where the load pin was located. A drop in load as shown in Figure 2.8 corresponds to the resulting shear crack. With a rapid static release of energy during a shear crack, no rate is to be determined and less data is gained compared to Mode I coupons of steady crack growth. All specimens experienced a linear increase before the crack propagated. Slope as well as the amount of cross-head displacement required for crack growth will depend on the material and the thickness of the specimen. Thinner carbon fiber specimens required greater displacement than fiberglass materials. Fiber bridging was not much of an issue for Mode II specimens, unlike the significant amount fiber bridging as observed in the Mode I specimens.

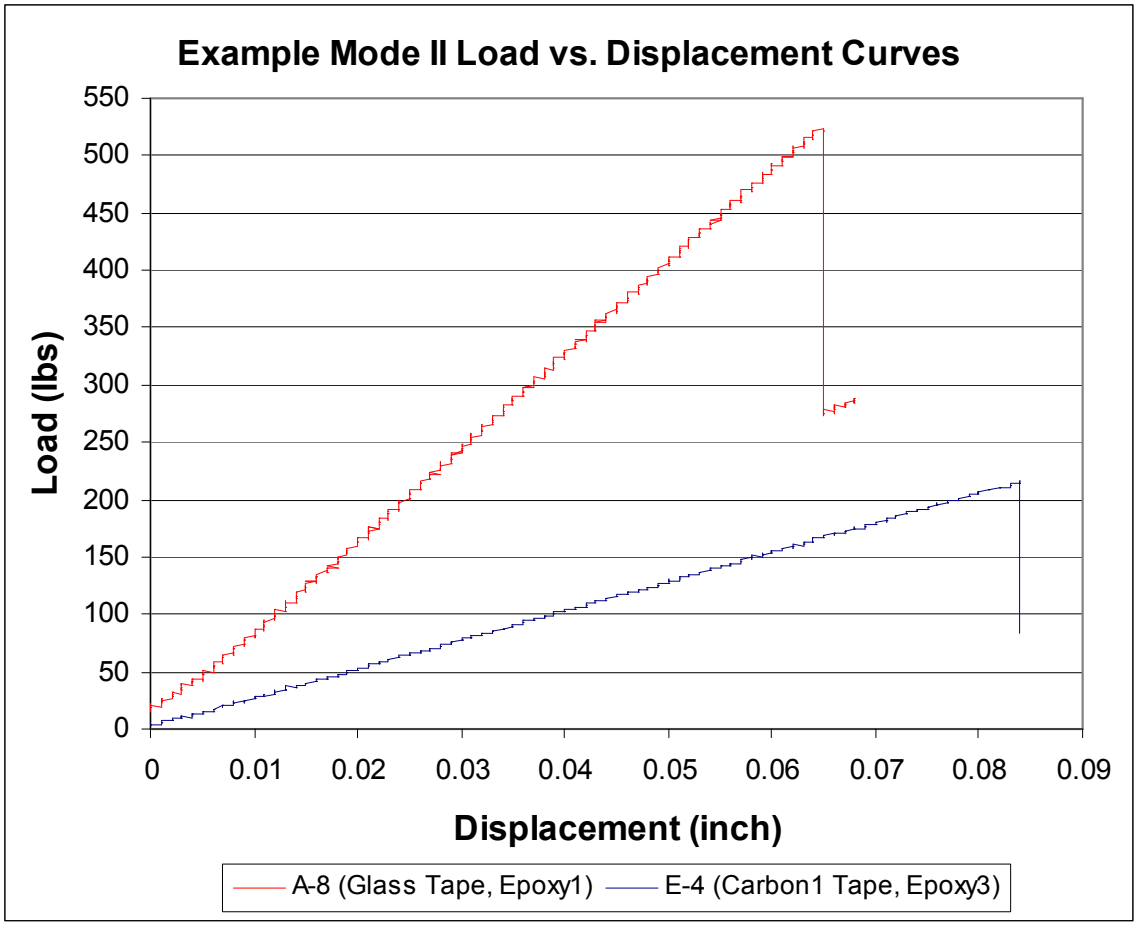

Figure 2.8: Load vs. cross-head displacement example curves of Mode II glass and carbon tape specimens.

The *Compliance Calibration Method* was used to obtain the strain energy released for ENF specimens. Finding the compliance response with varying crack length in the three-point bend test would yield half of the equation as follows:

$$G_{IIc} = \frac{P^2}{2b}\frac{\partial C}{\partial a} \qquad (2)$$

where again, P is the load, b is specimen width, C is compliance, and a is the crack length.

To find the compliance baseline or response of a material, the specimen is loaded at half the critical crack growth load for a given crack length. This crack length can be adjusted by moving the specimen (with a 2.0 inch (51 mm) PFTE insert) between the two

load points as shown in Figure 2.7. Example compliance vs. crack length curve is shown in Figure 2.9. After finding a best fit equation, enter the value for the actual wedged-open crack length as well as the test data to determine $\partial C / \partial a$ and ultimately Mode II strain release energy. Just like Mode I calculations, all G_{IIc} values were determined using the 5% offset/maximum load technique to be consistent. It was also used because the crack propagated so quickly that using the VIS method was not possible.

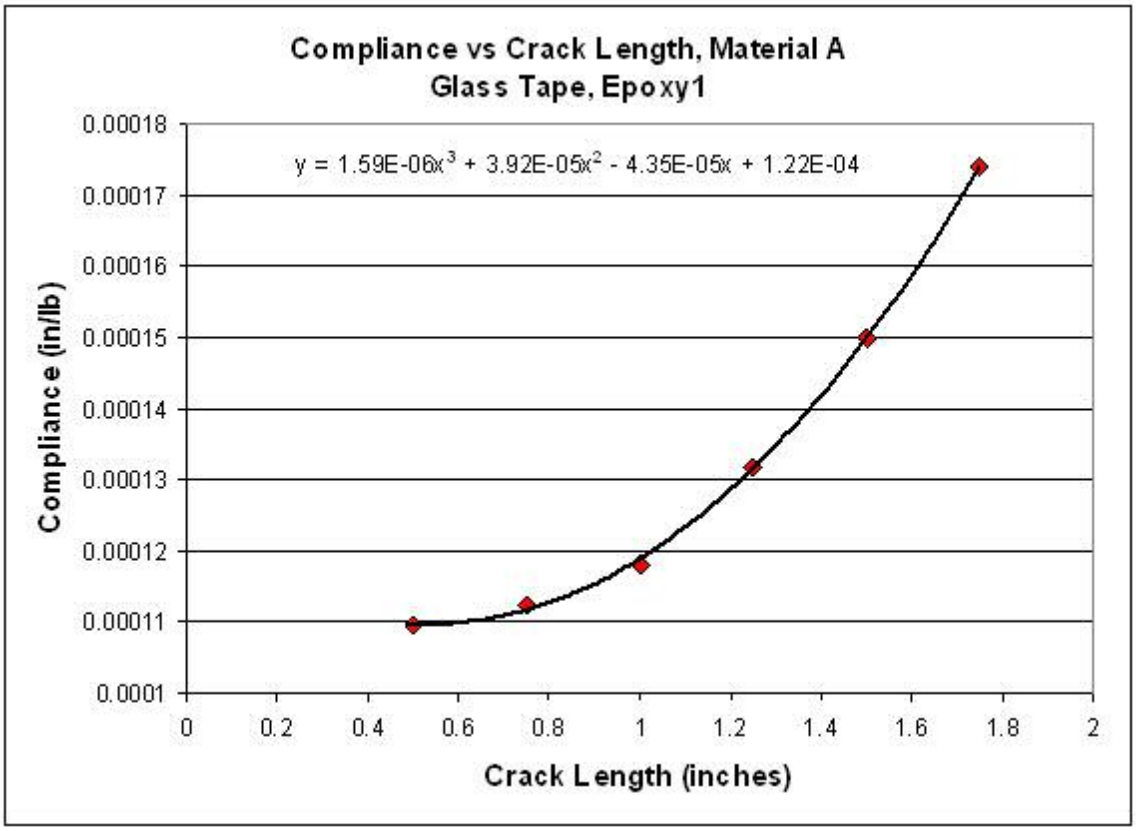

Figure 2.9: Example compliance vs. crack length curve to determine strain release energy for Mode II.

CHAPTER 3

FRACTORGRAPHY

Fractography is the detailed analysis of a fracture surface to determine the cause of the fracture and the relationship of the fracture Mode to the micro and macro structure of the material. Fractography techniques are used to locate the origin area of a crack and to determine what type of loading and/or outside forces that caused the crack to initiate. It is also used to determine the direction of crack propagation and the local loading mode that drove the crack. Other data can also be extracted such as structure-property relationship involving strength and failure of materials. Fractography provides useful information in evaluating new materials and in defining their response to mechanical, chemical, and thermal environments [1].

Fractography is important not only to the determination of the events during failure, but also for the identification of the state of stress (tension, compression, or shear) that existed at the time of fracture. Analytical techniques such as visual and optical macroscopy, optical microscopy, scanning electron microscopy (SEM), and transmission electron microscopy (TEM) are used to extract information from the morphology and other crack features. Together, these techniques are used with interpretative methods to determine the origin and direction of the failure, crack propagation type and mode, environmental affects, or any other material anomalies to reduce the material strength. For these reasons, it is important to have a standard fractography library.

3.1 Experimental Procedure

Two test specimens from each of the Mode I and II tests were examined and photographed using a Hitachi 3400 and a Hitachi 3700 SEM. Since the Mode I specimens fractured in half from testing, the surface of one of the halves was washed with acetone. After the specimen was dry, a thin layer of gold (approximately 200 Å) coated the surface by physical vapor deposition to reduce the amount of charging in the SEM and improve imaging. The same method was used for the Mode II specimens, except a cut had to be made near the end of the crack that extended to the loading pin (approximately 1 inch (25 mm)). Photographs were taken with accelerating voltages of 5-20KeV, but the majority were taken at 5KeV for less electron beam penetration and better fracture feature detail without a ghost-like image.

3.2 Fracture Morphology

There are two distinct delamination features both the two failure Modes that will be presented in the following sections. The primary feature of Mode I specimens are river patterns that initiate at the resin and fiber interface and flow "down stream" with the direction of the crack propagation. The primary features for Mode II specimens are hackle and scallop formations. Hackles appear saw-toothed on one side of the crack face with the scallops on the mating surface that appear wave-like. Both of these common Mode I and II delamination features will vary with the toughness of the resin systems and fiber modulii. More delamination features will be discussed and explained below.

3.2.1 Mode I

Mode 1 is the weakest fracture type in which the maximum tensile stress lies perpendicular to the plane of failure for interlaminar and intralaminar fractures. As a

result, brittle cleavage of the matrix occurs and fiber fracture rarely happens. Macroscopically, the surface is typically flat and shiny in appearance. Higher magnifications with a SEM reveal cohesive resin fracture between the areas of fiber-matrix interface. These areas have pronounced river markings and resin microflow, where crack propagation would be in the direction of "down river flow".

Fiber bridging is another typical characteristic of Mode I loading (see the physical model in Figure 3.1). The resin-rich areas between adjacent fibers undergo significant deformation revealing river markings with fibers appearing clean without resin. This is different from the event where the crack front experiences severe resin deformation.

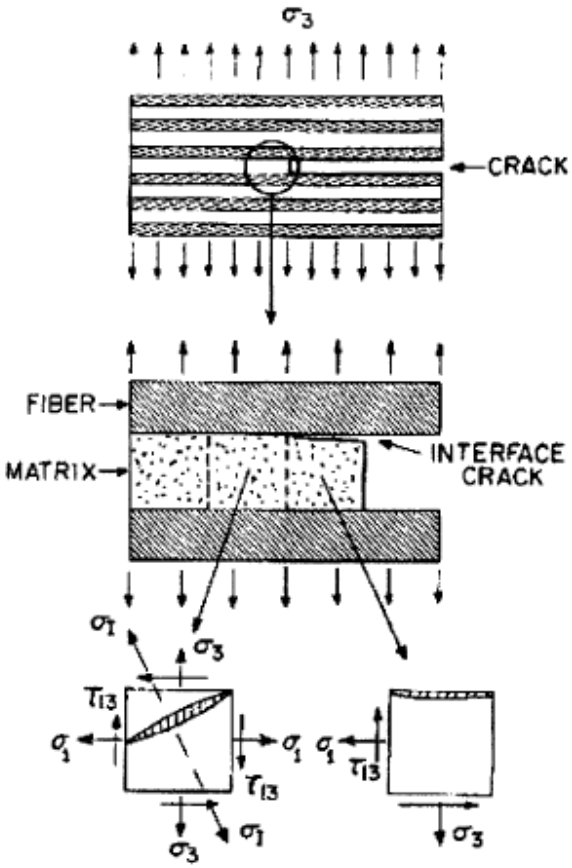

Figure 3.1: Physical model explaining crack branching under Mode I loading.

Since the matrix is relatively brittle, failure occurs where the tensile stress is maximum. At the crack front, the tensile stress occurs at the interface normal to the fiber. Away from the crack front, the tensile stress tends to incline in the direction of crack growth due to the presence of shear. Since the loading systems has very low compliance, the high energy release rate causes crack bifurcation along the fiber matrix interface and along the normal to the maximum tensile stress ahead of the crack tip [11].

Material A (Glass Tape, Epoxy1)

Typical Mode I river patterns were not as apparent in this resin system as opposed to other systems. River patterns were visible, however the pockmarked surface, that was most likely due to volatiles trapped during the fabrication of the panels, may have retarded the development and growth of river patterns. Micro-cracks also may have formed ahead of a crack front at these small voids. Areas of unorganized fracture features did not aid in determining delamination direction. A small percentage of the fracture surface contained hackles or mixed-mode features that may have arisen from a complex state of stresses from fiber bridging or fiber pull-out. In some areas, resin adhesion was found on the fibers, but most fibers had a clean appearance with no sheathing of resin. This resin system did not have a particularly strong indication of desirable interfacial bonding.

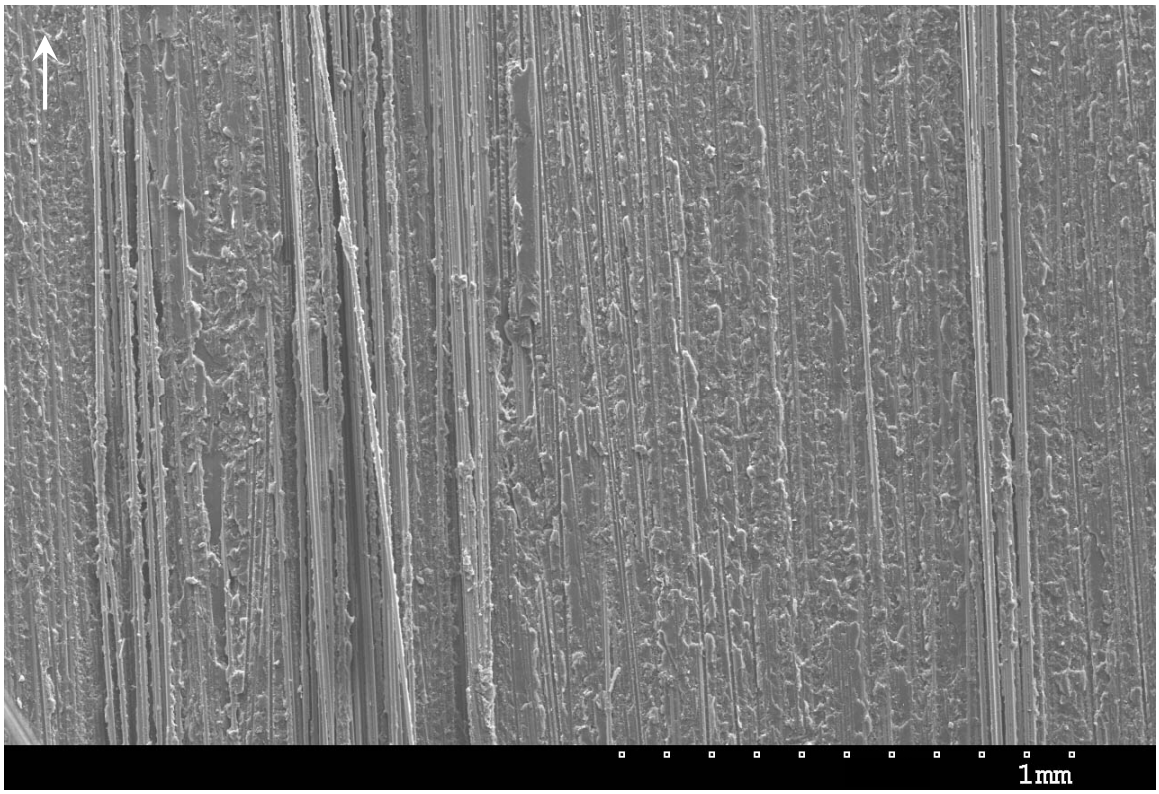

Figure 3.2: Overall view of Material A tested under Mode I loading showing fiber bridging on the fracture surface (arrow indicates crack direction).

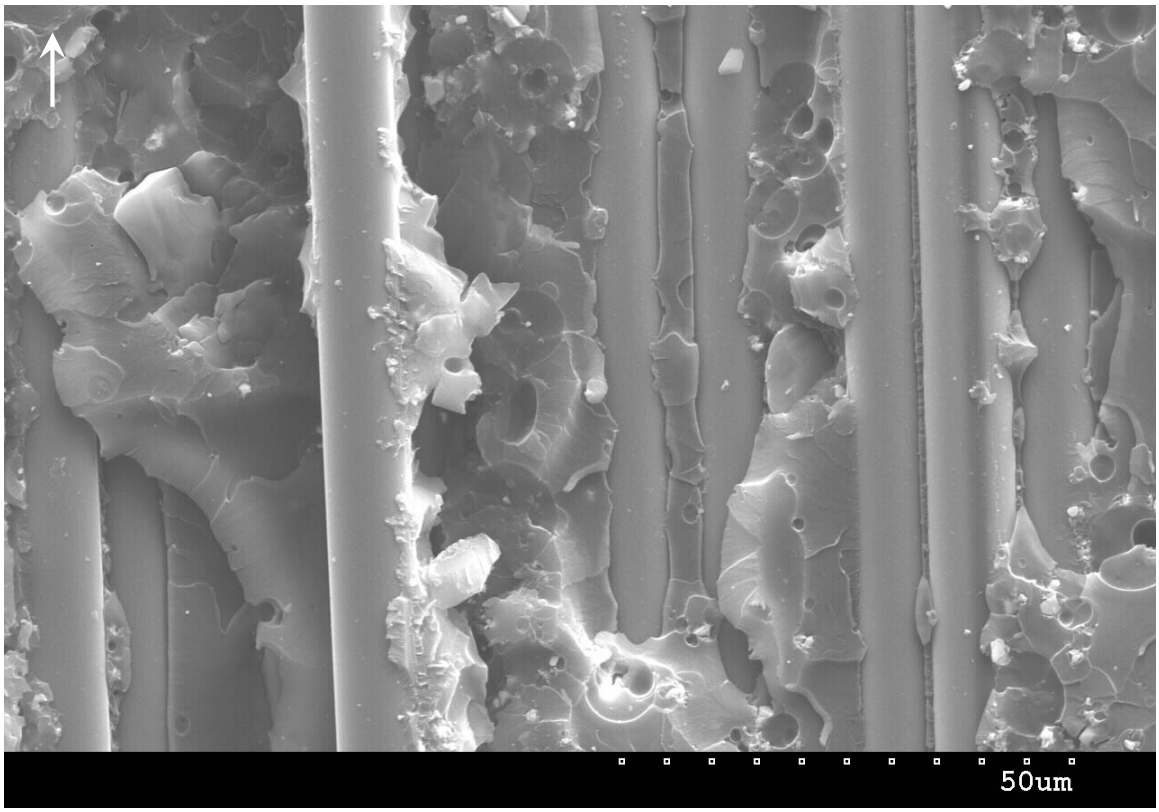

Figure 3.3: Close-up view of fiber bridging, partial fiber/resin adhesion and unorganized fracture features.

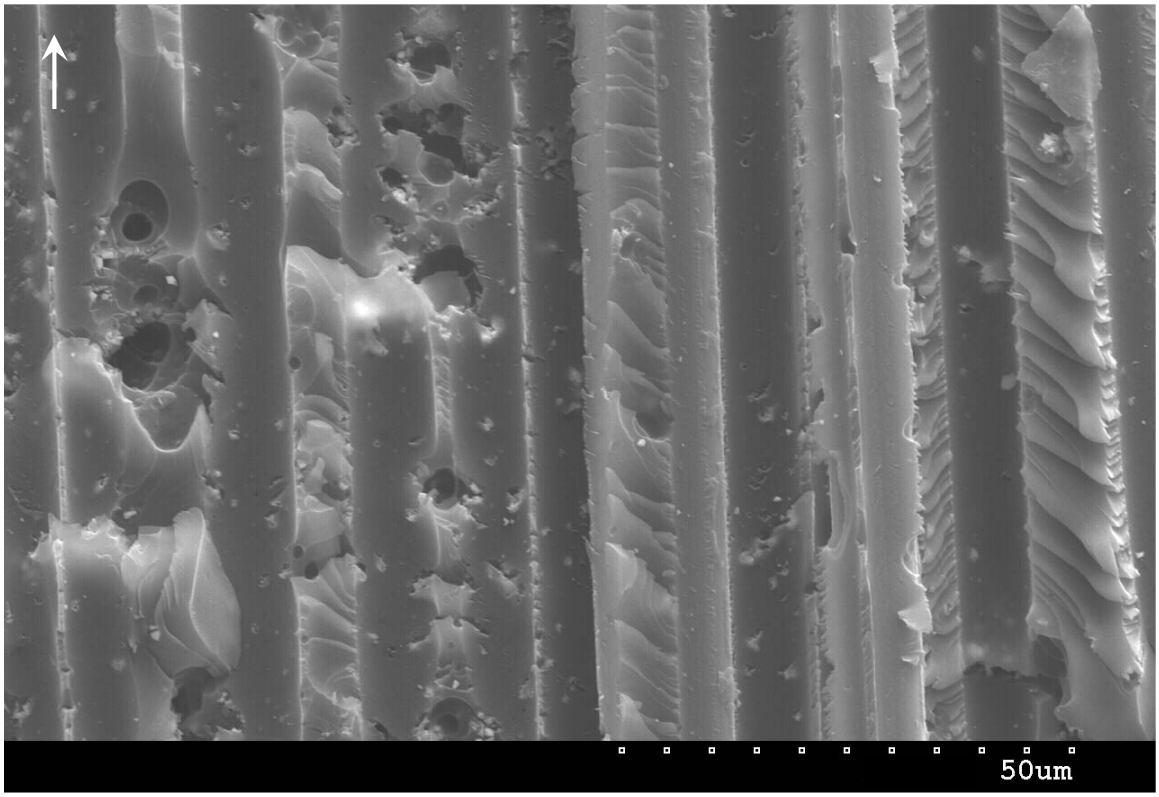

Figure 3.4: Pockmarked surface with areas of river patterns and mixed-mode features possibly from fiber bridging or fiber pull-out.

Material B (Glass Roving, Epoxy1)

A larger amount of fiber bridging was easily noticed as compared to the Material A that has the same fibers and resin system, but in different forms. Areas of unorganized fracture features were found as well as tiny pores, but plenty of river patterns helped indicate a crack growth direction. Some fiber/resin adhesion was also observed, but the majority of the fracture surface had no adhesion and poor interfacial bonding. An example of micro-resin flow that is characteristic for all resin systems is shown below. This can also be used to determine the local crack growth direction as well as the resin's toughness and cohesive integrity.

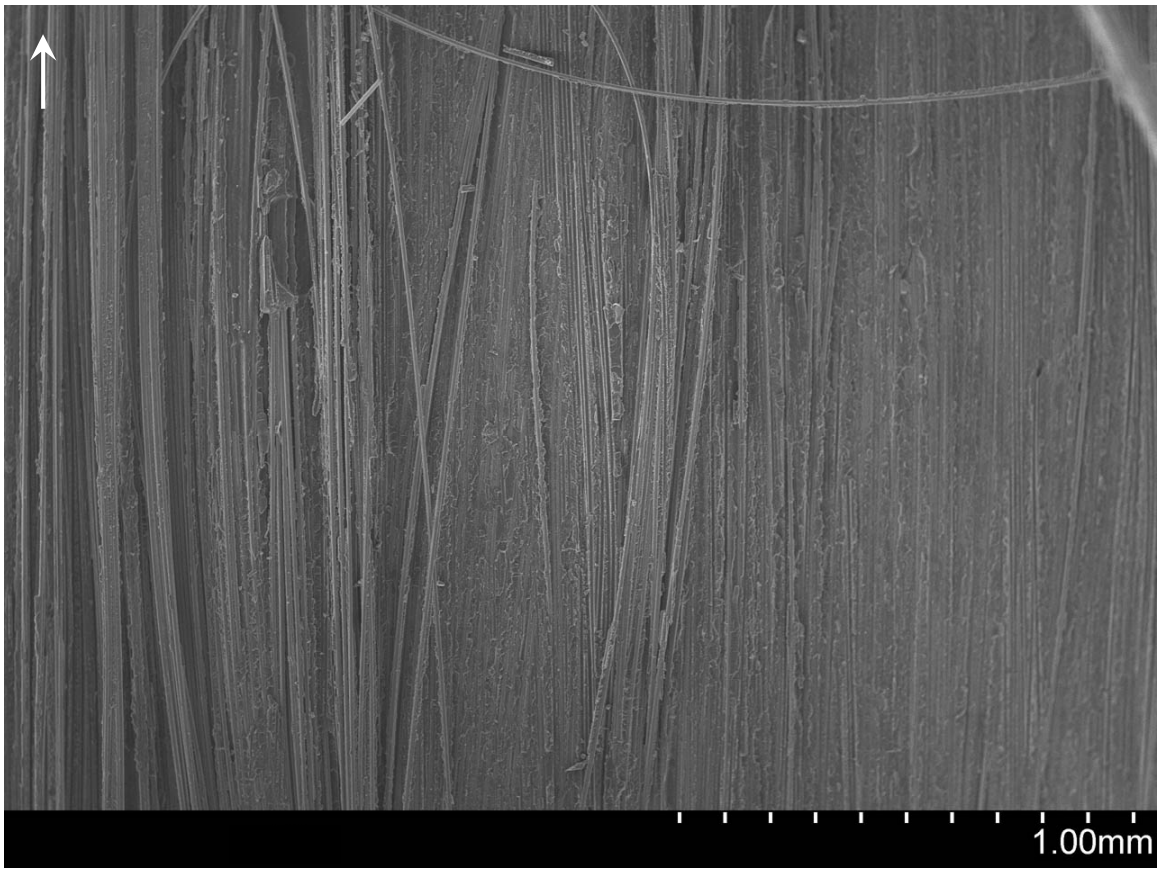

Figure 3.5: Overall view of Material B tested under Mode I loading showing a larger amount of fiber bridging (arrow indicates crack direction).

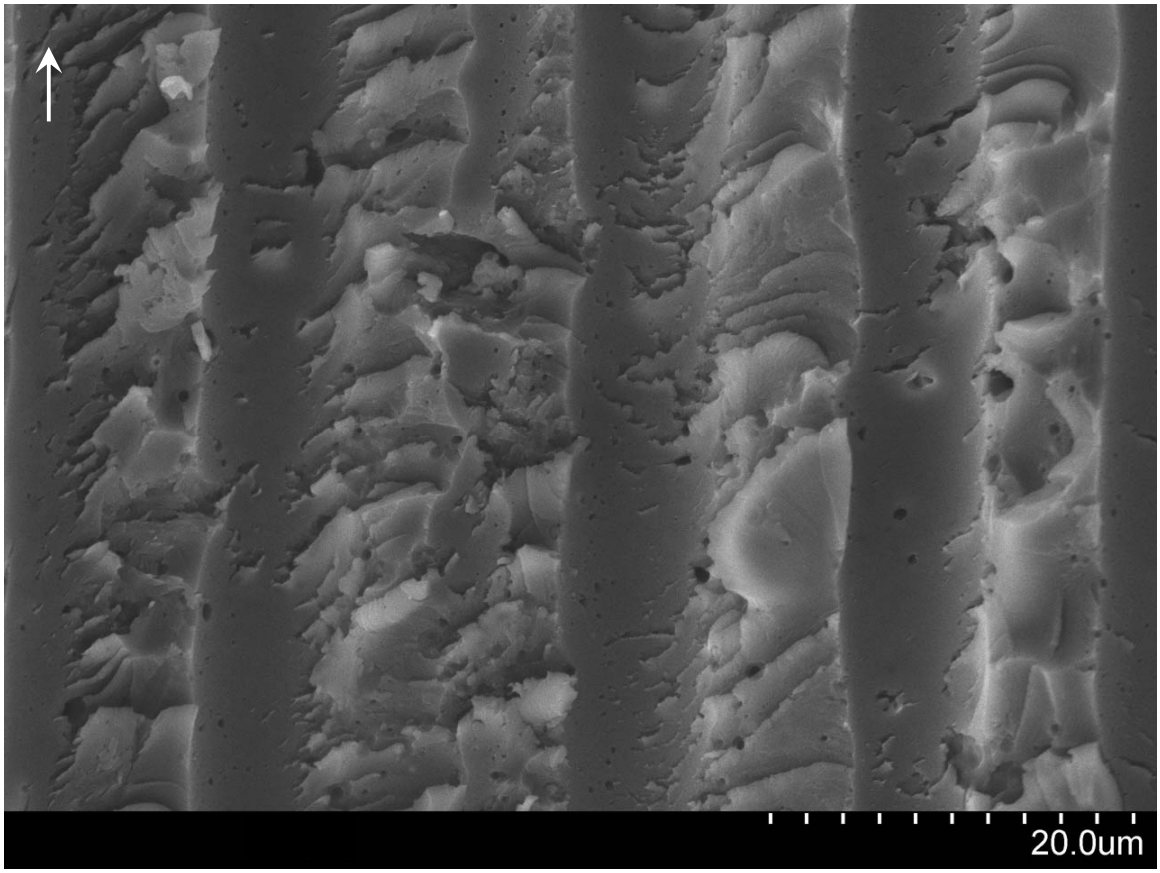

Figure 3.6: Unorganized resin deformation with negative fiber impressions showing some fiber/resin adhesion.

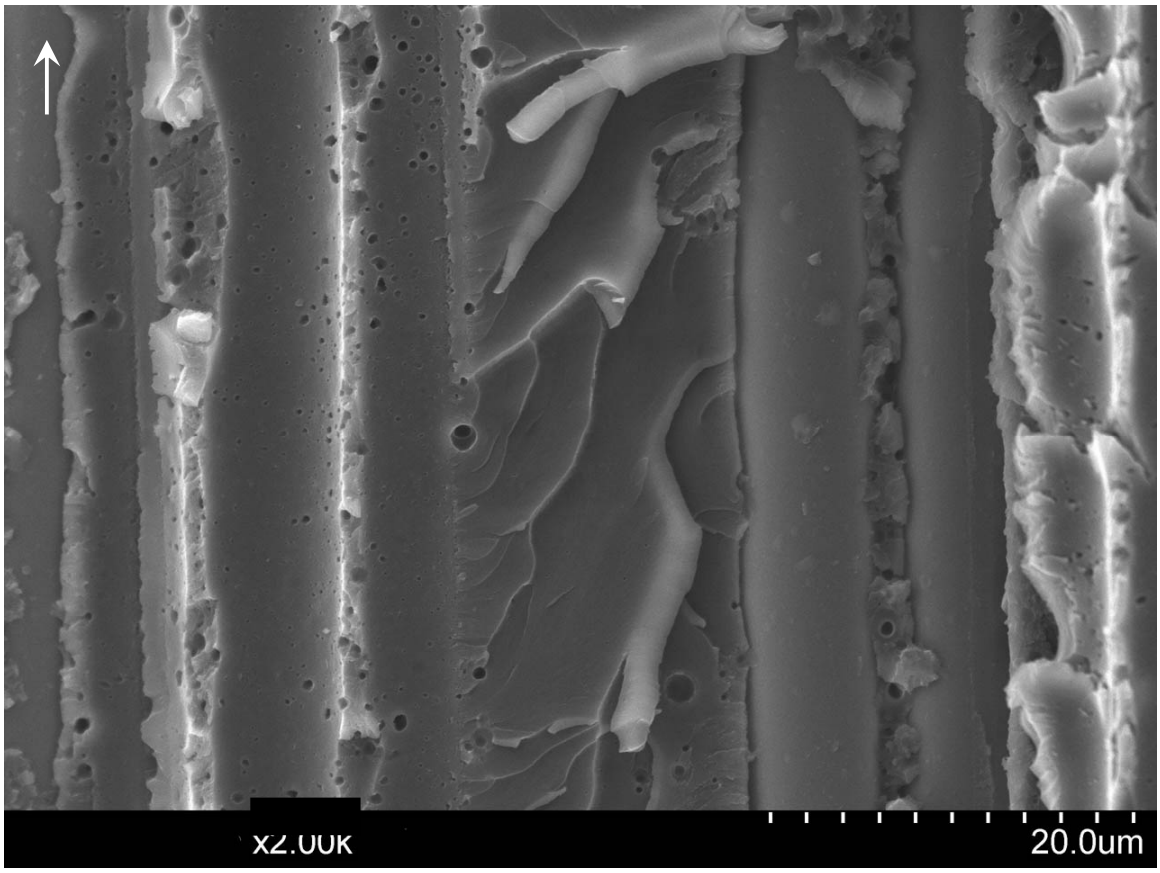

Figure 3.7: Examples of river patterns and a small amount of porosity.

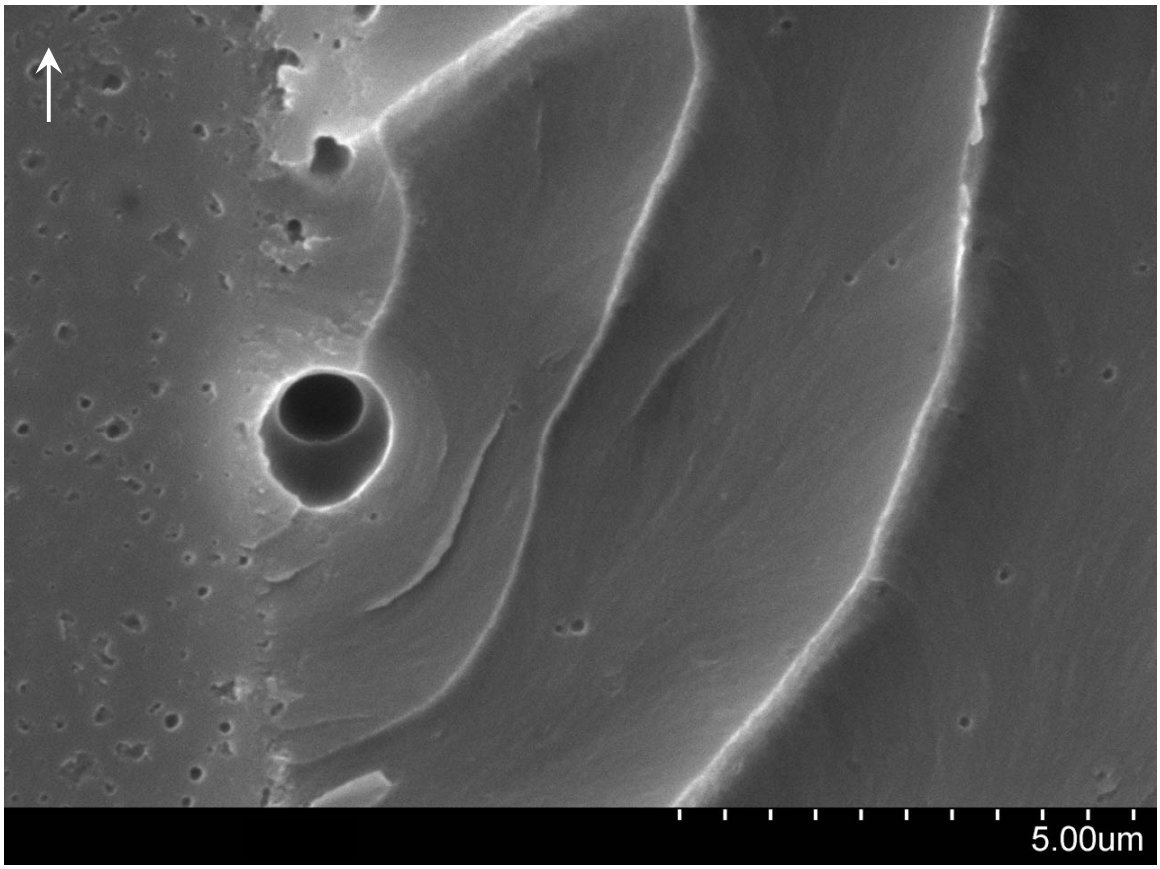

Figure 3.8: High magnification view of micro resin flow between river patterns.

Material C (Glass Tape, Epoxy2)

The fracture surface for Material C had a large amount of resin deformation and surface area as well an uneven fractures surface that both indicate a much improved strain energy needed for failure. Micro resin flow was easily apparent at lower magnifications than what more brittle resin systems require. Fiber/resin adhesion was visible over the majority of the exposed fiber surface. A small amount of fiber breakage was observed on the fracture surface that may be due to increased fiber/resin adhesive strength since fiberglass has a relatively lower modulus.

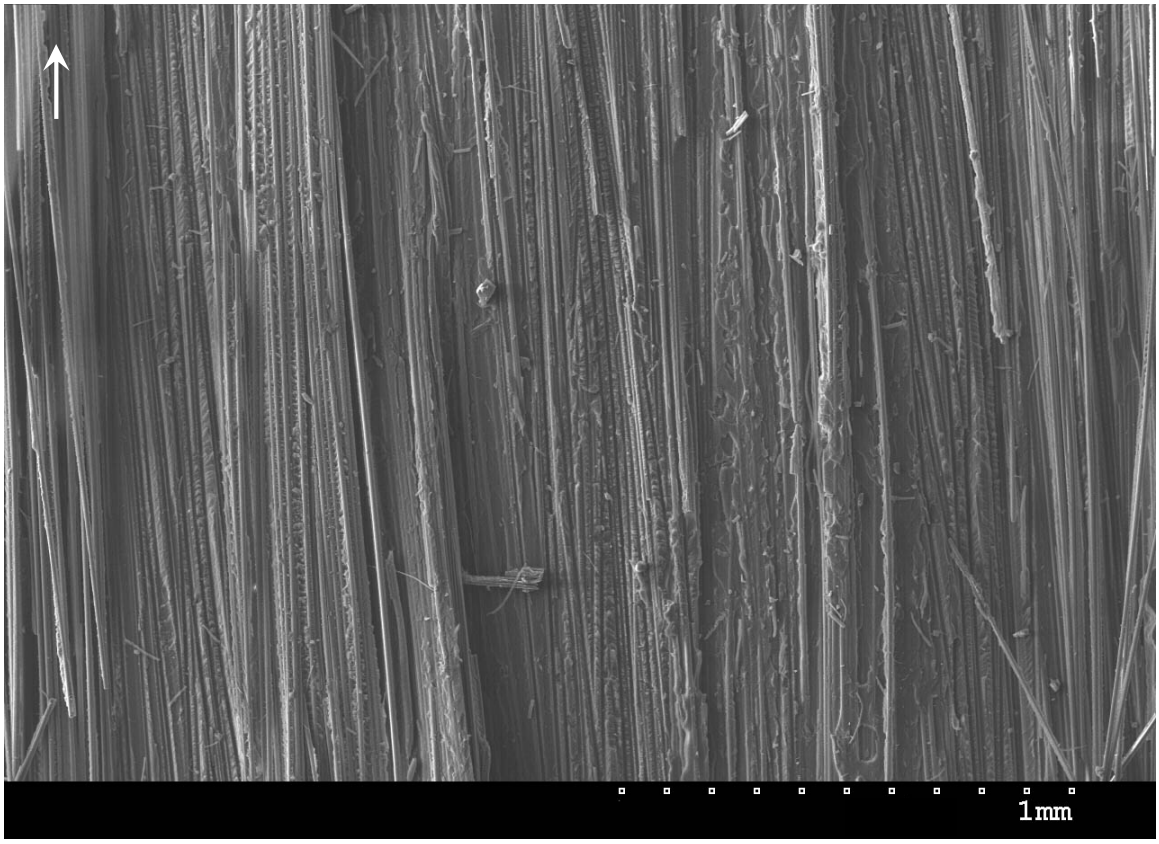

Figure 3.9: Overall view of Material C tested under Mode I loading revealing an uneven and rough fracture surface and fiber bridging (arrow indicates crack direction).

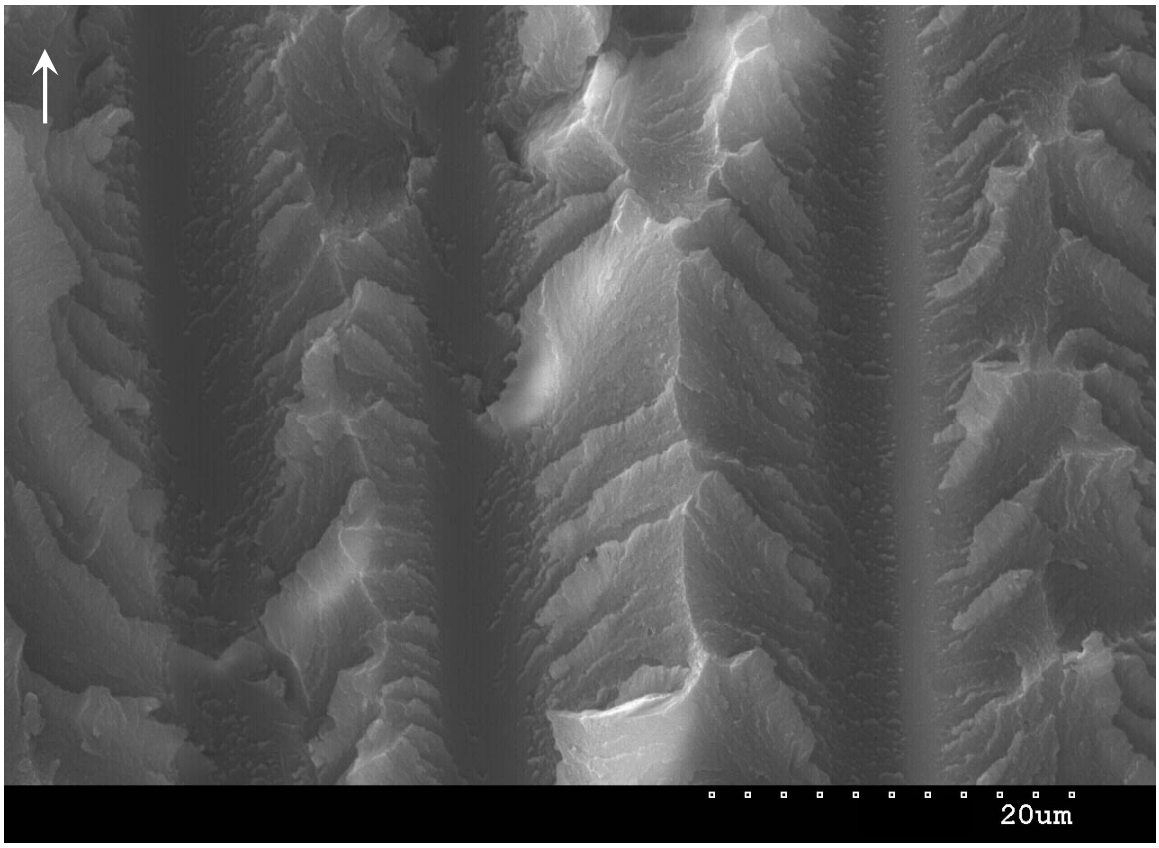

Figure 3.10: A large amount of resin surface area could be seen with increased fiber/resin adhesion of negative fiber impressions. Some mixed-mode features from fiber bridging or fiber pull-out were observed.

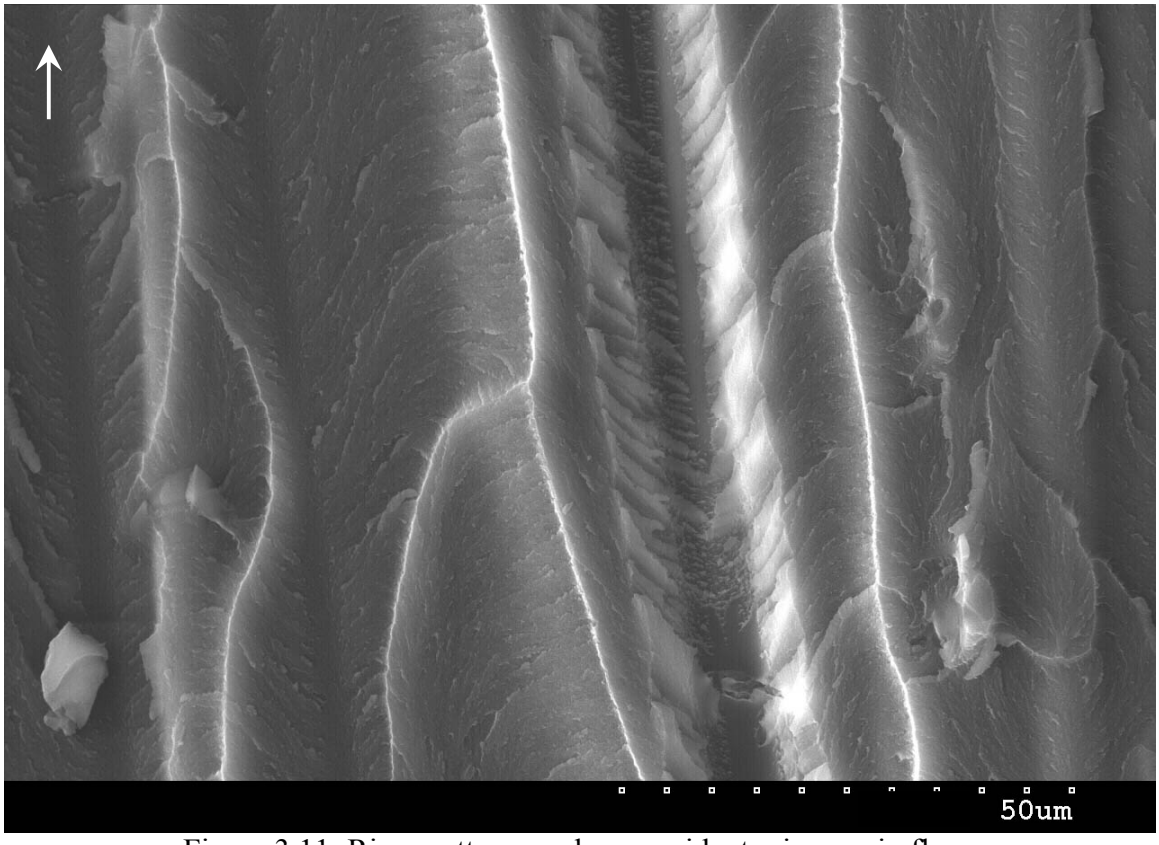

Figure 3.11: River patterns and very evident micro resin flow.

Material D (Glass Roving, Epoxy2)

Figure 3.12 shows a large amount of fiber bridging that has been apparent in all of the fiberglass specimens. Much like Material C with the same resin system, the fibers of Material D was in the form of roving with overlapping tows. Several large intralaminar cracks that were most likely due to the separated tows were observed. River patterns and micro resin flow were both easily visible. A resin sheath covered almost the entire fiber surface, indicating excellent interfacial bonding. Because of this, the majority of the fracture surface comprised of resin yielding and deformation.

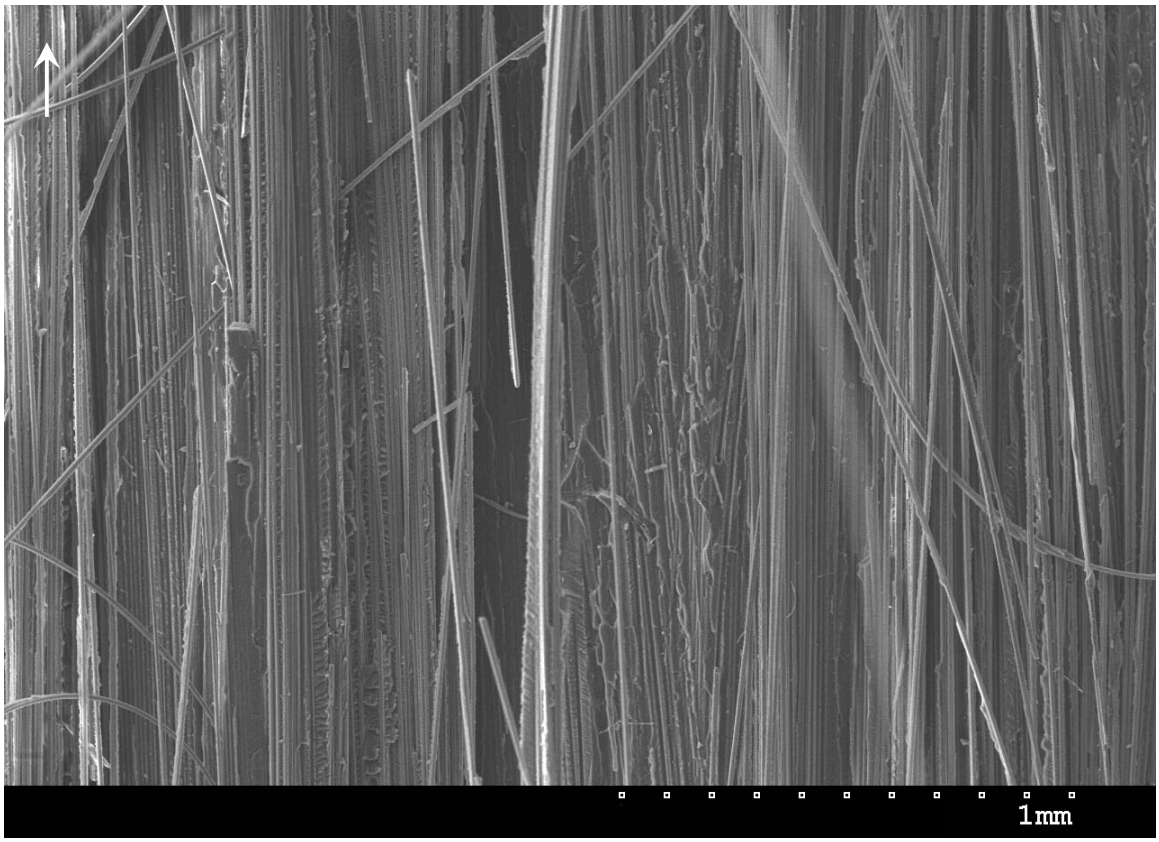

Figure 3.12: Overall view of Material D tested under Mode I loading depicting an intralaminar crack and fiber bridging (arrow indicates crack direction).

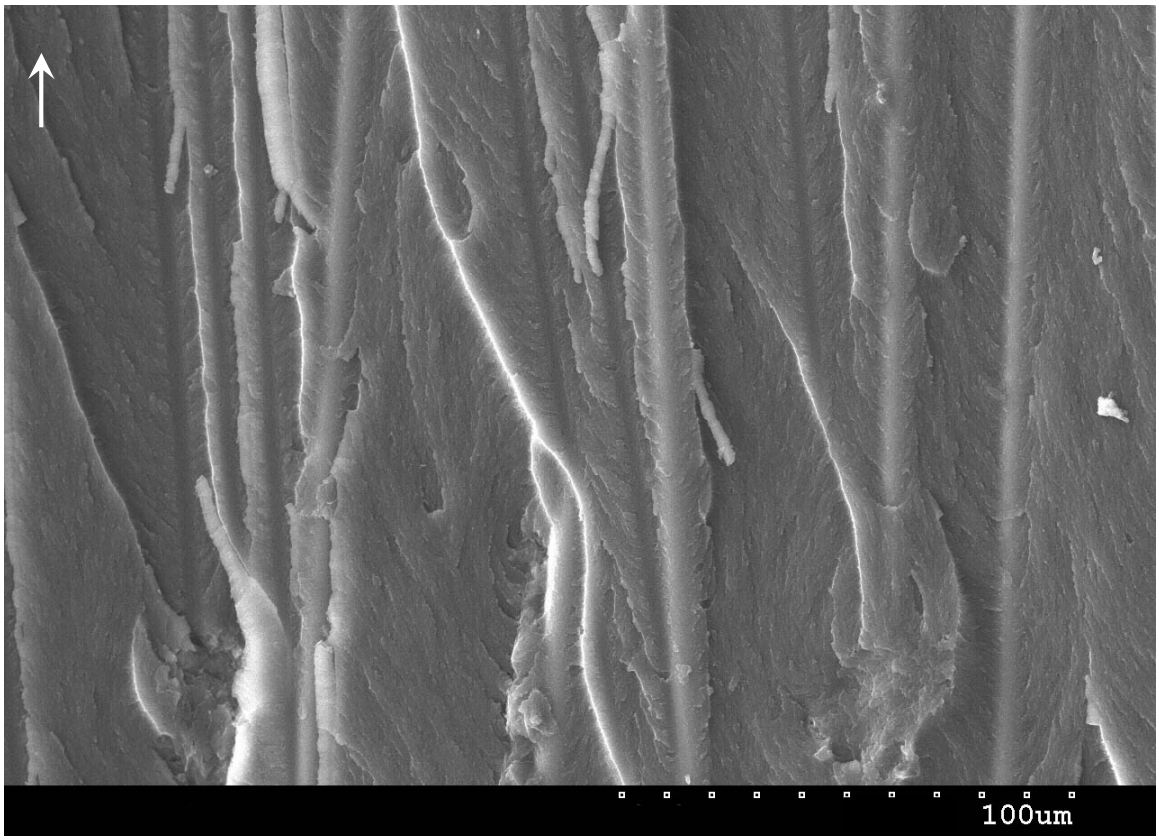

Figure 3.13: View of river patterns, resin sheath on fibers and easily visible micro resin flow.

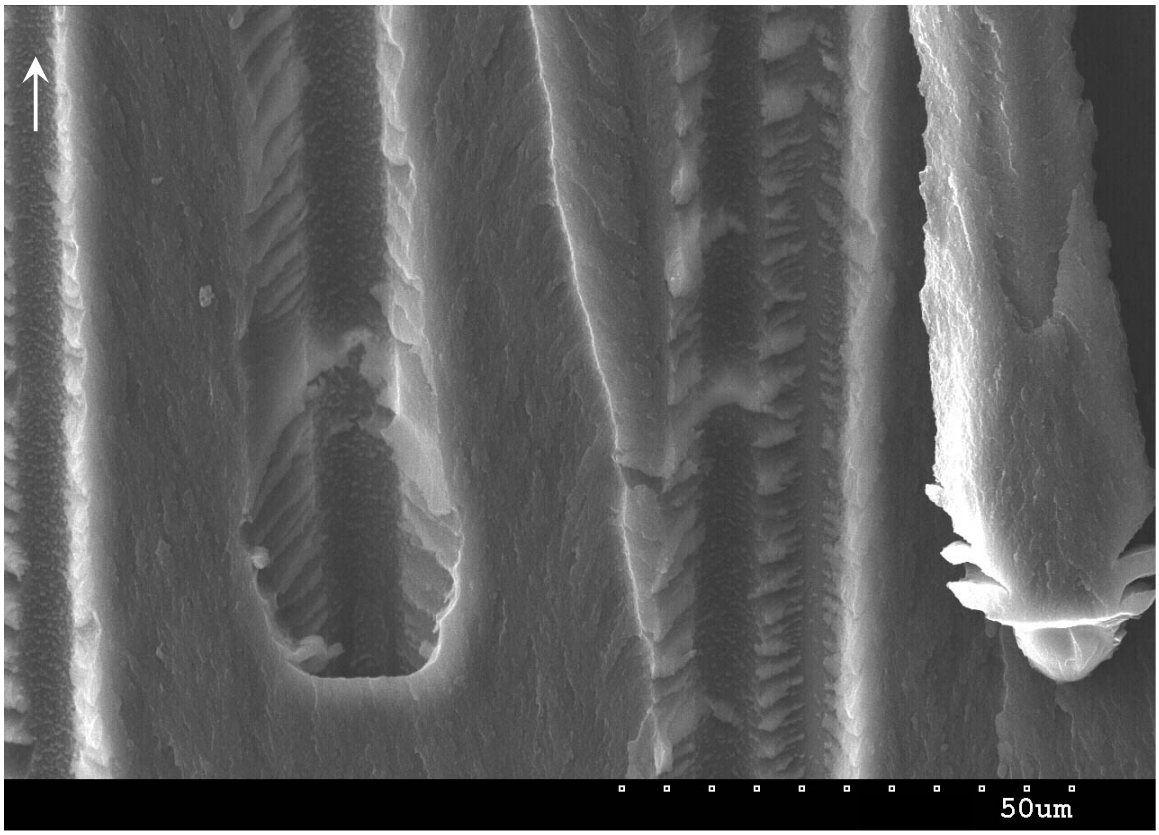

Figure 3.14: Example of mixed-mode features associated with fiber pull-out and micro resin flow.

Material E (Carbon1 Tape, Epoxy3)

Caron fiber has a much higher modulus than fiberglass and results in more frequent fiber breakage of Mode I test specimens. This particular resin system showed evidence of being very brittle because of very weak fiber/resin adhesion and almost no micro resin flow at high magnifications. However, an uneven fracture surface was observed, which would increase surface area and fracture toughness.

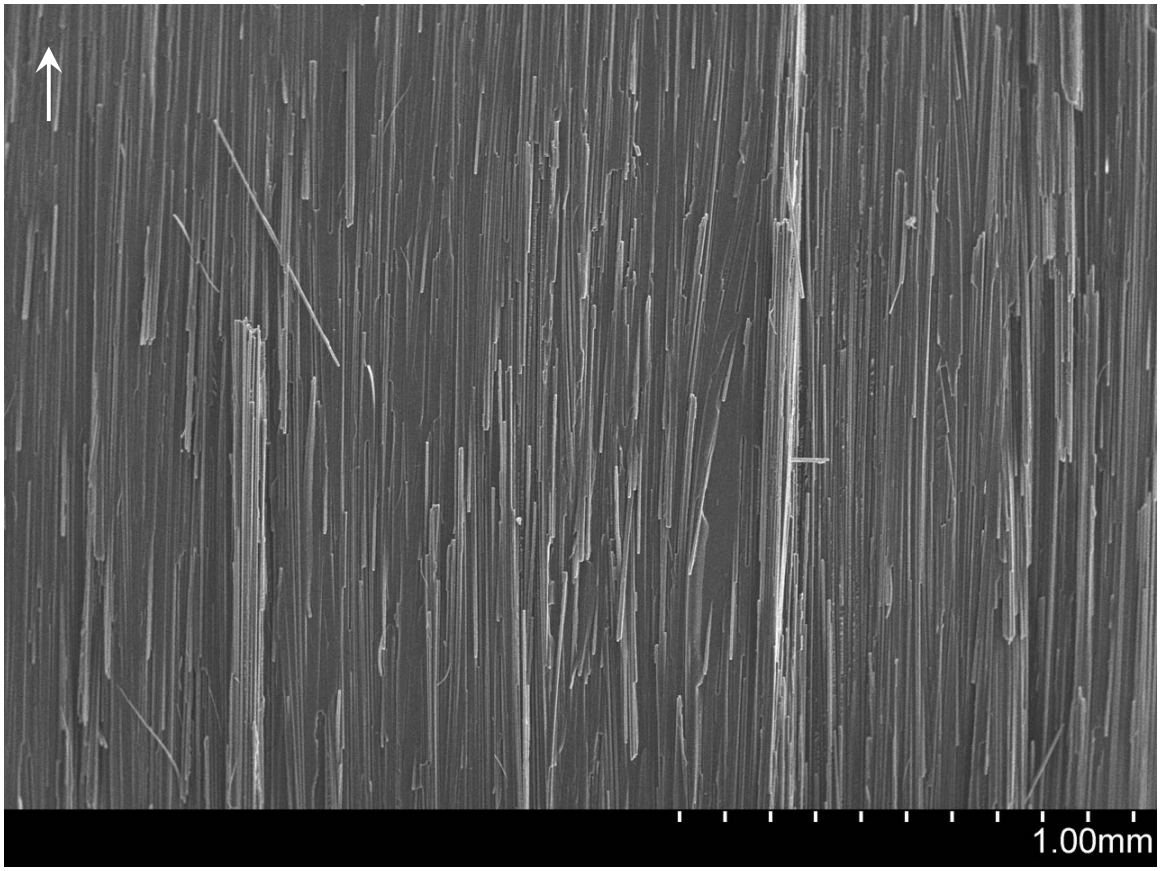

Figure 3.15: Overall view of Material E tested under Mode I loading revealing fiber breakage and a relatively smother fractures surface than fiberglass materials (arrow indicates crack direction).

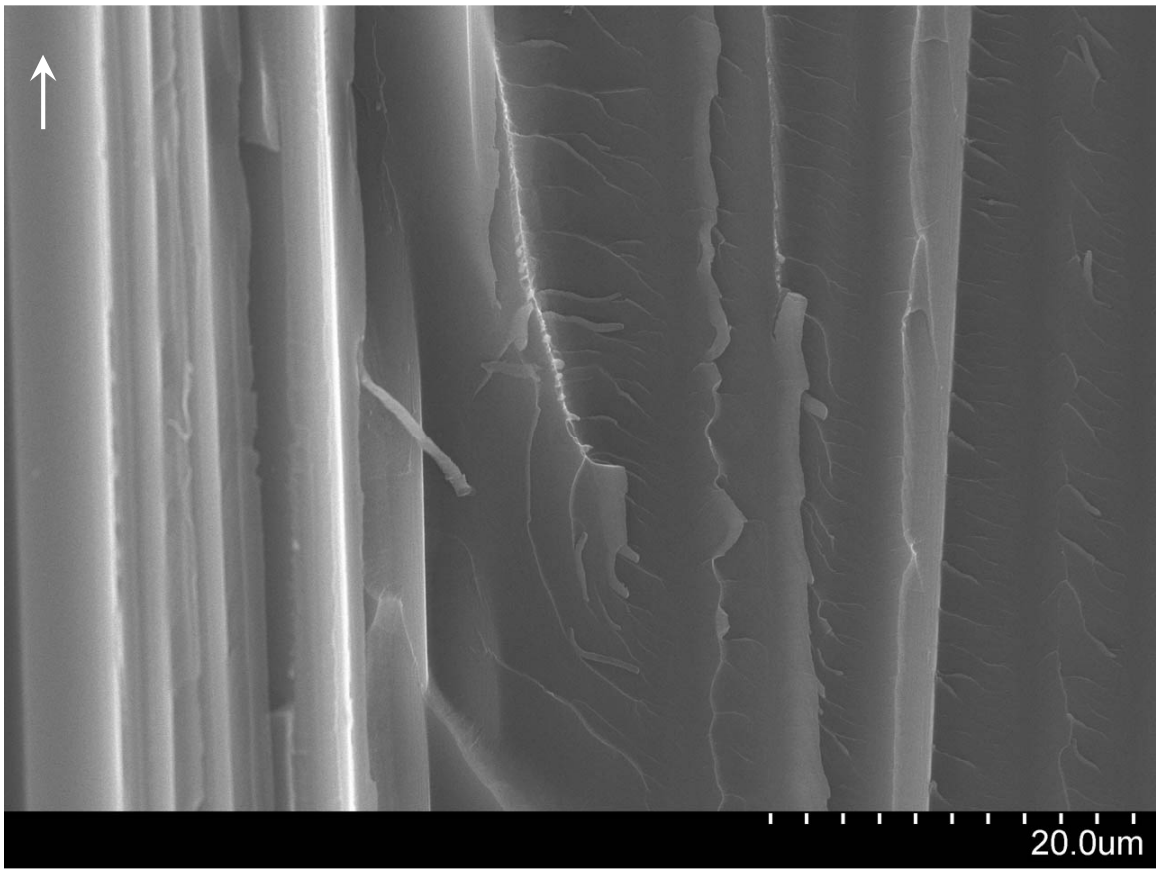

Figure 3.16: Brittle resin fracture and river patterns.

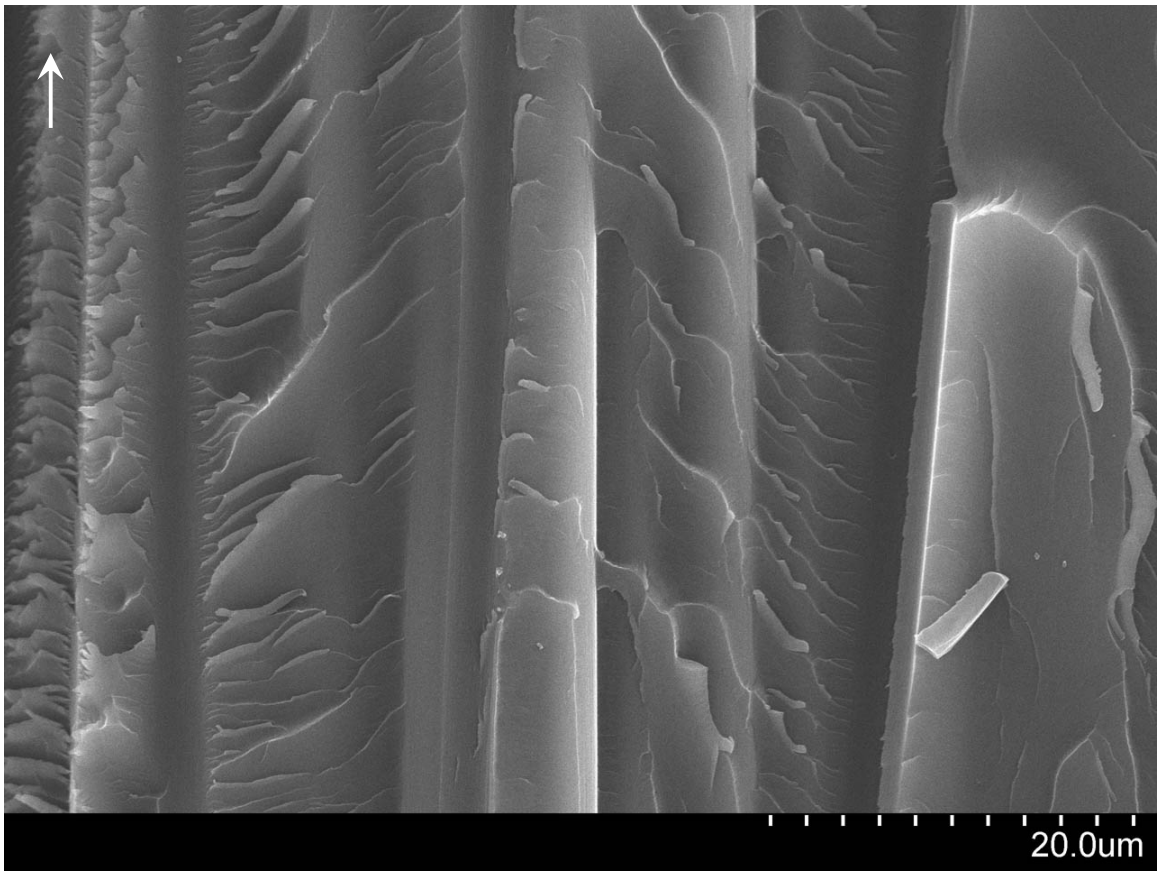

Figure 3.17: River patterns and no fiber/resin adhesion from the negative fiber impressions. Almost no micro resin flow was visible.

Material F (Carbon2 Tape, Epoxy1)

Material F has the same resin system as in Materials A and B, which coincides with the observation previously made with respect to pockmarked features from small voids formed by volatiles during fabrication, and poor fiber/resin adhesion. The fracture surface was extremely flat. River patterns were observed originating from fiber surface or voids and a small amount of micro resin flow could be seen at high magnifications. The failure mechanism was almost completely brittle resin fracture.

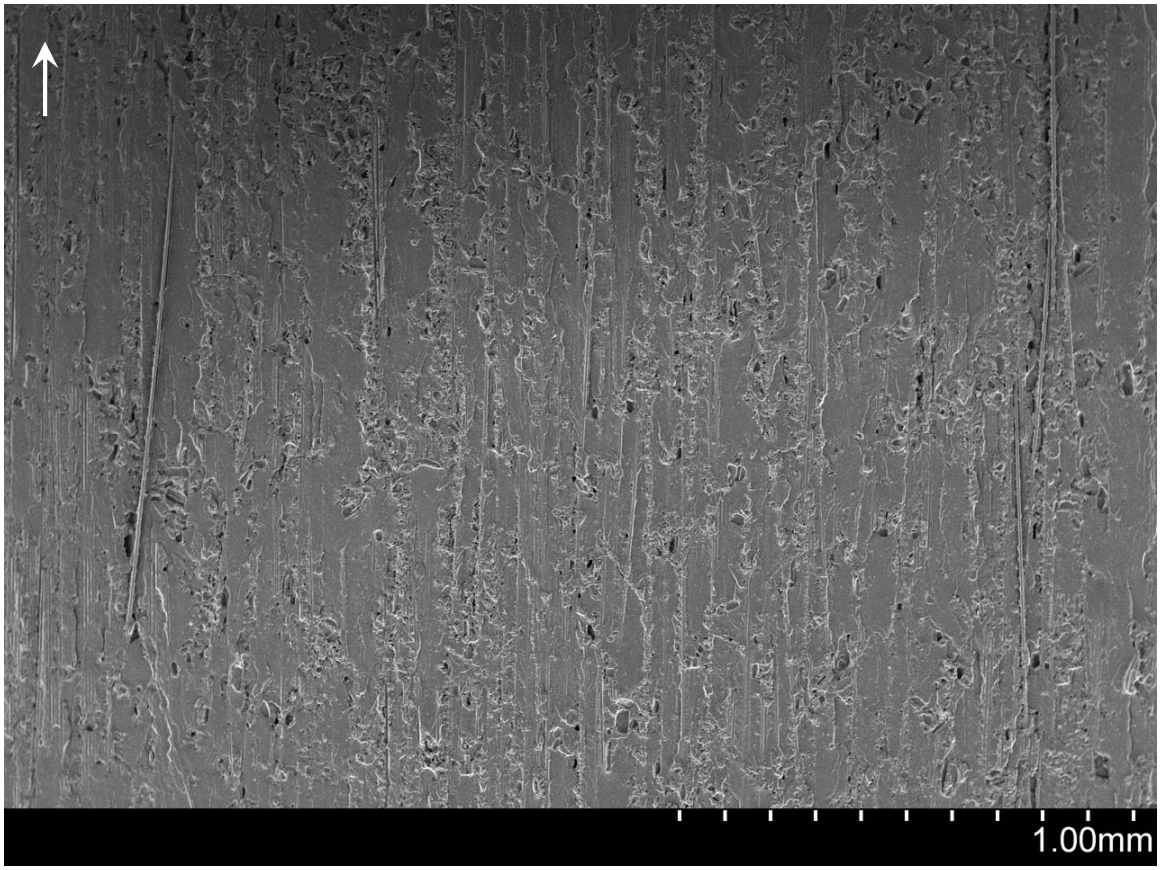

Figure 3.18: Overall view of Material F tested under Mode I loading showing a flat surface with a few porous areas. Fiber pull-out and fiber bridging were sometimes observed (arrow indicates crack direction).

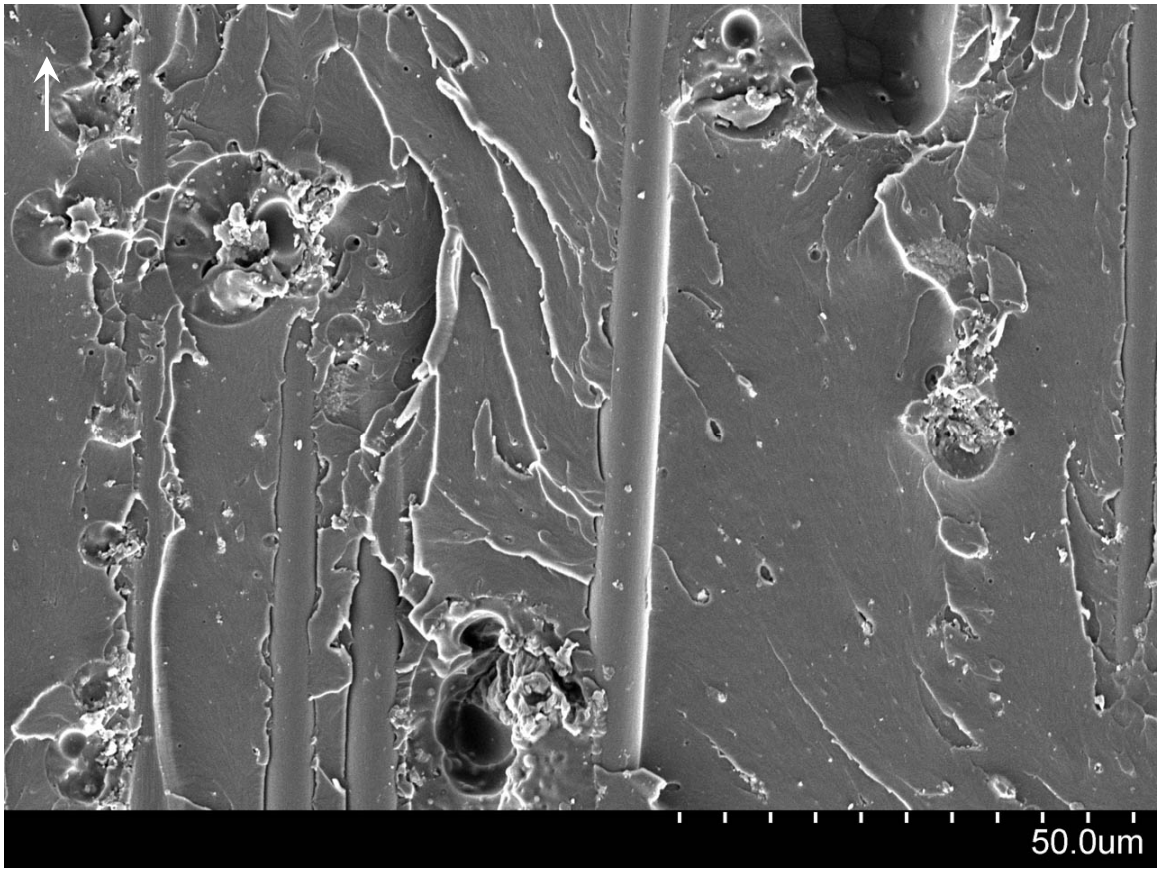

Figure 3.19: A relatively flat fracture surface with very little resin sheath on the fibers.

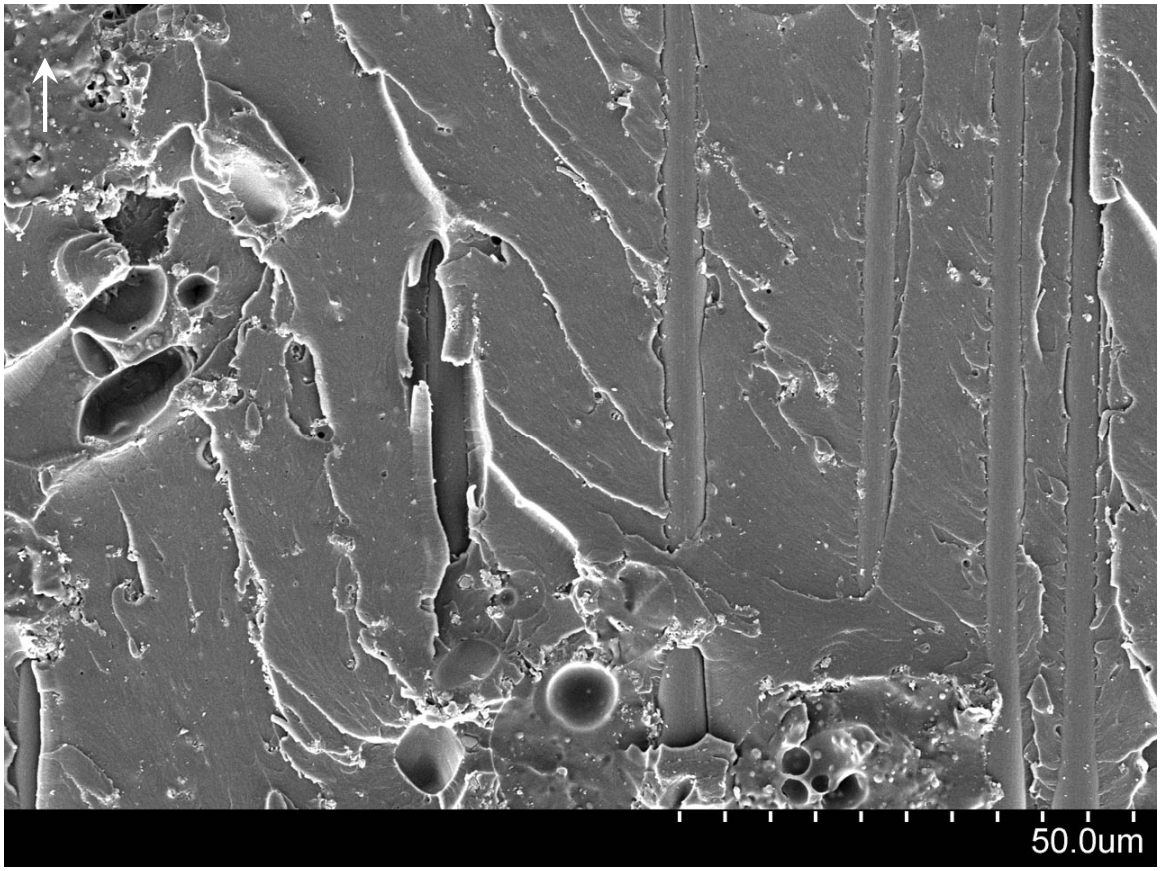

Figure 3.20: View of more voids and river patterns.

Material G (Carbon4 Tape, Epoxy4)

From Figure 3.21, an uneven and rough fracture surface was visible as well as some fiber bridging. Although fiber/resin adhesion was not as apparent as other materials tested, a significant amount of resin plastic deformation was found. Maximum resin deformation was located in the center of adjacent fibers with river patterns flowing up the deformation slopes away from the fibers and in the direction of crack growth. Micro resin flow could be seen at relatively lower magnifications. Because of the lack of fiber/resin adhesion, failure of this laminate was primarily due to the superior toughness of the resin system.

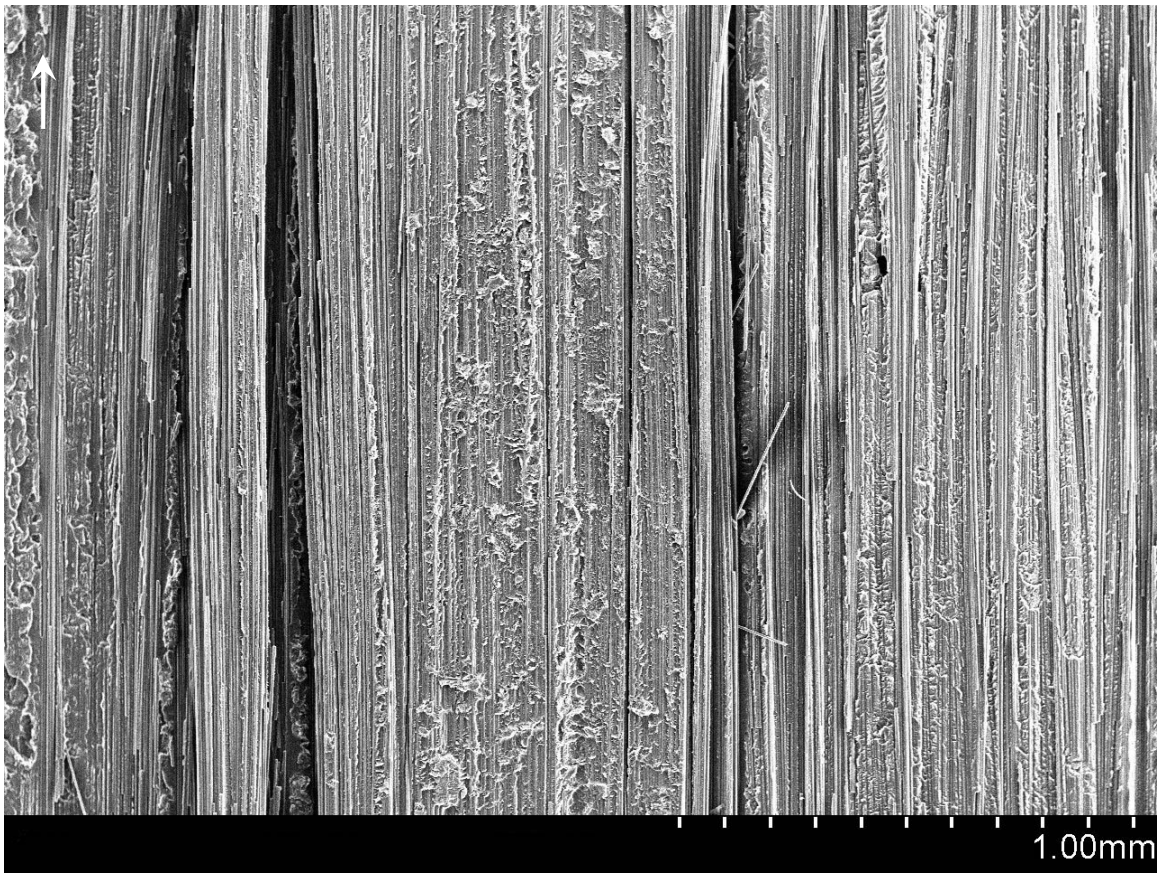

Figure 3.21: Overall view of Material G tested under Mode I loading depicting a rough and uneven fracture surface. Fiber bridging was also found (arrow indicates crack direction).

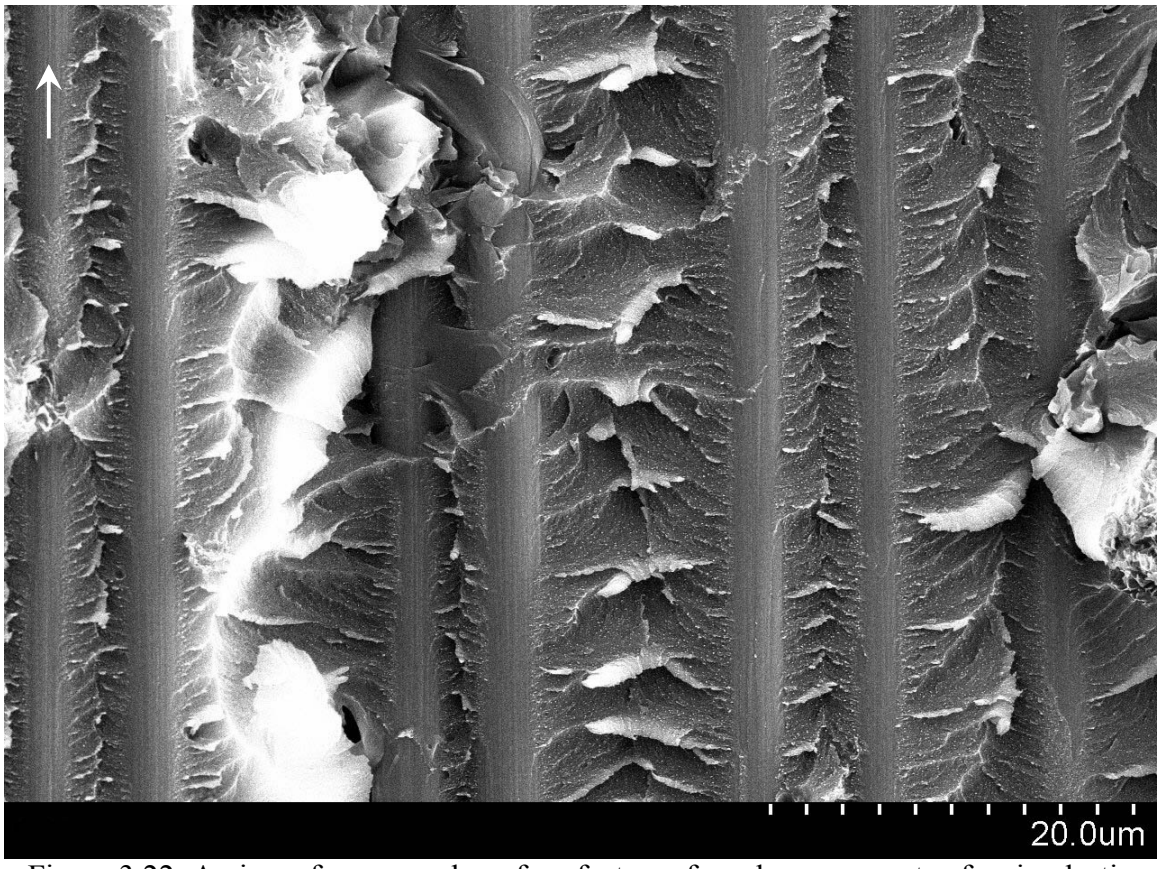

Figure 3.22: A view of very rough surface features from large amounts of resin plastic deformation. Little fiber/resin adhesion was observed.

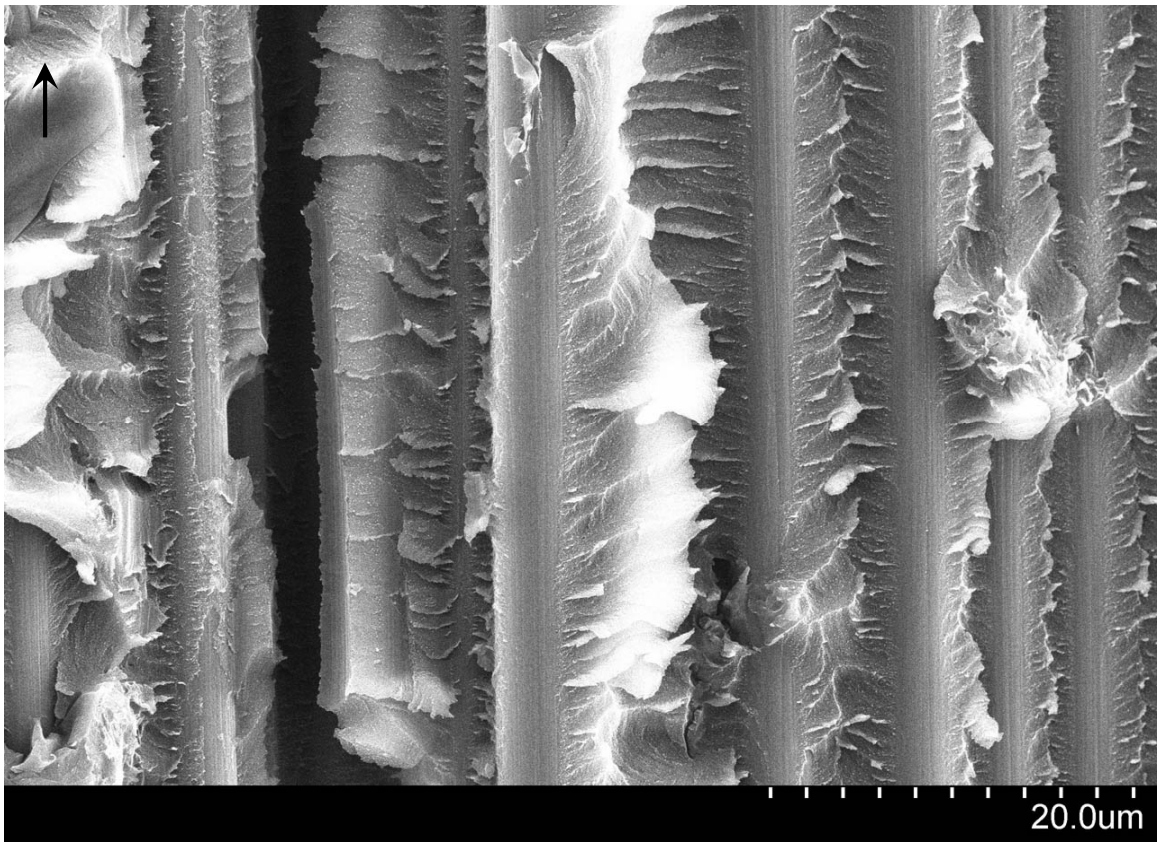

Figure 3.23: Close-up view of an intralaminar crack and river patterns leading up to the area of maximum resin deformation.

Material H (Carbon5 Tape, Epoxy5)

Long resin-rich areas that were parallel with the fiber orientation could be seen through the fracture surface of the test specimens. These stretches of resin-rich areas had little micro resin flow, but still had resin yielding, indicating a relatively high strength resin system. Although weak fiber/resin adhesion was not prevalently found, fiber breakage still occurred. River patterns were visible to aid in crack growth direction. Small voids from volatiles during fabrication were also found.

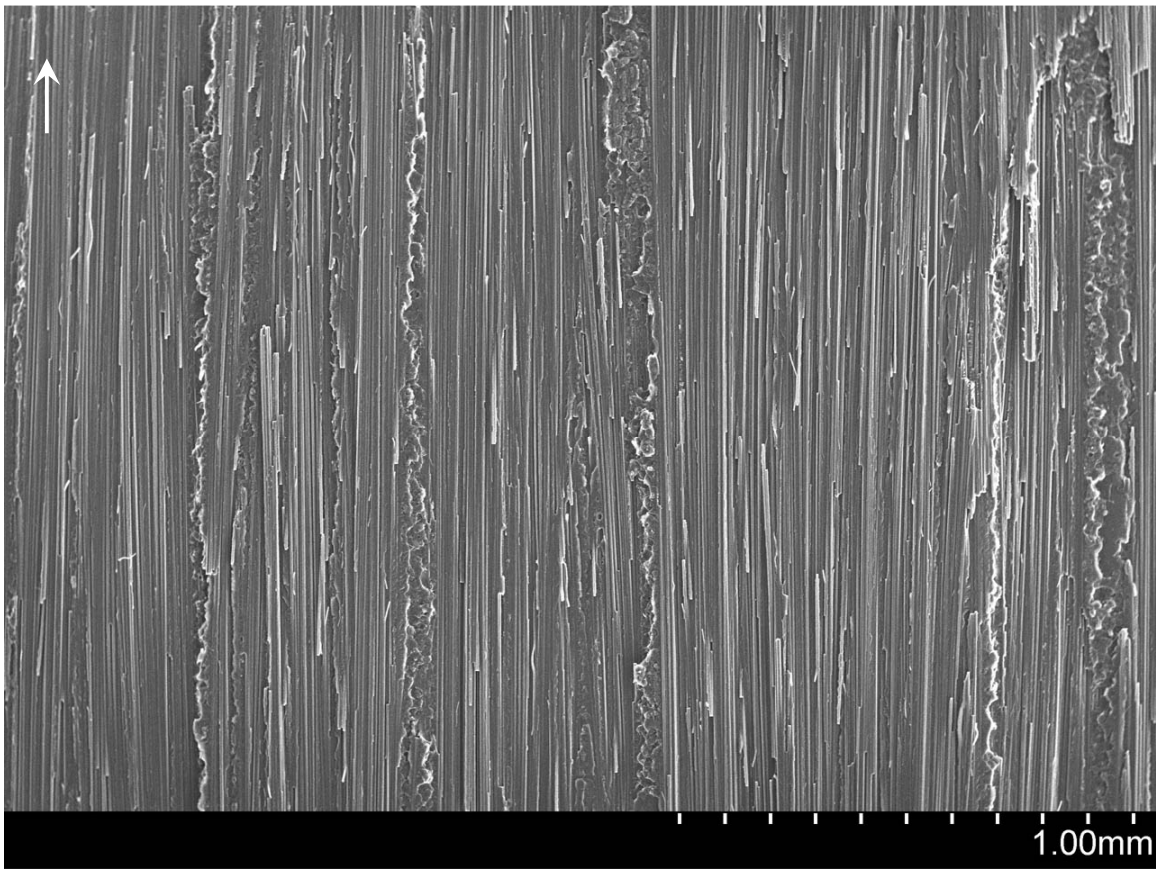

Figure 3.24: Overall view of Material H tested under Mode I loading depicting resin-rich areas parallel with fiber orientation and fiber breakage (arrow indicates crack direction).

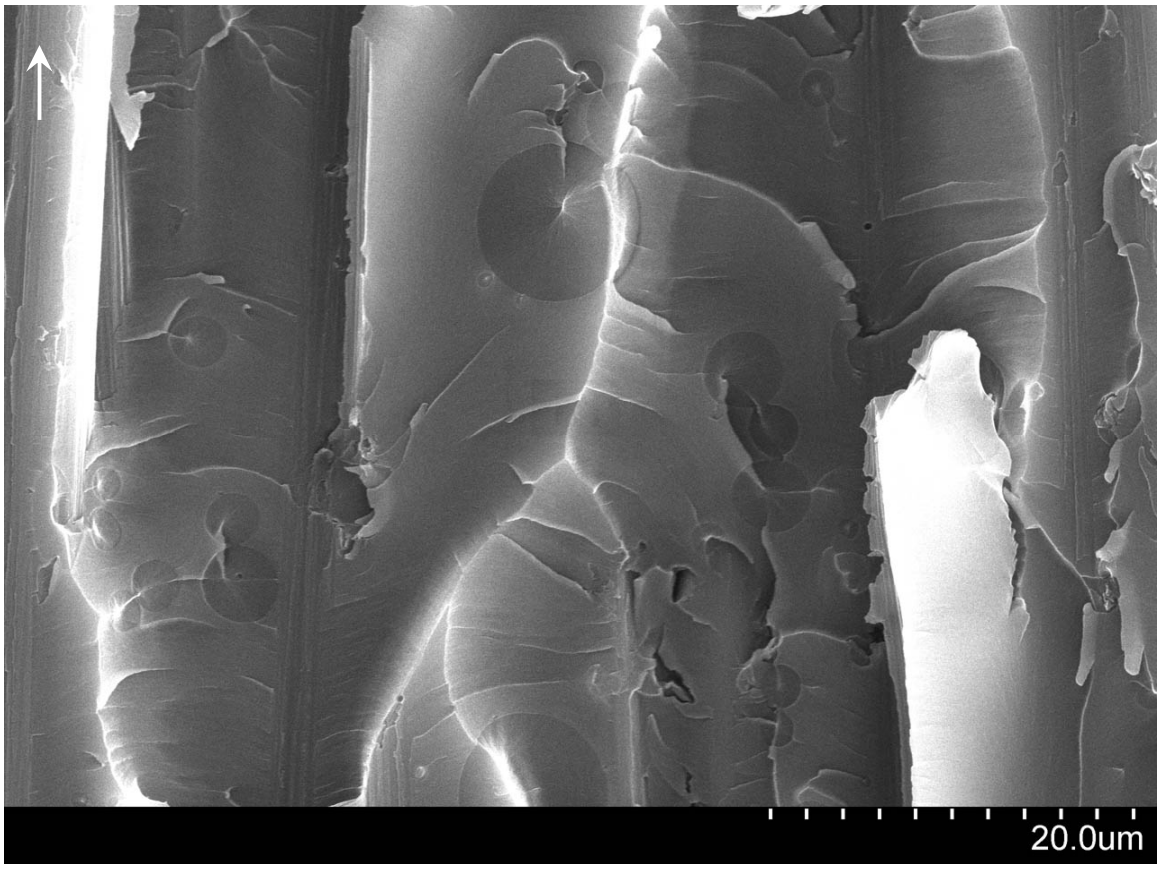

Figure 3.25: Close-up view of a resin-rich area with little micro resin flow features and a few voids from volatiles.

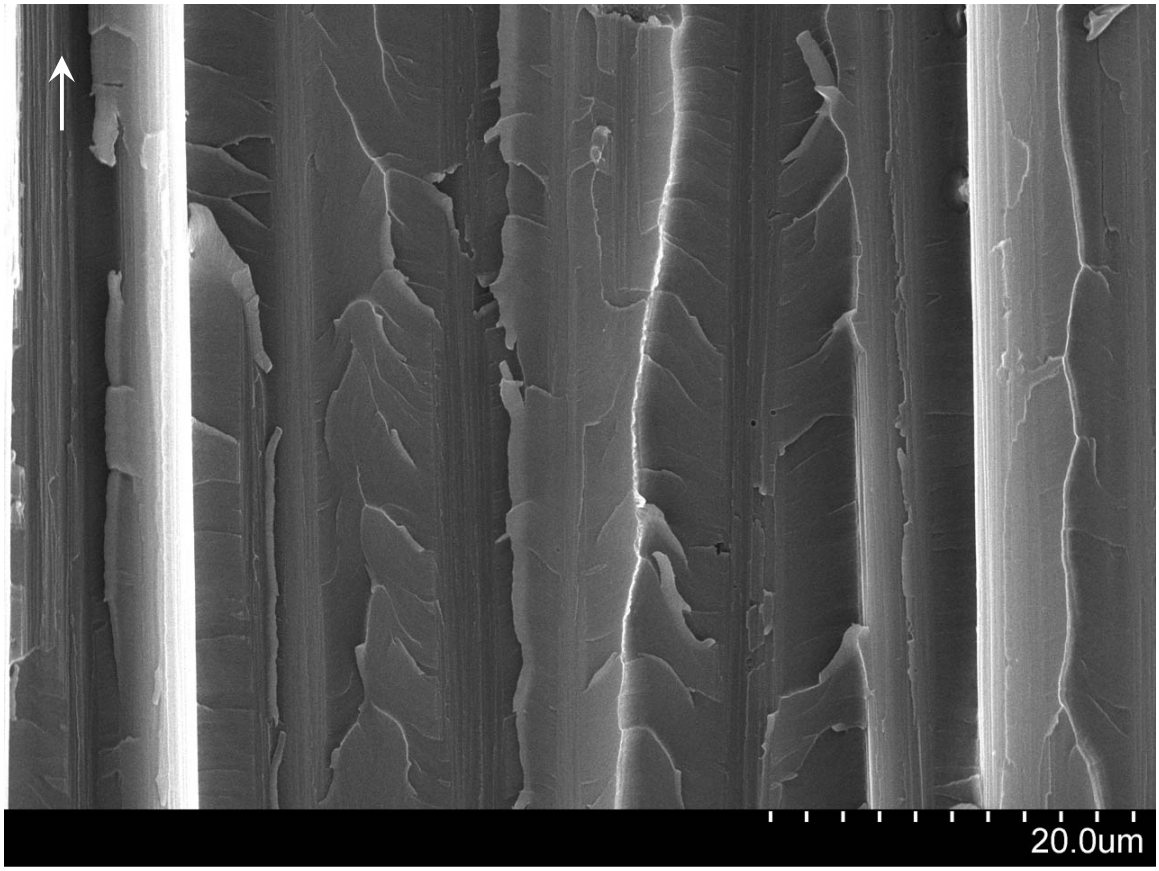

Figure 3.26: River patterns and little fiber/resin interfacial bonding.

Material I (Carbon3 Slit Tape, Epoxy2)

Material I had an uneven fracture surface similar to the other fiberglass slit tape and roving specimens, but the carbon fibers experienced fiber breakage. Resin deformation was somewhat limited to the extent that large amount of plastic yielding was not observed, yet the resin fracture surface was very rough. Majority of the fibers had a sheath of resin, which indicates excellent interfacial bonding and less resin cohesive strength. This evidence and the lack of river patterns and the appearance of small hackle formation could be due to the slit tape form of a high modulus carbon fiber material.

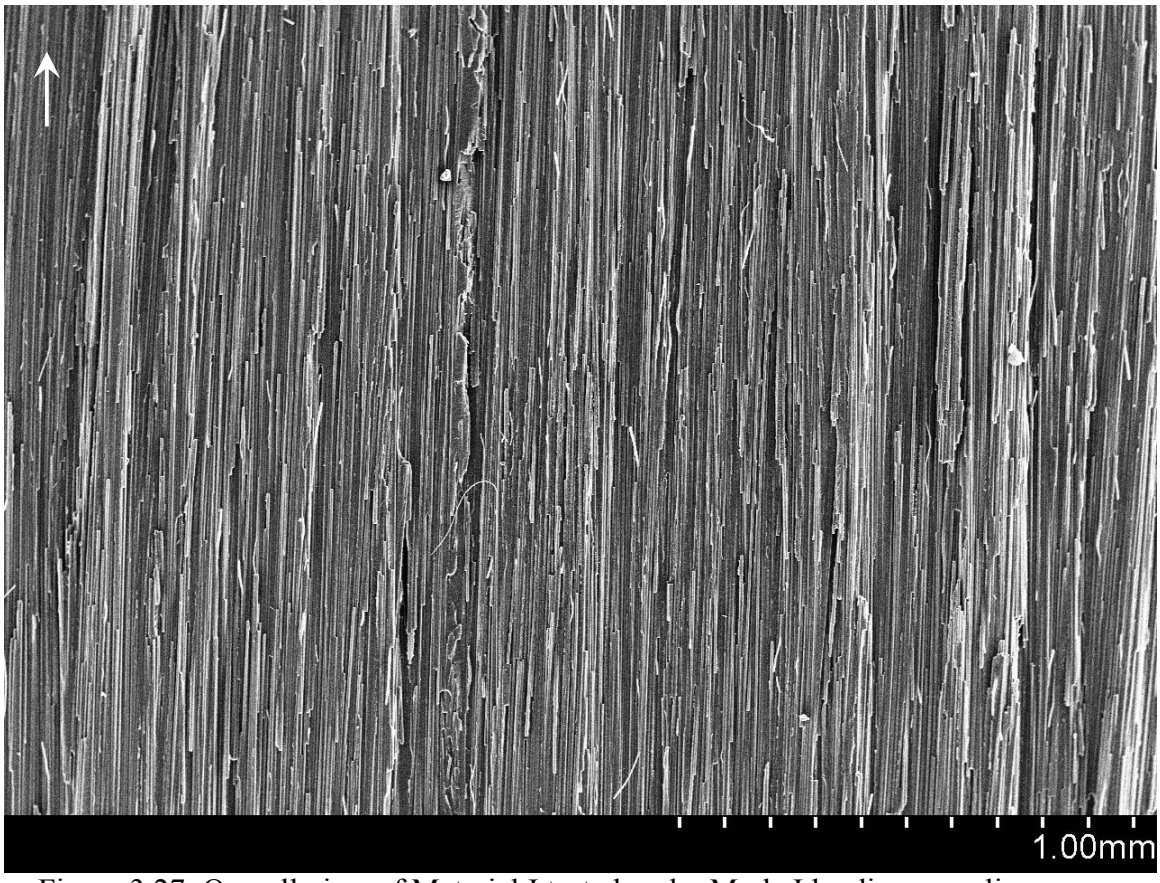

Figure 3.27: Overall view of Material I tested under Mode I loading revealing a very rough uneven surface as well as fiber breakage (arrow indicates crack direction).

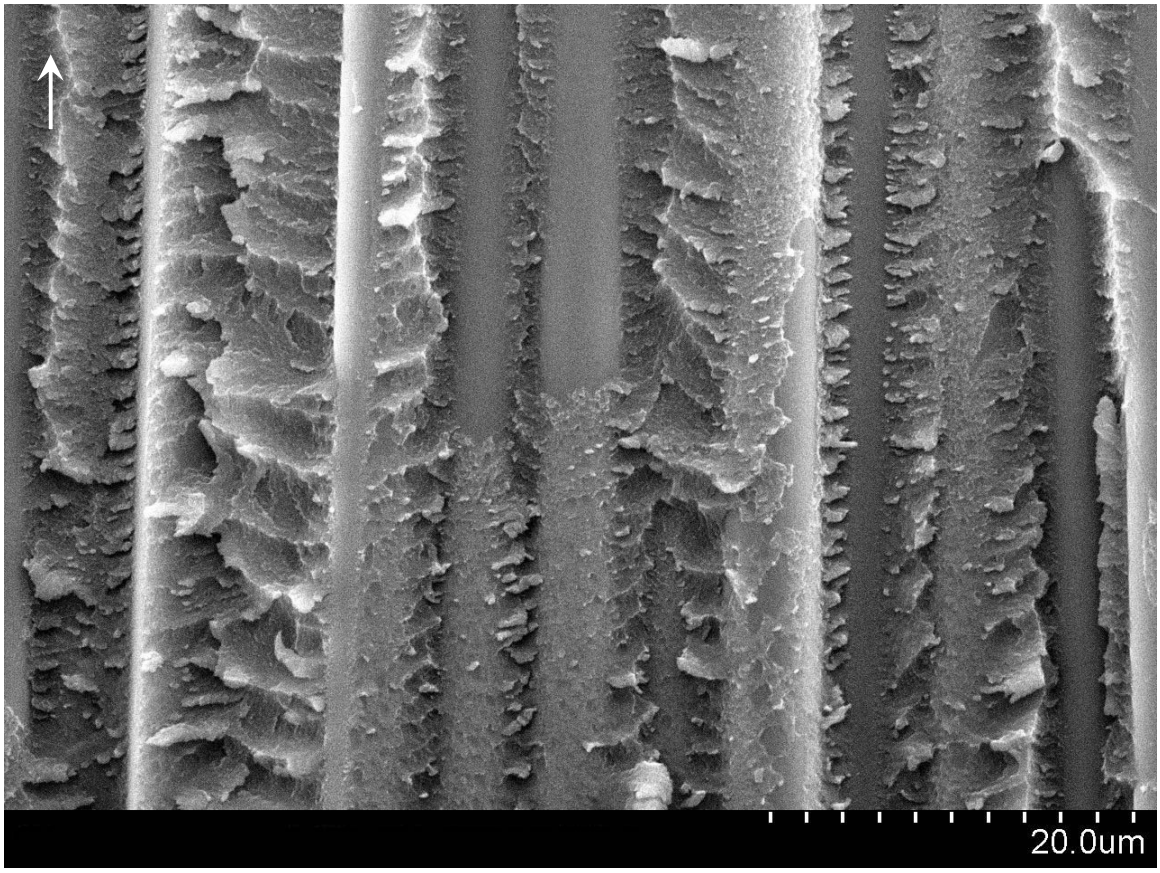

Figure 3.28: A high degree of resin sheathing on the fiber surfaces and some small hackles were noted.

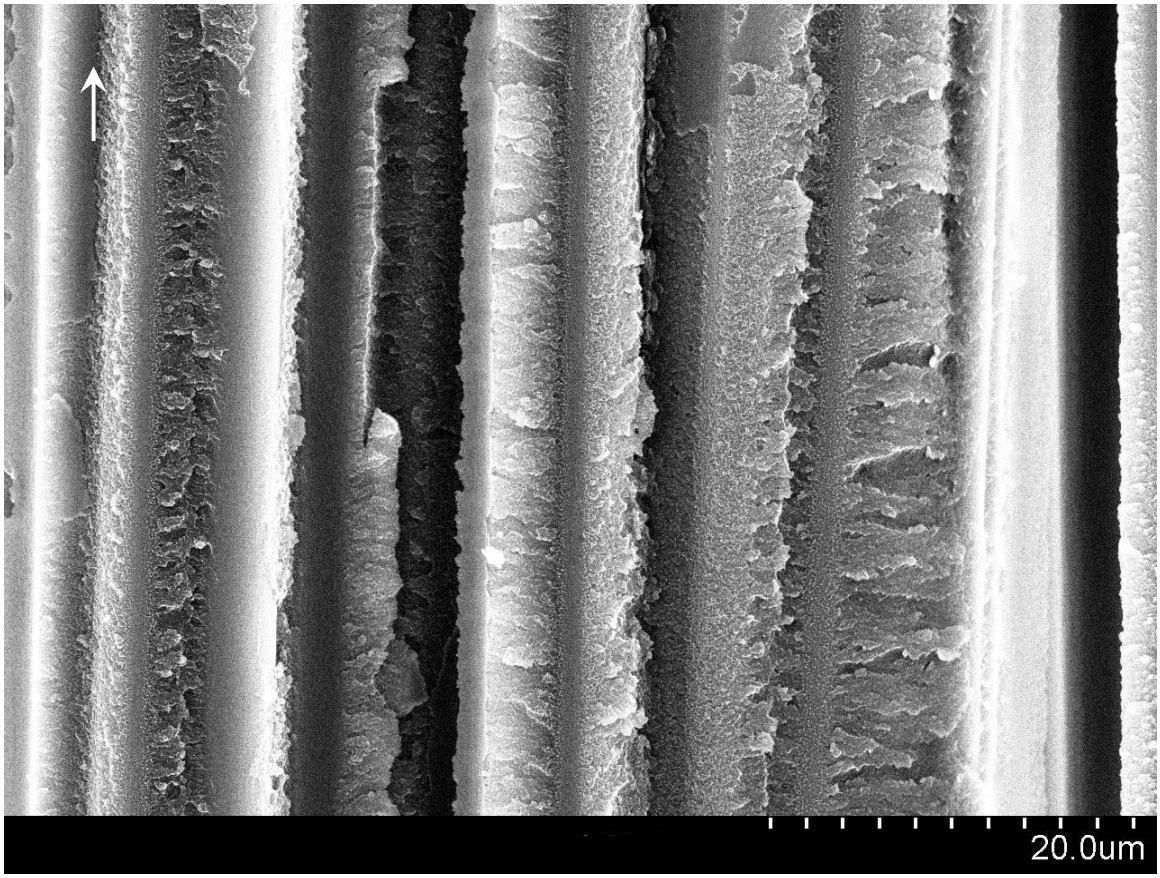

Figure 3.29: Close-up view of an uneven surface with average resin deformation.

3.2.2 Mode II

Ply shear fractures occur within or adjacent to plies that are orientated in the direction of maximum loading. The fracture surface of a brittle tensile sheared specimen has a dull, milky appearance from the light being scattered by resin hackles. These hackles are found in the narrow resin fracture zones between fibers. During in-plane shear loading, the principle tensile stresses are orientated at 45° to the plane of applied shear as shown in Figure 3.30 [11]. These parallel micro-cracks that are inclined away from the direction of applied stress, normal to the maximum tensile stress, grow under increased shear loading, resulting in upright hackles. The separation of hackles can result by either Mechanisms A or B (see Figure 3.31). In Mechanism A, hackle separation occurs such that they are on the side in which the direction of crack propagation coincides with the locally applied shear direction. In Mechanism B, the hackles are on the opposite side of the locally applied shear direction. Thus, the direction of Mode II crack growth cannot be determined as easily as Mode I growth. However, if the fibers are orientated at an angle to the direction of crack growth, triangular asymmetric hackles and scallops form. The tilt of the triangular hackles is mostly parallel to the direction of crack propagation.

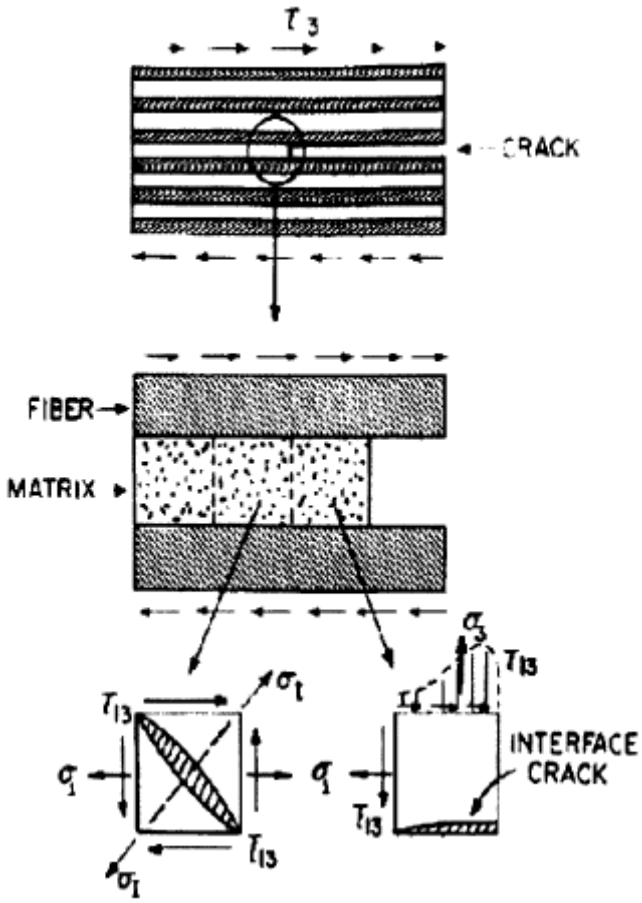

Figure 3.30: Physical model explaining crack formation under mode II loading.

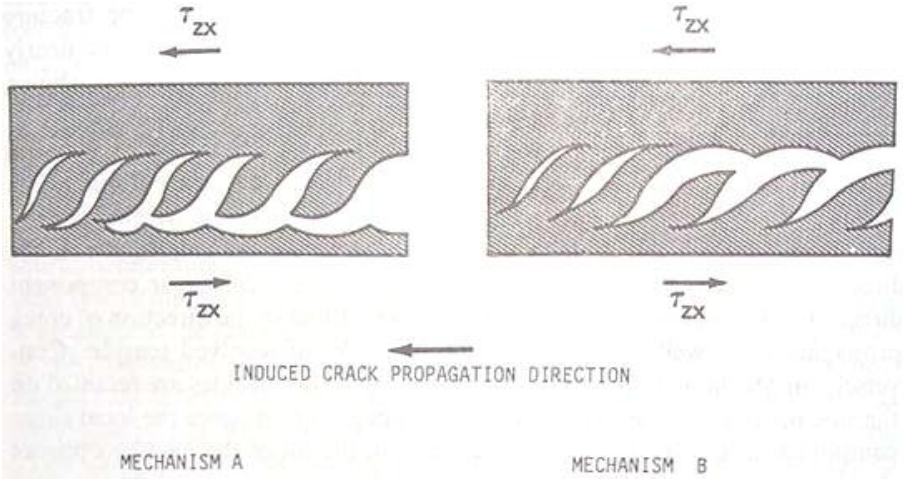

Figure 3.31: Two possible hackle separation mechanisms in Mode II. On side forms plate-like hackles while the opposite side from wave-like scallops.

Material A (Glass Tape, Epoxy1)

The majority of hackle formation was organized, but a portion of the fracture surface had unorganized fracture features that was also characteristic of Mode I loading. The surface was uneven, which increases the surface area and amount of energy for the crack to propagate. Some fibers had resin adhering to the surfaces, but the majority of the fibers did not. Figure 3.34 shows easily visible micro resin flow of the scallops formed opposite of hackles.

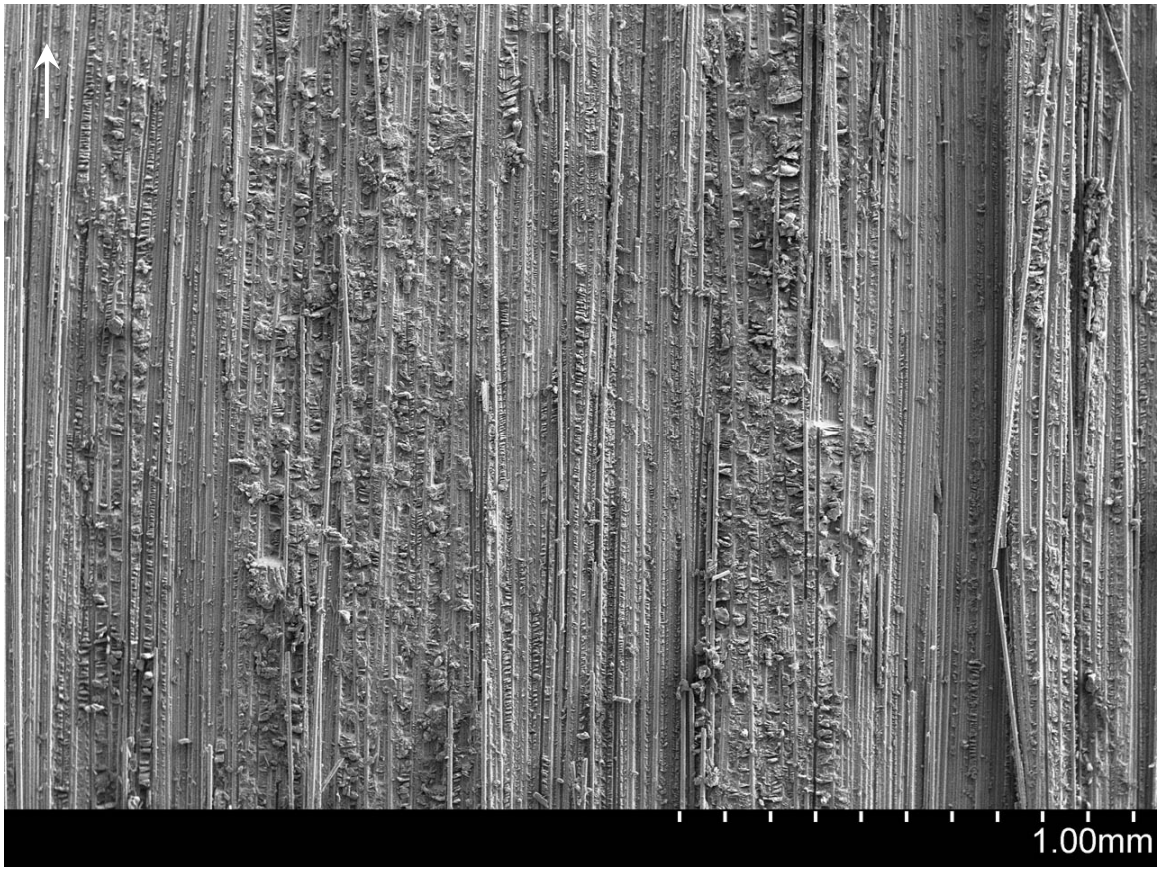

Figure 3.32: Overall view of Material A tested under Mode II loading showing a rough surface typical of pure shear fracture (arrow indicates crack direction).

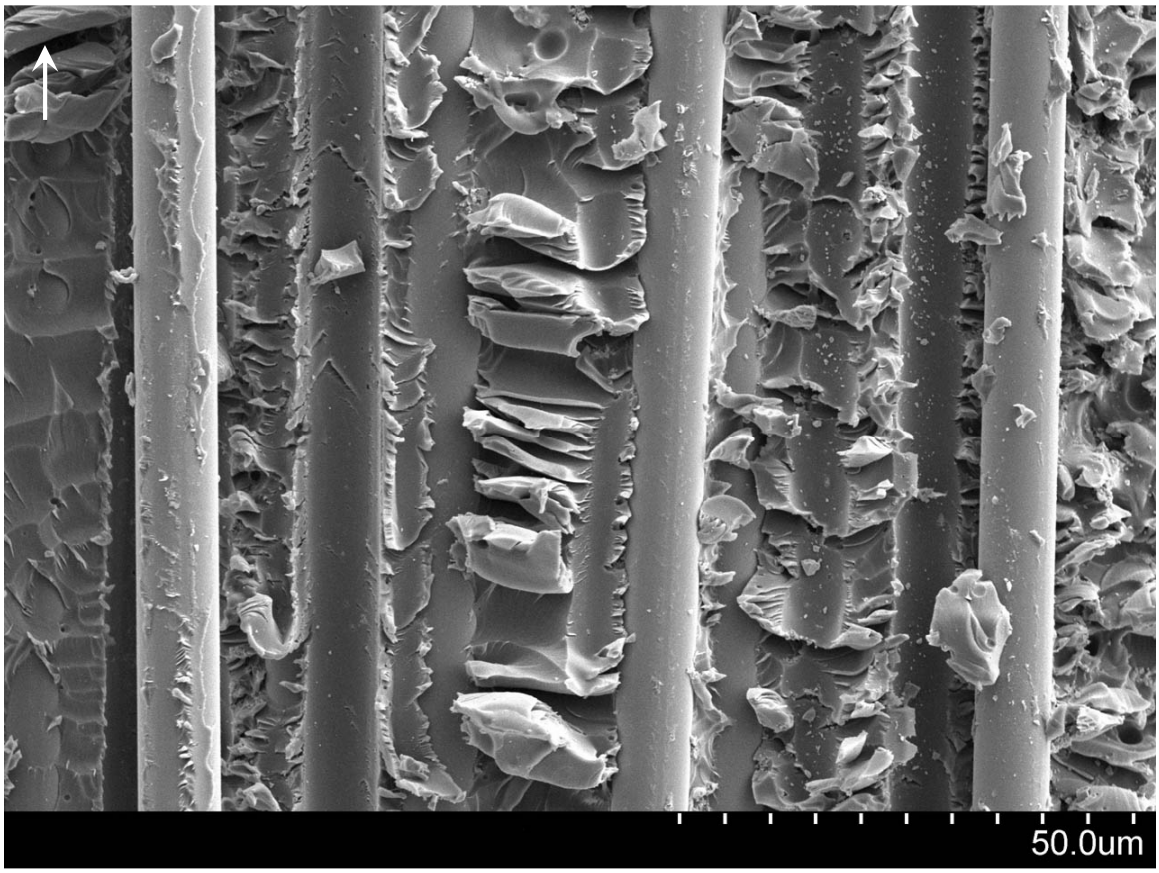

Figure 3.33: Hackle formation with some unorganized features with some resin adhering to the fibers.

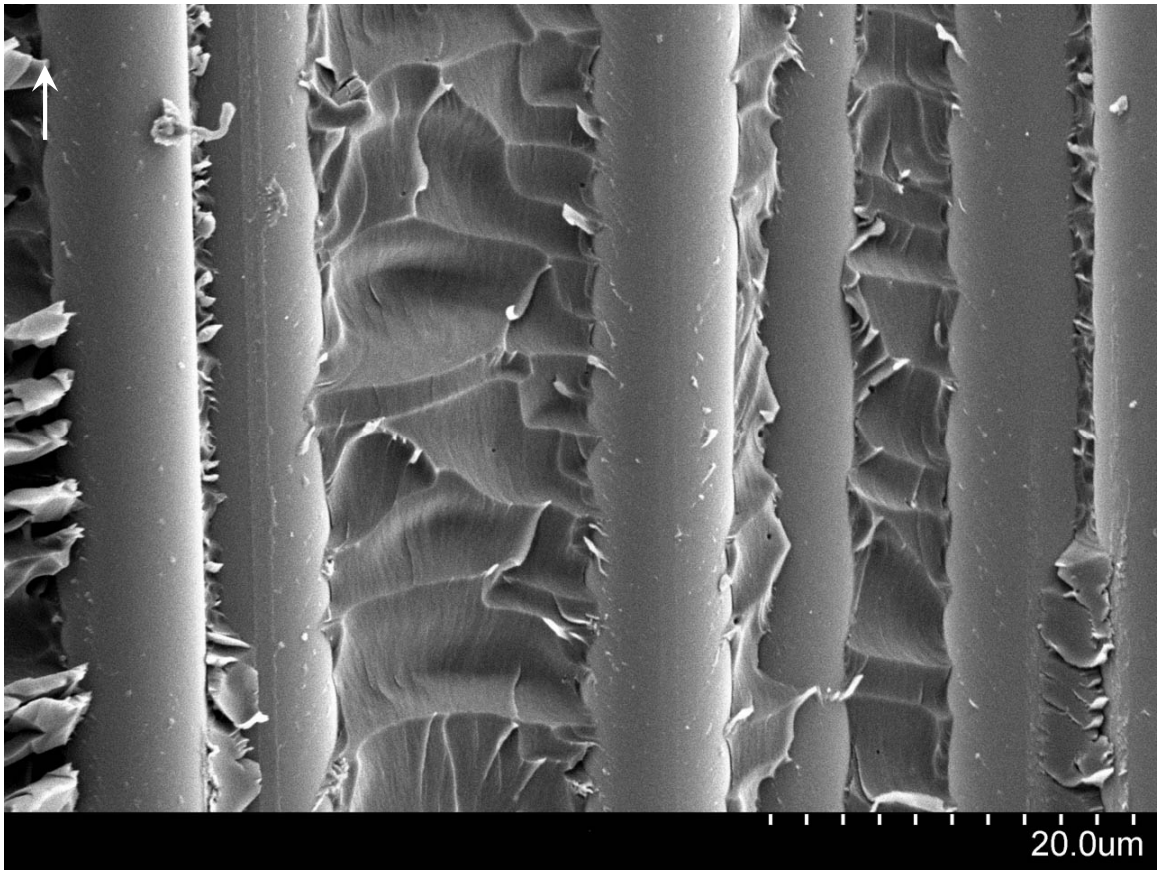

Figure 3.34: Scallop formation with visible micro resin flow and an uneven crack front.

Material B (Glass Roving, Epoxy1)

A small amount of fiber bridging was found on the fracture surface, which is due to the roving fiber form, otherwise the surface was relatively flat at lower magnifications. Just like the Mode I specimens, tiny pores from volatiles during panel fabrication were found in the middle of scallops, which would not be the primary location for microcrack nucleation. Viewing the flat surfaces of hackles would only confirm if the microcrack was initiated from a void, but would be very difficult to observe. Very little resin/fiber adhesion was apparent, but micro resin flow and river patterns on the hackles and scallops could be seen. In some areas, compact microcracks or undeveloped hackles were noted within unorganized fracture features.

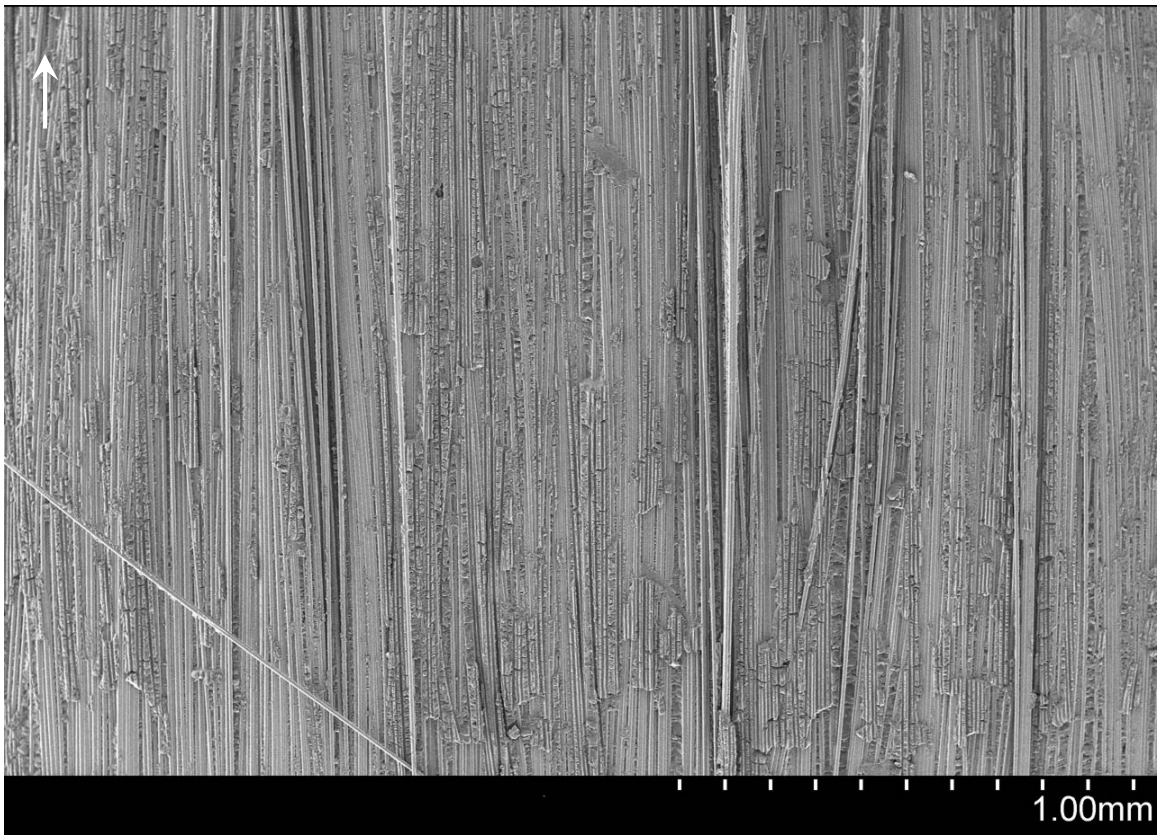

Figure 3.35: Overall view of Material B tested under Mode II loading revealing a small amount of fiber bridging, but a relatively smooth fracture surface (arrow indicates crack direction).

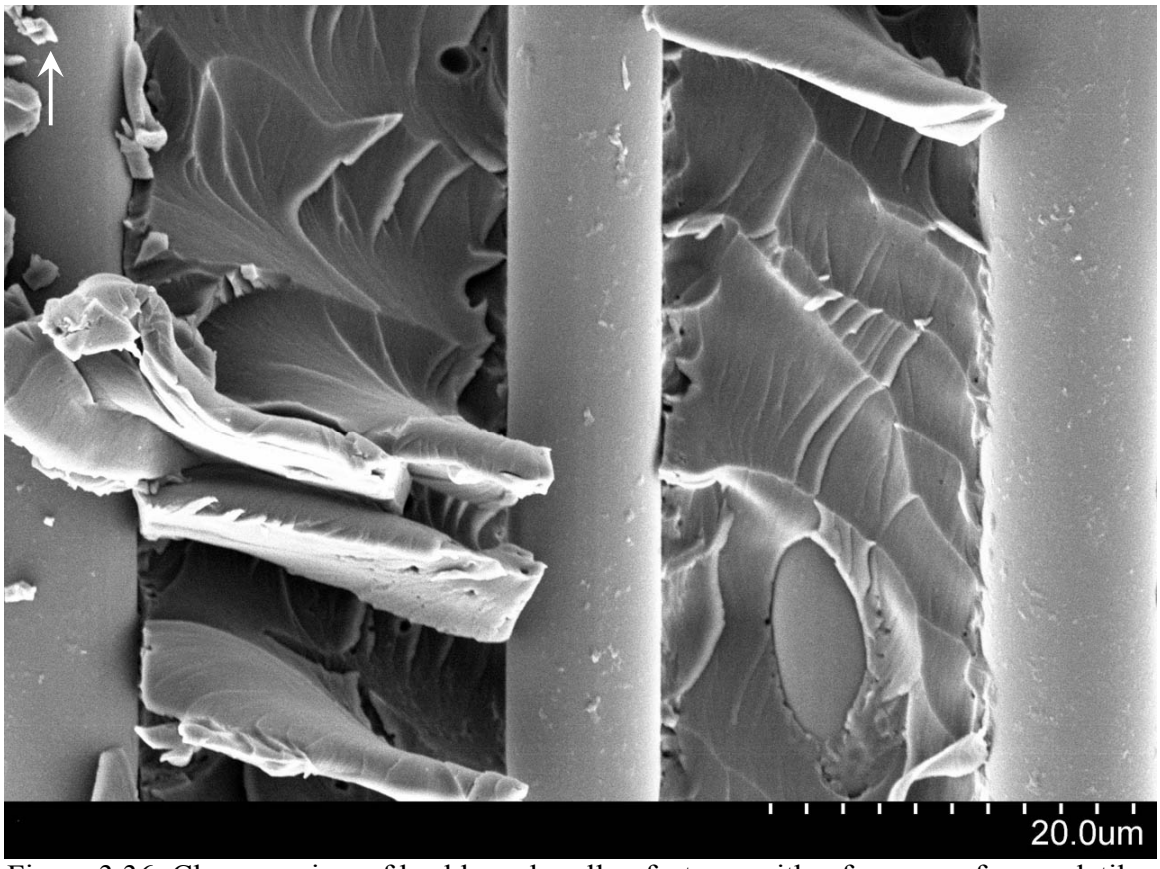

Figure 3.36: Close-up view of hackle and scallop features with a few pores from volatiles during fabrication.

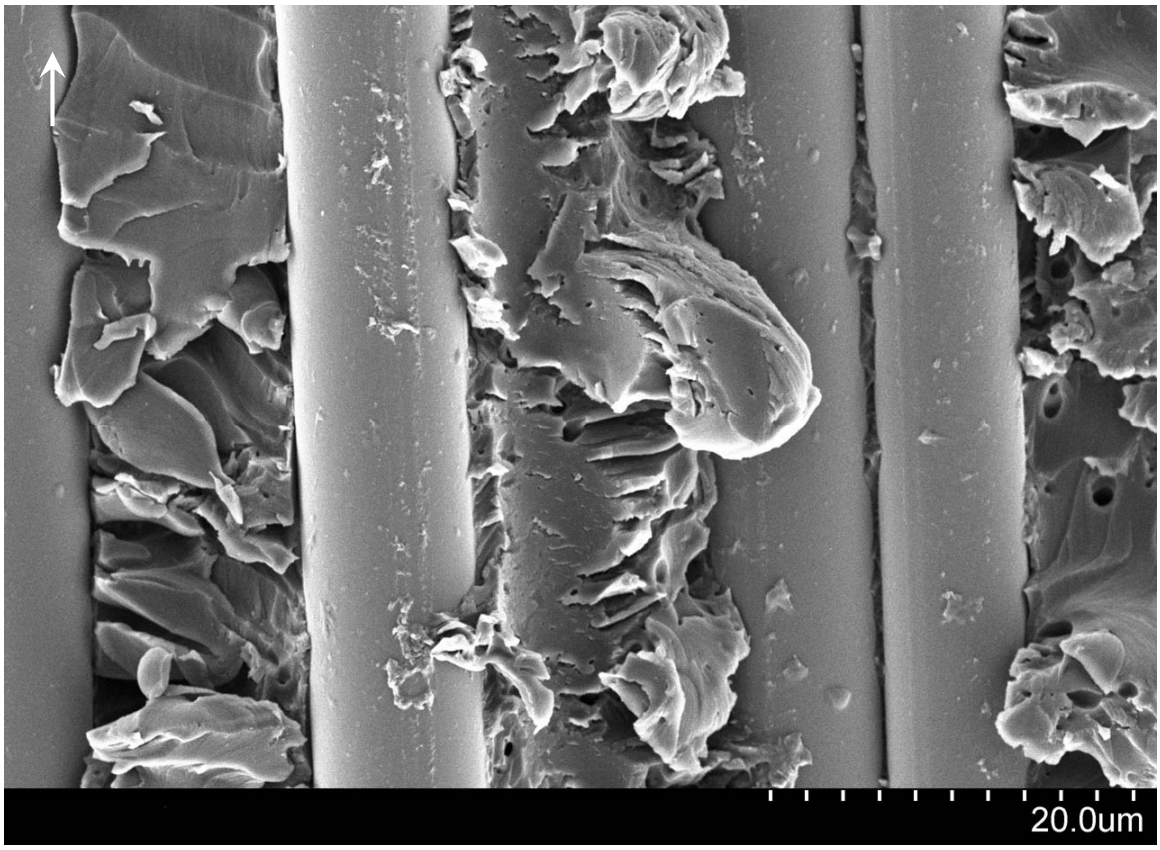

Figure 3.37: Little resin/fiber adhesion was found and very compact resin microcracks or undeveloped hackles in unorganized features were observed.

Material C (Glass Tape, Epoxy2)

Material C had fiber breakage as viewed on the fracture surface. A rough surface aids in the required energy for a crack to propagate, but the best indicator for this resin system was the amount of resin/fiber adhesion. Most of the fibers were covered with a rough resin sheath. Not only were the hackle and scallop surfaces easily visible micro resin flow on the surfaces, but river patterns could also be seen.

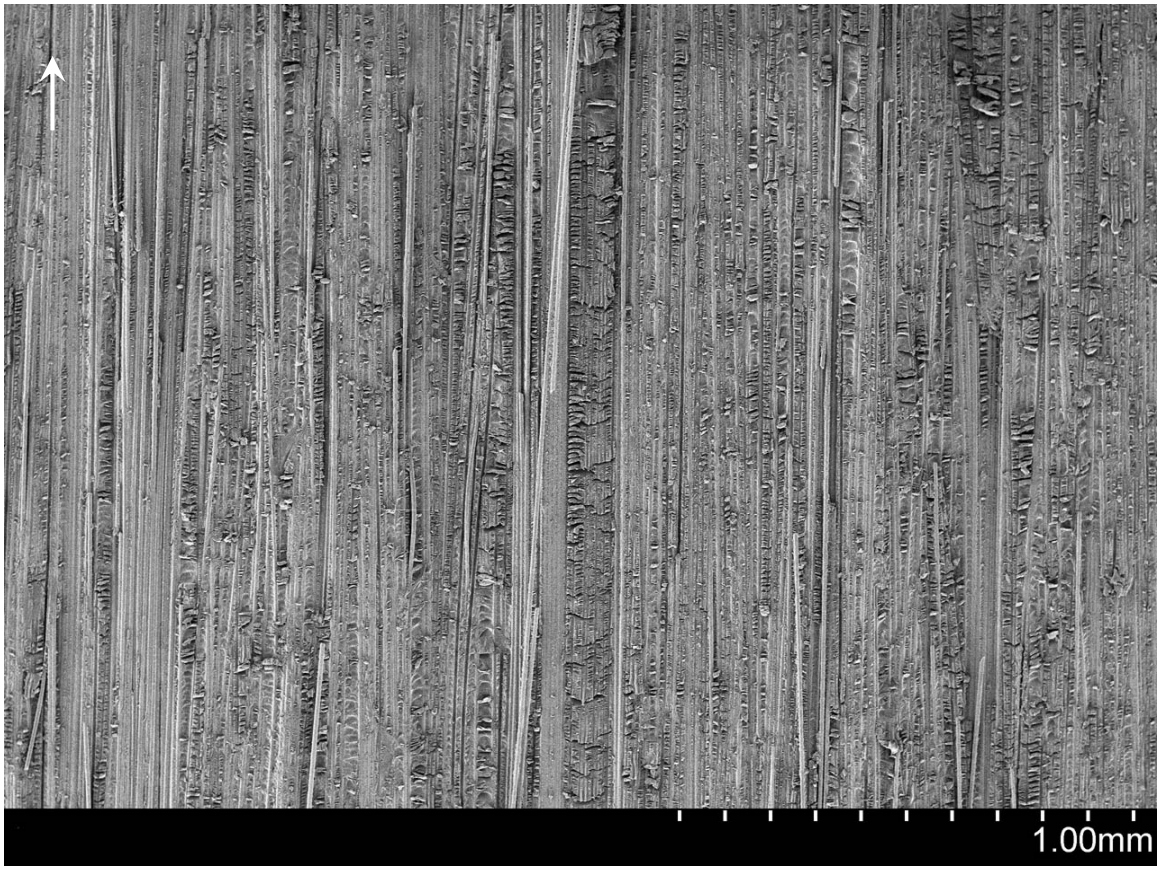

Figure 3.38: Overall view of Material C tested under Mode II loading depicting fiber breakage and a rough surface (arrow indicates crack direction).

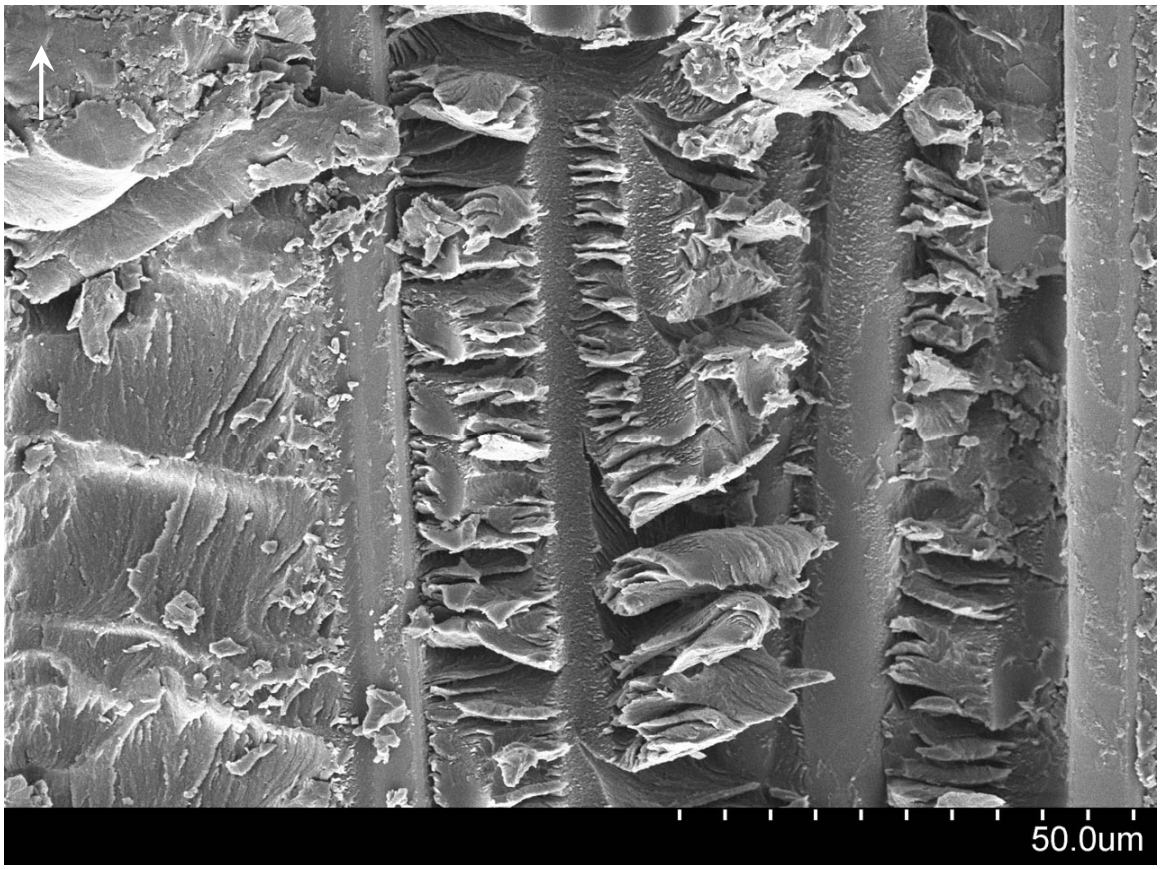

Figure 3.39: Large and small hackles and resin/fiber adhesion were visible.

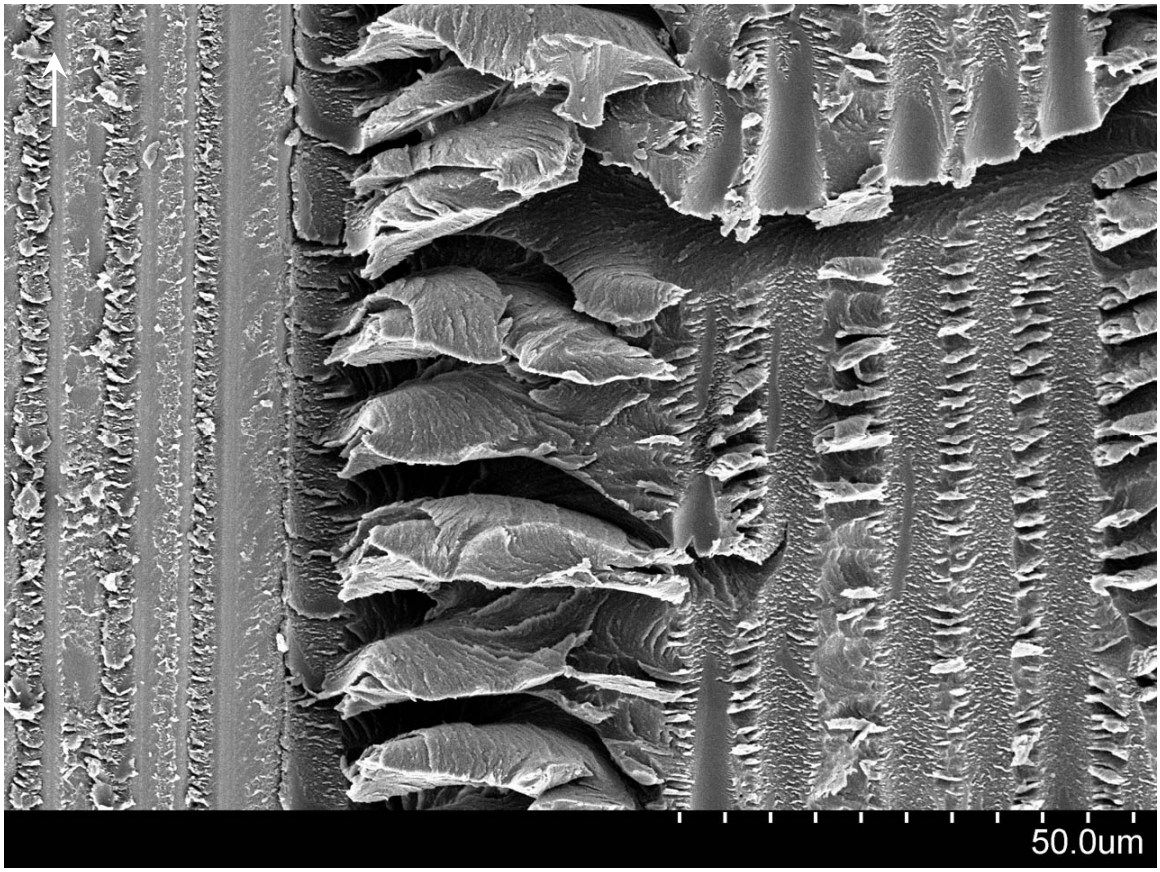

Figure 3.40: More examples of resin/fiber adhesion from the very rough negative fiber impression.

Material D (Glass Roving, Epoxy2)

The fracture surface was slightly more uneven than what was visible for Material C with the same resin system, but of different fiber forms. The fracture surface was also rough with similar hackle and scallop formations. On the hackles and scallops, micro resin flow could be easily seen with river patterns also present on the small surfaces. The resin/fiber adhesion covered nearly the entire fiber surface.

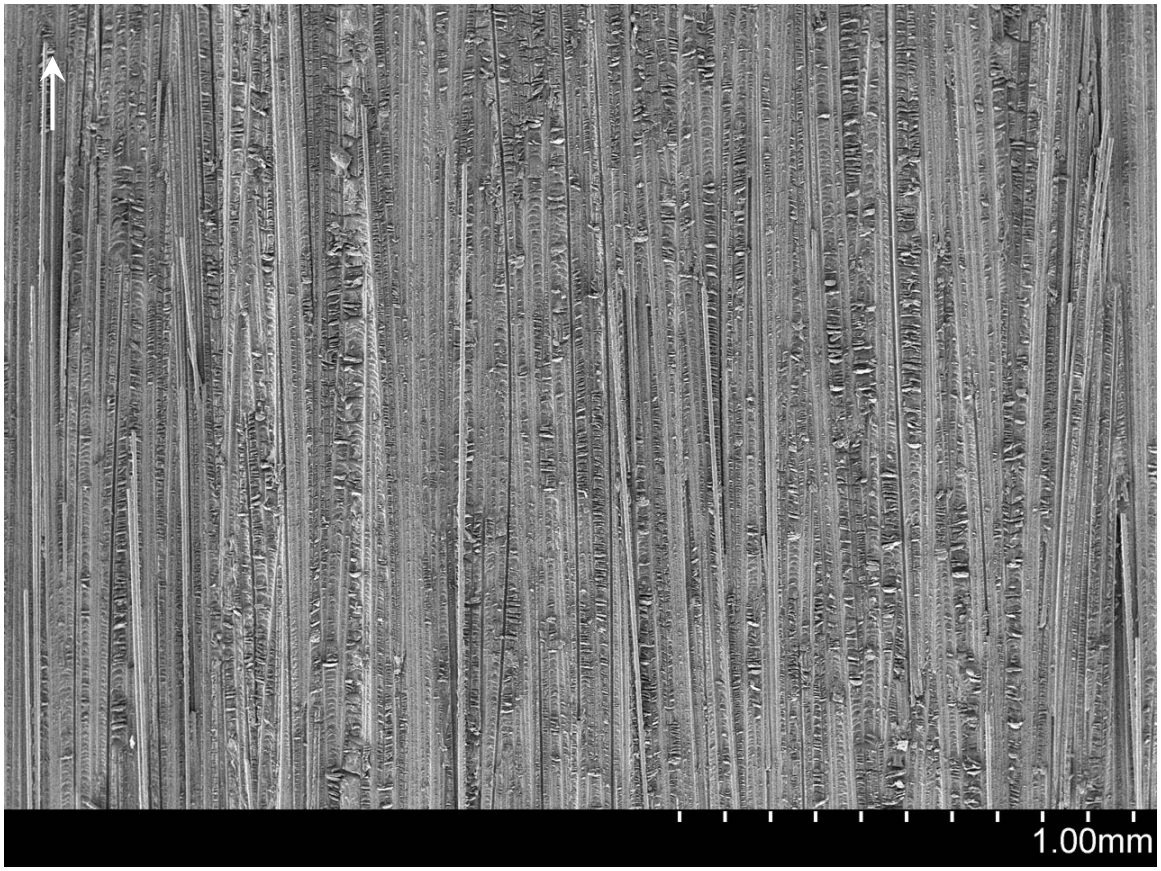

Figure 3.41: Overall view of Material D tested under Mode II loading showing fiber breakage with a few areas of grouped fibers debonding (arrow indicates crack direction).

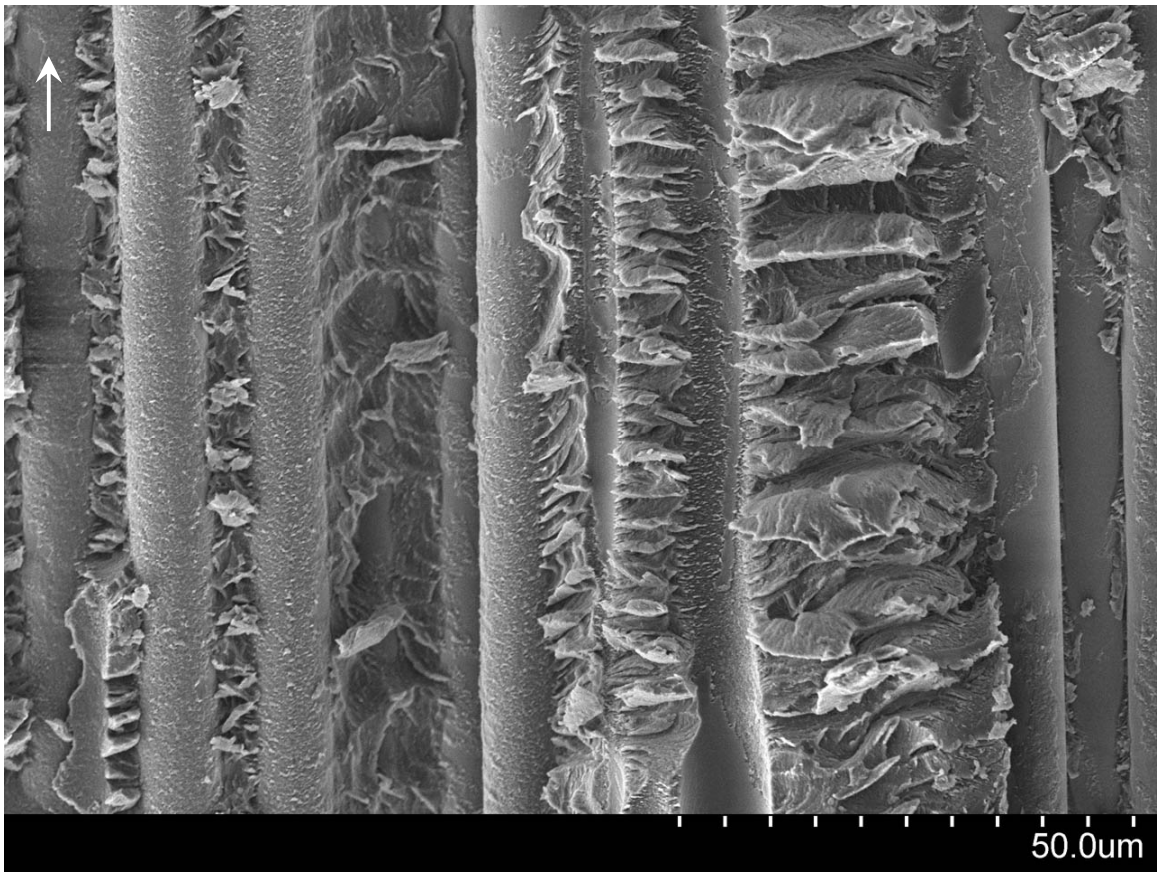

Figure 3.42: An uneven surface and a rough resin sheath were both observed.

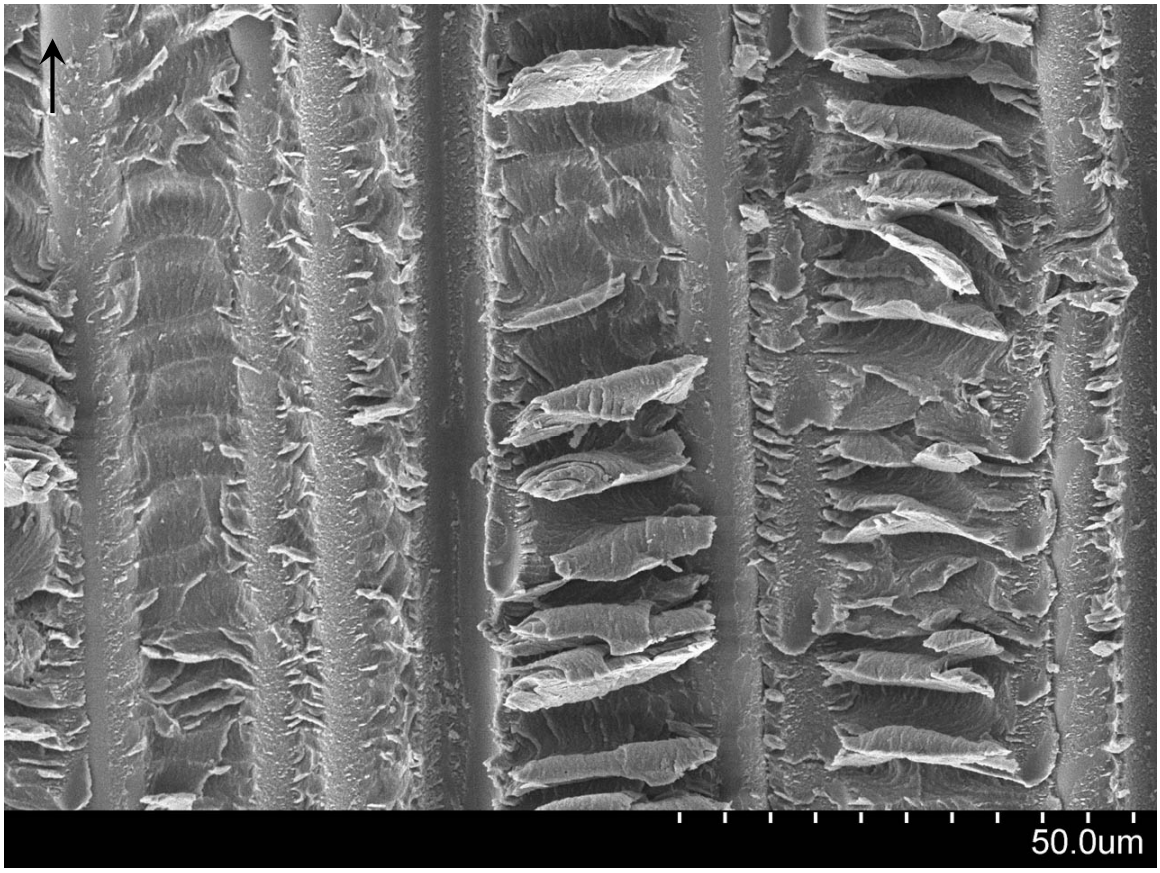

Figure 3.43: Hackle and scallop formations.

Material E (Carbon1, Epoxy3)

A rough fracture surface of Material E specimens was noted, but was not as rough as other laminate fractures. Besides the formation of hackles and scallops, other fracture features did not seem to contribute to a tough resin system. Micro resin flow was only visible at high magnifications. Resin/fiber adhesion was observed as minimum fiber coverage.

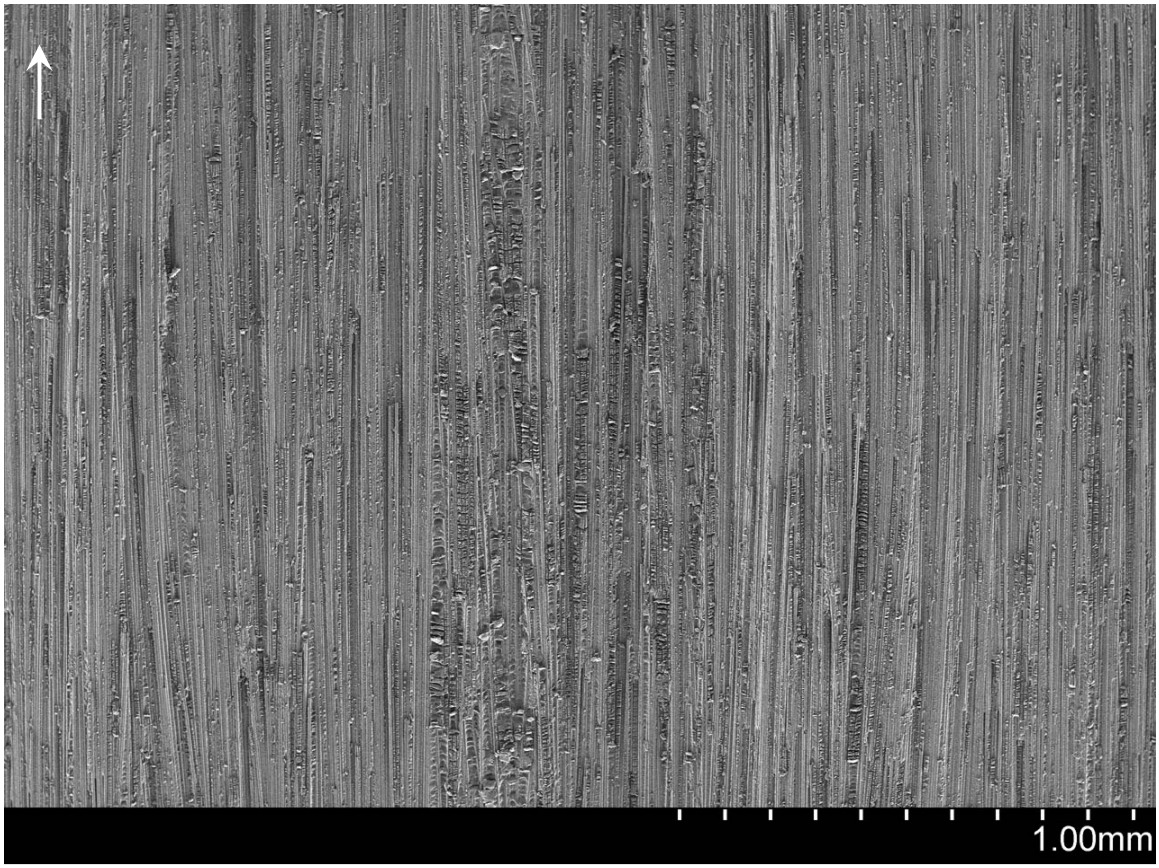

Figure 3.44: Overall view of Material E tested under Mode II loading (arrow indicates crack direction).

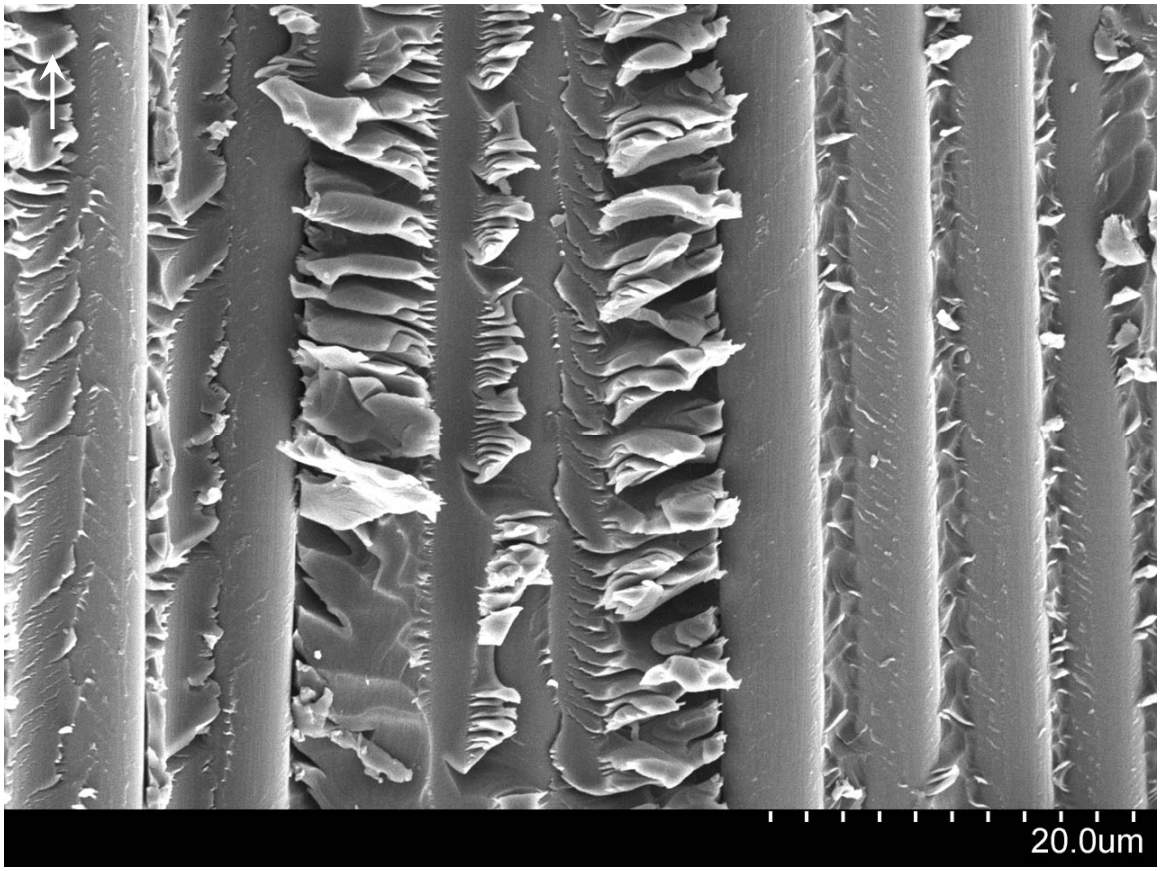

Figure 3.45: Relatively little resin/fiber adhesion was found.

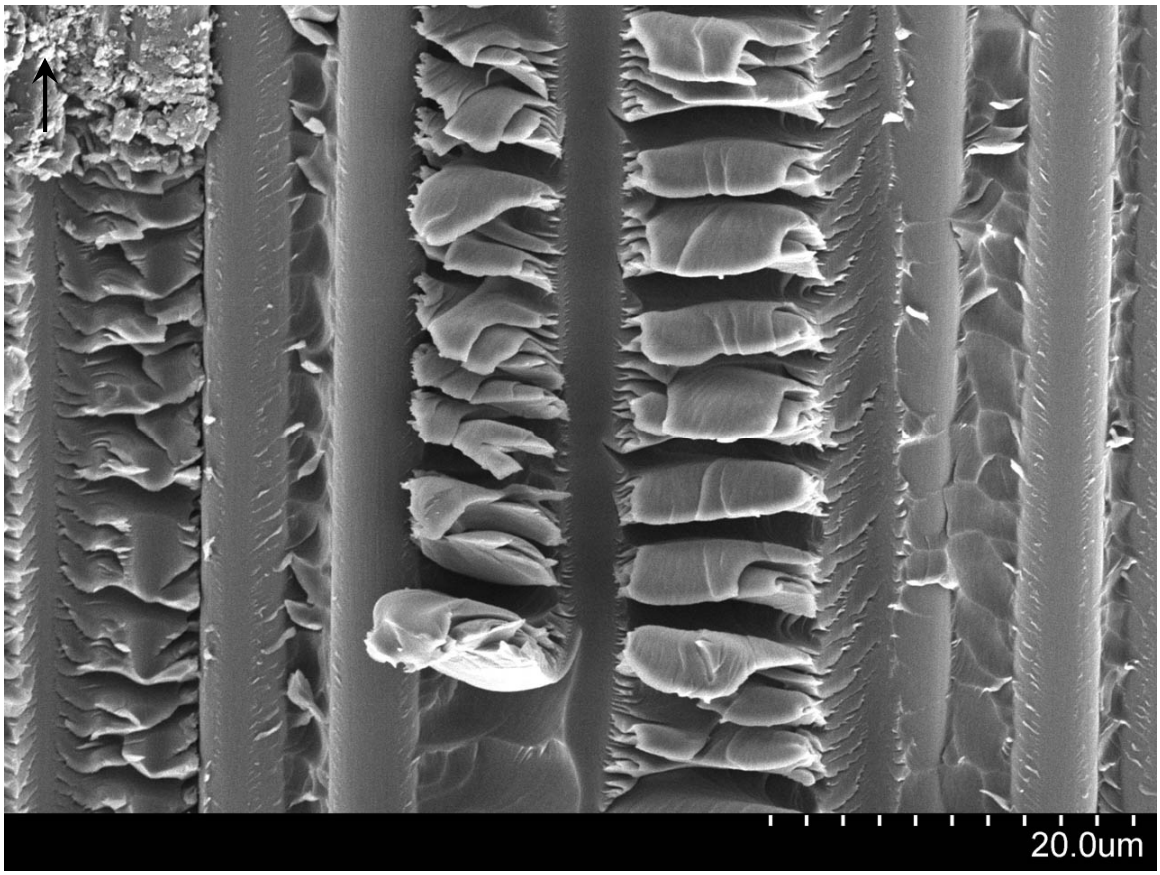

Figure 3.46: Micro resin flow could only be seen at high magnifications.

Material F (Carbon2 Tape, Epoxy1)

Overall, the fracture surface did not appear to have a particularly rough surface or much unevenness to aid in a tougher laminate. Microcracks were observed within hackles. Compact microcracks would absorb energy and increase toughness. Micro resin flow was observed just as in the fiberglass laminates, but to a slightly less extent. No resin/fiber adhesion could be found.

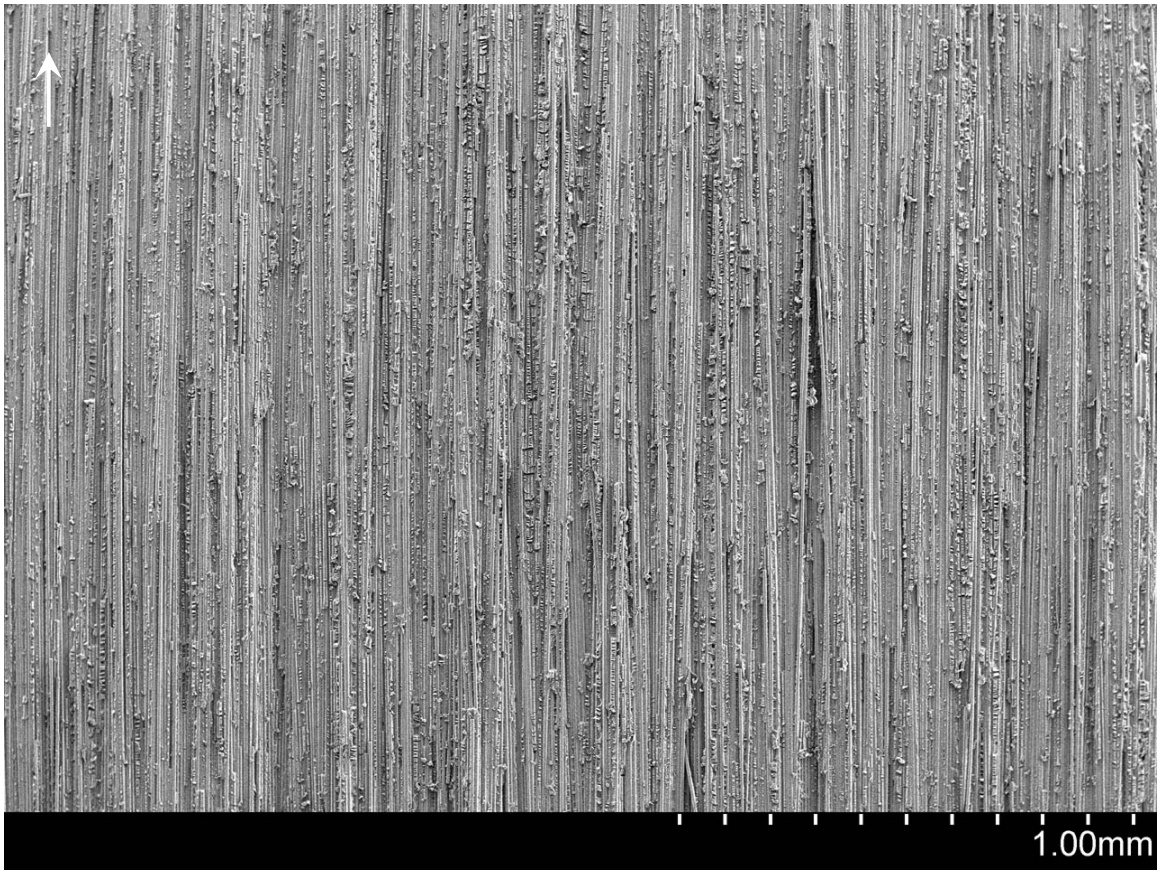

Figure 3.47: Overall view of Material F tested under Mode II loading (arrow indicates crack direction).

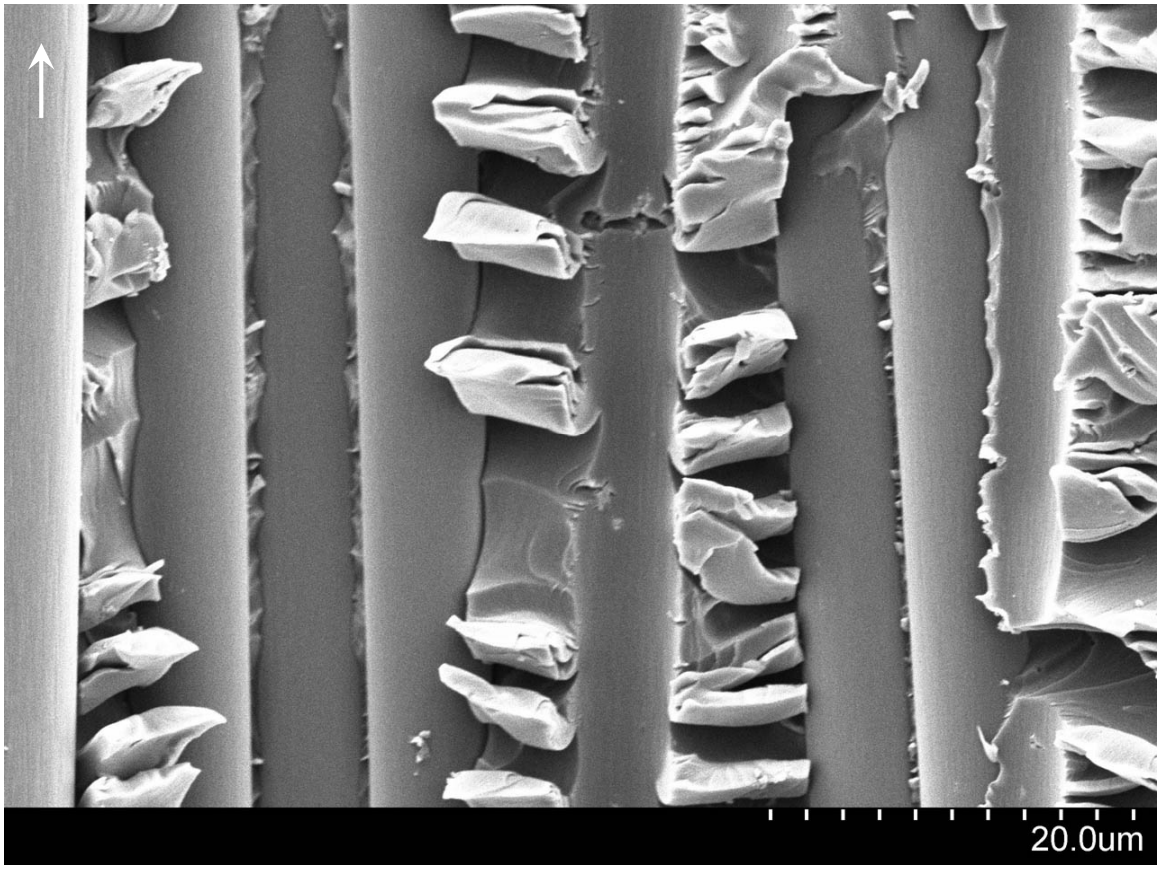

Figure 3.48: Microcracks were visible within hackles and no resin/fiber adhesion could be found.

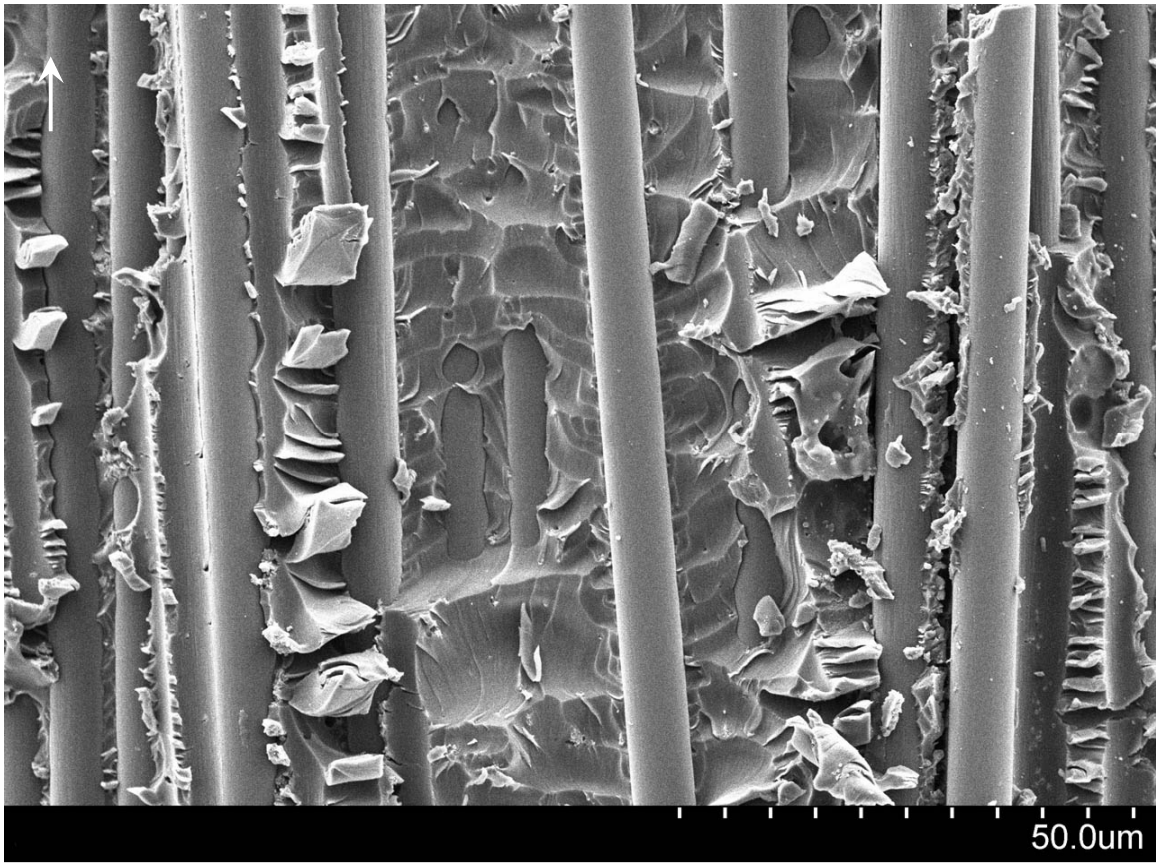

Figure 3.49: An area of unevenness and micro resin flow on scallops.

Material G (Carbon4 Tape, Epoxy4)

Material G had a resin system that was very unique in several aspects compared to other systems studied. The fracture surface had an extremely rough surface with resin-rich areas subjected to shear deformation. Upon closer examination, the surface was uneven with large resin platelets that somewhat resembled hackles, but were the length of one to several fiber diameters. Some hackles were found between fibers that had a crest in the middle with a hackle resemblance on both sides. River patterns could also be seen as well as tensile resin failure. The fibers had length-wise scores on the surface, which increased the surface area for resin adhesion that was found in some areas.

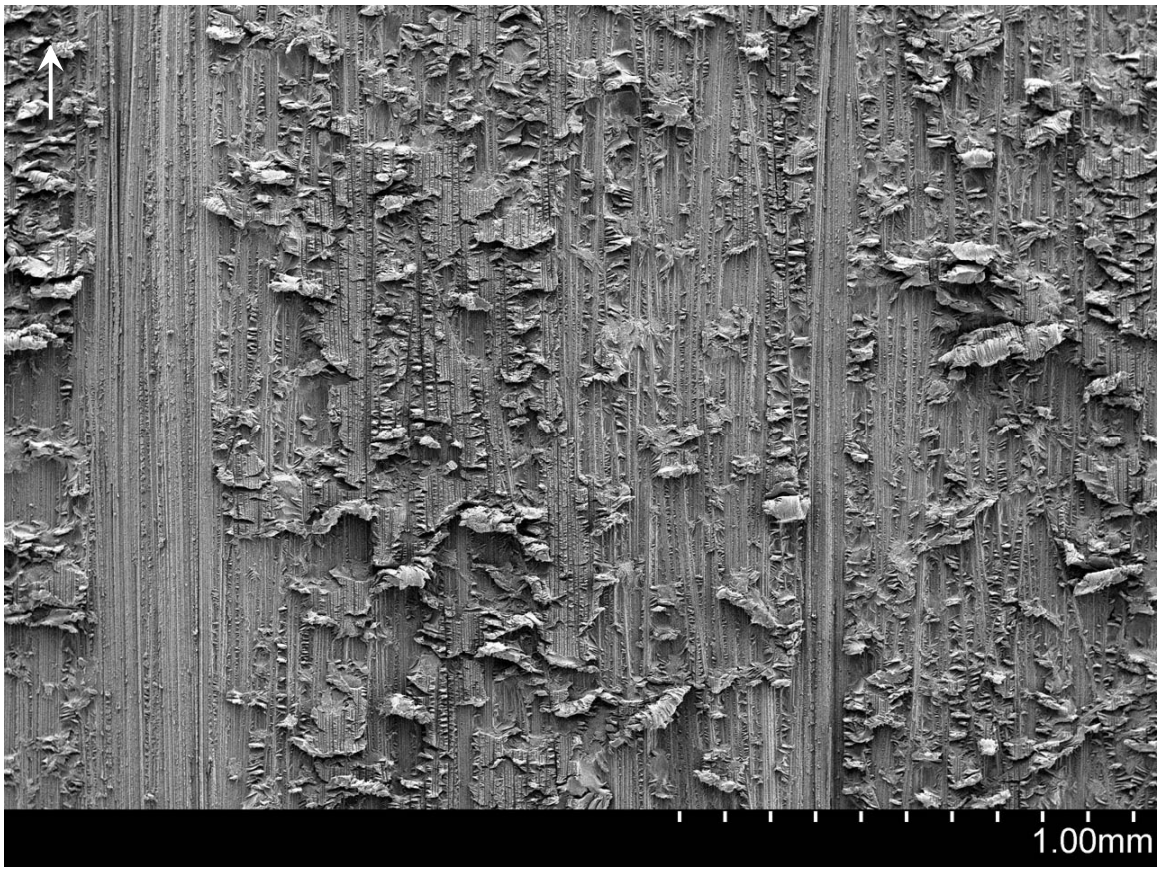

Figure 3.50: Overall view of Material G tested under Mode II loading revealing an extremely rough surface with large resin patches (arrow indicates crack direction).

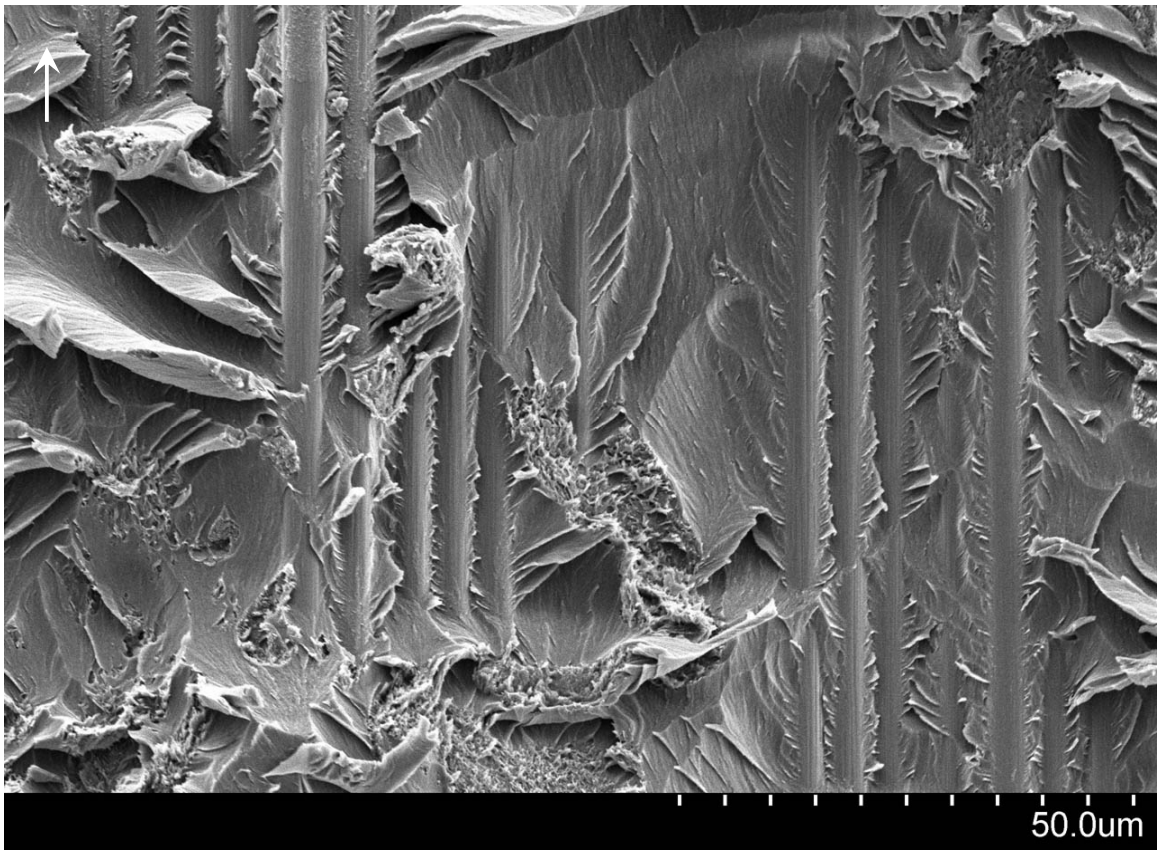

Figure 3.51: Large resin platelets, river patterns, easily visible micro resin flow, tensile resin failure, and an uneven surface were all found on the fracture surface.

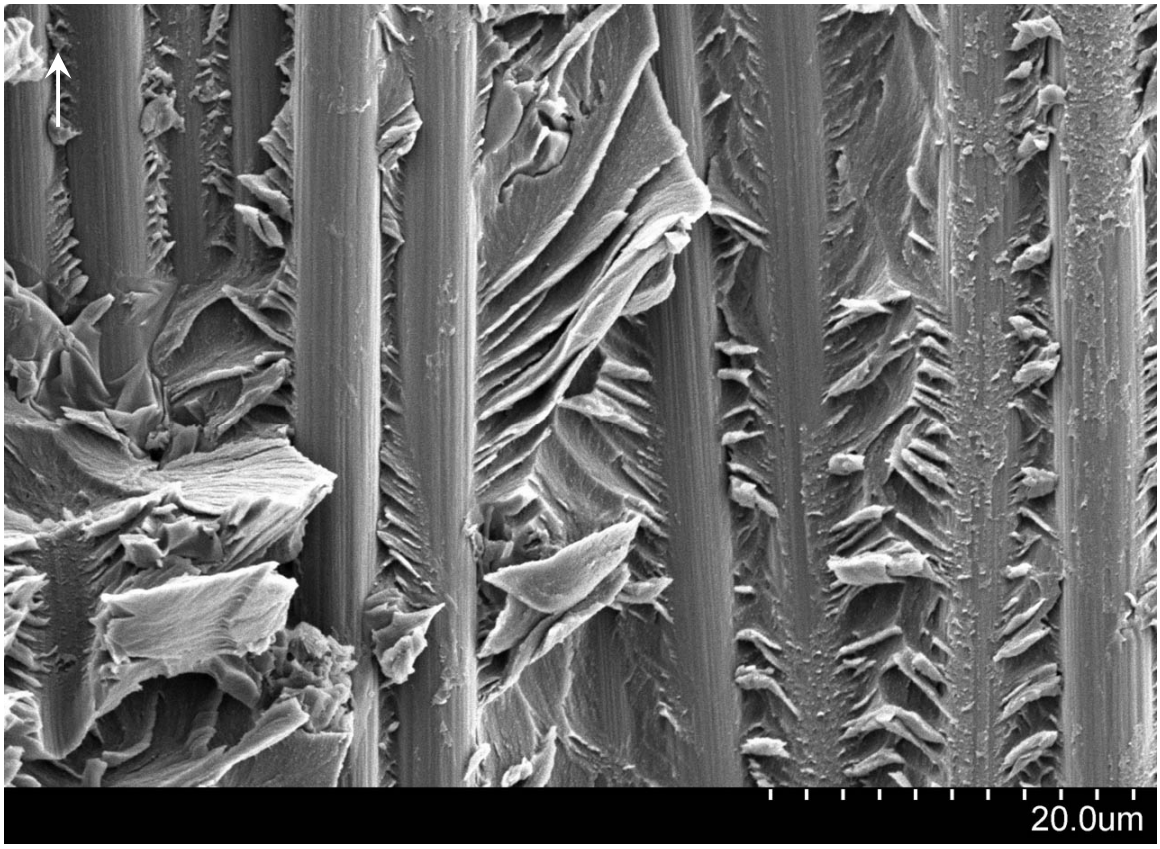

Figure 3.52: The laminate had fibers with a rough surface and partial resin/fiber adhesion is shown (arrow indicates crack direction).

Material H (Carbon5 Tape, Epoxy5)

Resin-rich areas were found on the rough fractures surface. Within the resin-rich areas, hackle-like formations experienced a large amount of plastic deformation. The negative fiber impressions were observed wavy, which could have occurred after the fiber separated away from the resin at the crack tip and the resin continued to deform. This is also supported by the fact that little resin/fiber adhesion was found even with a larger fiber surface area from length-wise scoring. Micro resin flow and river pattern could easily be seen. Away from the resin-rich areas, typical hackle and scallop formations were observed.

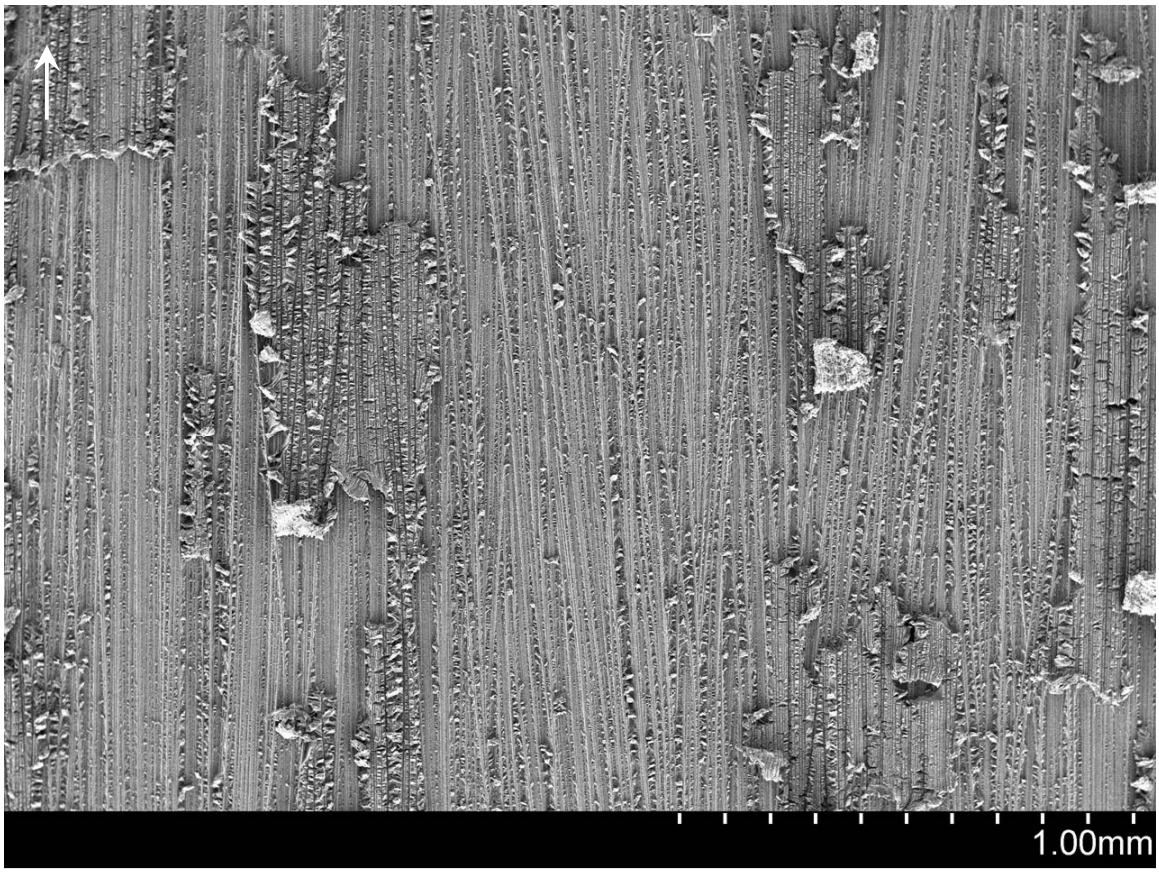

Figure 3.53: Overall view of Material H tested under Mode II loading showing a rough surface and resin-rich areas.

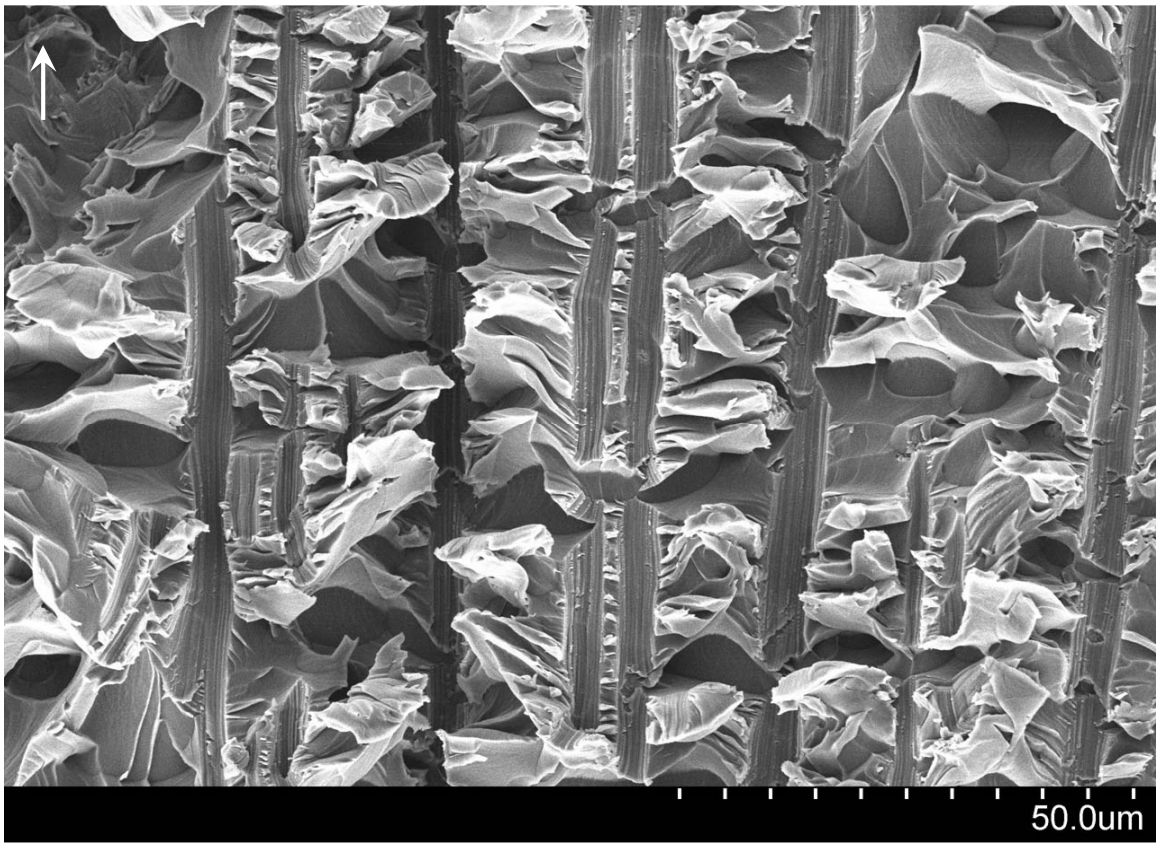

Figure 3.54: Irregular hackle-like formations and deformed fiber impression in the resin were noted.

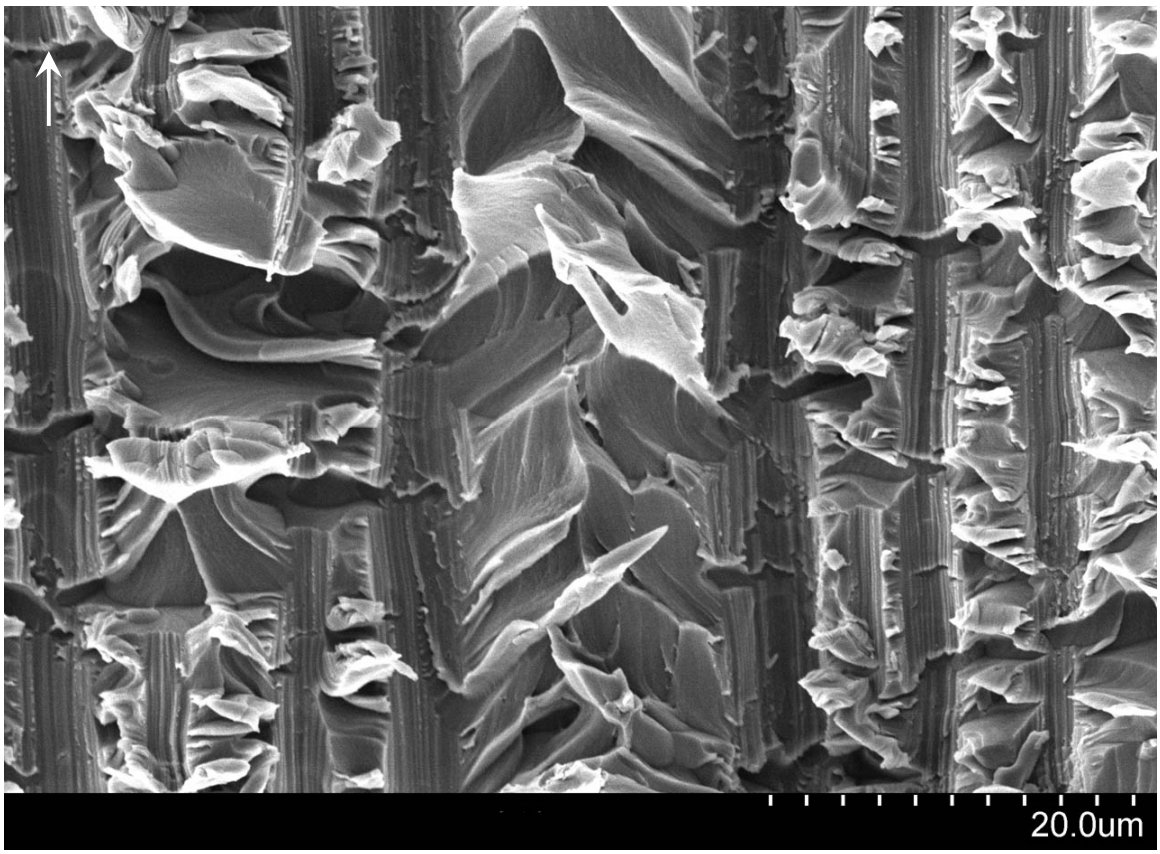

Figure 3.55: Extreme resin plastic deformation, micro resin flow, and length-wise scoring in the negative fiber impressions were observed.

Material I (Carbon3 Slit Tape, Epoxy2)

The fractured laminate had a fairly rough surface with fiber breakage. Typical hackle and scallop formations were observed with a lot of surface area from easily visible micro resin flow present. Overall, excellent resin/fiber adhesion was found.

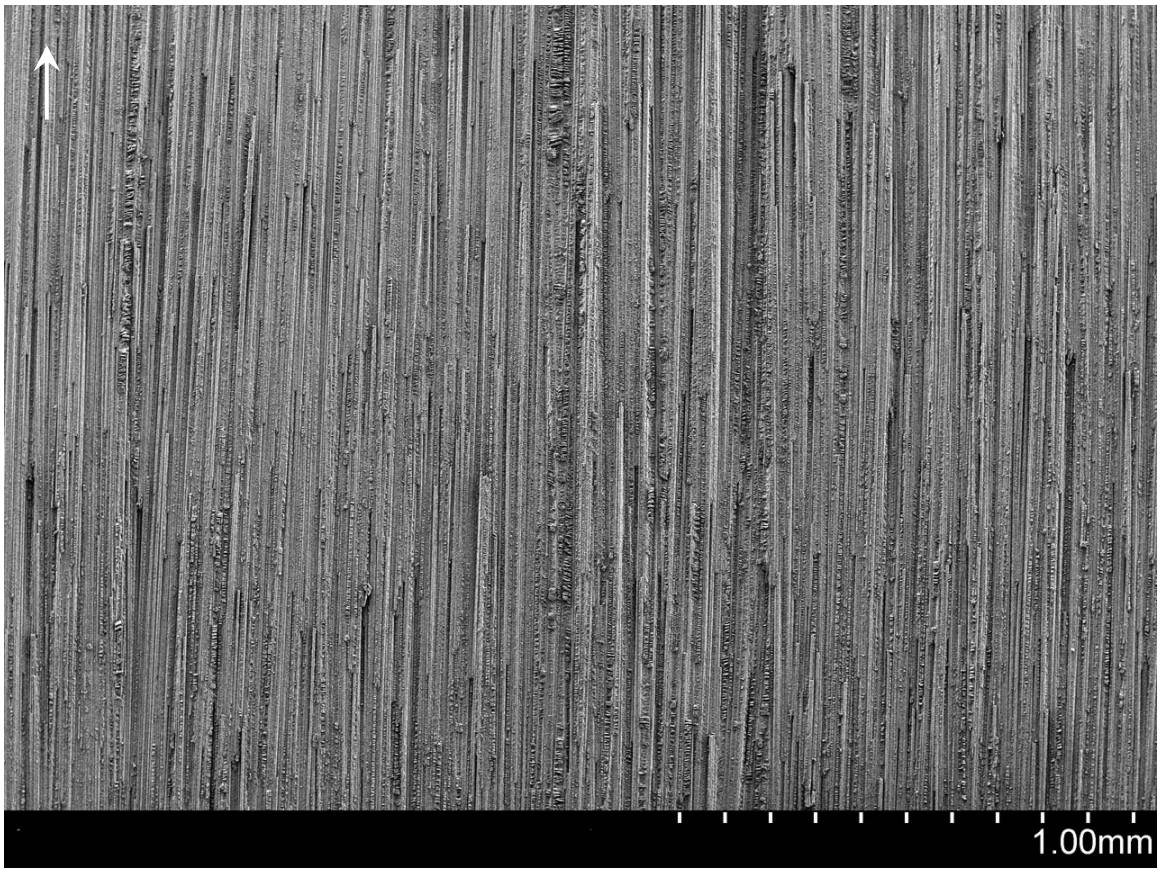

Figure 3.56: Overall view of Material I tested under Mode II loading depicting fiber breakage and a rough surface (arrow indicates crack direction).

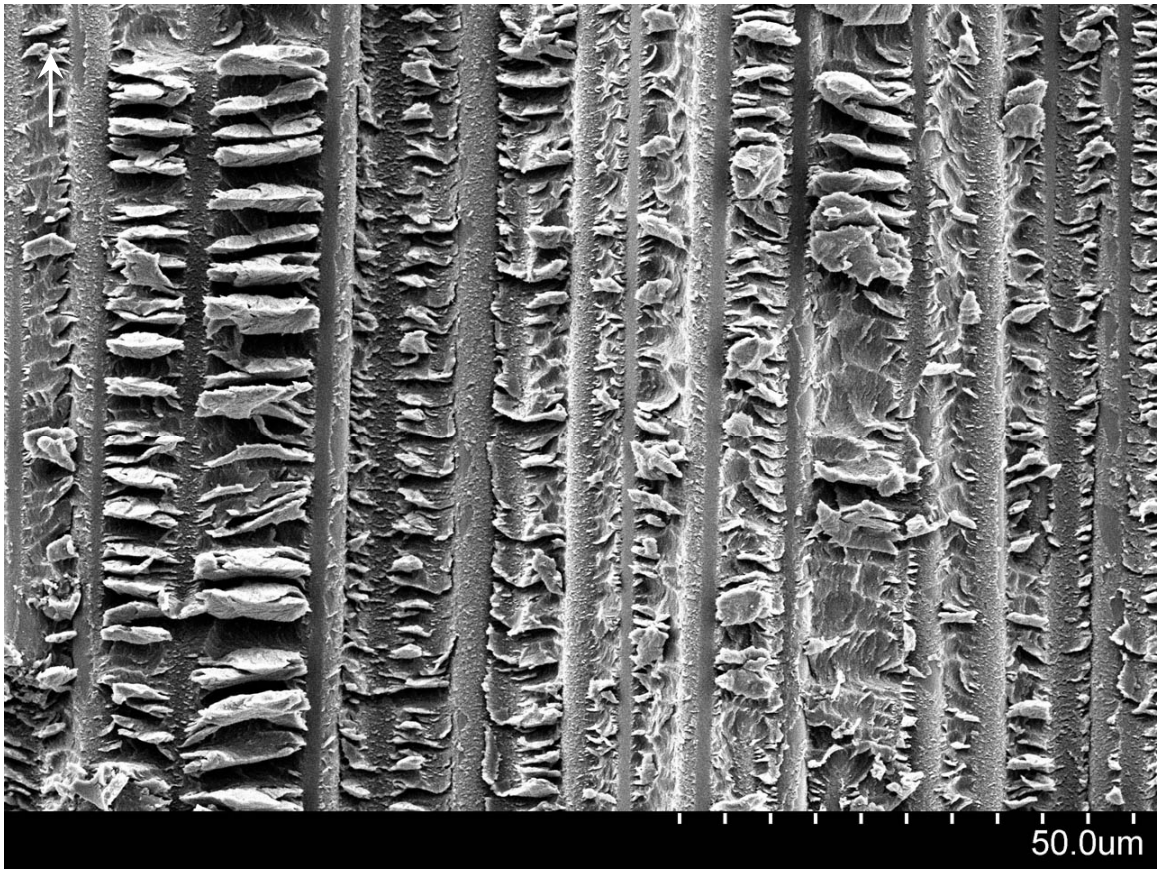

Figure 3.57: View of hackle and scallop formation.

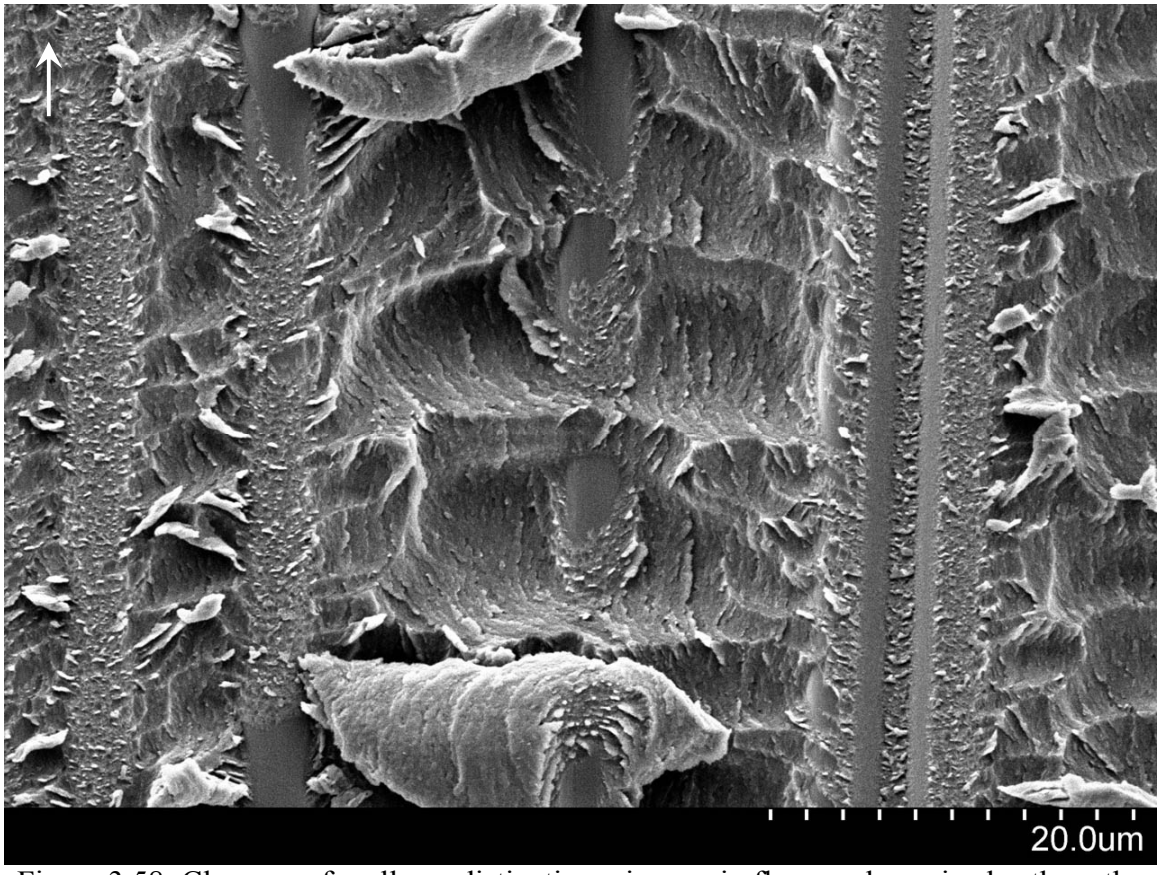

Figure 3.58: Close-up of scallops, distinctive micro resin flow, and a resin sheath on the fiber surfaces.

CHAPTER 4

RESULTS AND DISCUSSION

For toughened resin systems, the fracture surface can exhibit a series of complex features as a result of the interaction of the crack tip with rubbery or rigid particles within the resin system. Possible failure processes that can contribute to the formation of these features include fiber and resin mechanical properties, shear band formation near rubber particles, fracture of rubber particles after cavitation, stretching, debonding and tearing or rubber particles, trans-particle fracture, debonding of hard particles, crack deflection by hard particles, cavitation or voided rubber particles, crazing, plastic zone at craze tip, diffuse shear yielding, shear band/craze interaction, and pinning of the crack front [1]. All mechanisms contribute to the absorption of energy.

Toughening mechanisms may be classified into two general categories, (1) processes that occur along the crack plane, such as crack bridging, crack bowing/pinning, or fiber pullout and (2) toughening mechanisms such as phase transformation, microcracking, plastic void growth, and shear deformation determine the toughness in a finite-width fracture process zone that can extend past several fibers thick [1].

4.1 Fiberglass Strain Energy for Modes I and II

All fiberglass Mode I specimens exhibited fiber bridging as shown in Figure 4.1 that continued to increase as the delamination propagated (see Figures 4.2-4.5). For this reason, only the onset of Mode I strain energy release rate can be used for comparison

with other specimens. Table 4.1 lists the fiberglass strain energy release rate data for Modes I and II specimens. The fracture toughness for all fiberglass and resin systems could be correlated with their respective fracture morphology as discussed below.

Materials A and B, which have the same resin system (Epoxy1) but different forms, tape and roving, yielded similar Mode I and II fracture toughness results. Roving had a slightly higher G_I onset average as well as higher values as the crack propagated (approximately 1.7 in-lb/in² or 35% over Material A). This can be contributed to the fact that roving has overlapping tows of twisted fibers during manufacture, where tape is a flat unidirectional sheet that does not overlap within each ply.

Similar results were found for Materials C and D, which are also tape and roving specimens, but with a different resin system (Epoxy2). The Mode I G_I onset average was nearly identical; however Mode II was 15% higher for Material D (roving). It is possible that since this resin system is much tougher in comparison with Epoxy1 (Materials A and B) that roving would show a greater dependence of the fracture surface unevenness over tape specimens. Unfortunately, Mode I specimens did not show an increase in G_I onset. Roving had slightly higher fiber bridging values as the crack propagated (approximately 0.5 in-lb/in² or 6% over Material C). During fracture morphology analysis, it could easily be seen why Materials C and D had both greater onset and fiber bridging fracture toughness over Materials A and B due to the increased surface area of the river patterns or hackle and scallop formations, resin/fiber adhesion, micro-resin flow, and lack of porosity from volatiles during manufacture. Materials C and D also had a higher required cured resin content than Materials A and B (Table 3.2).

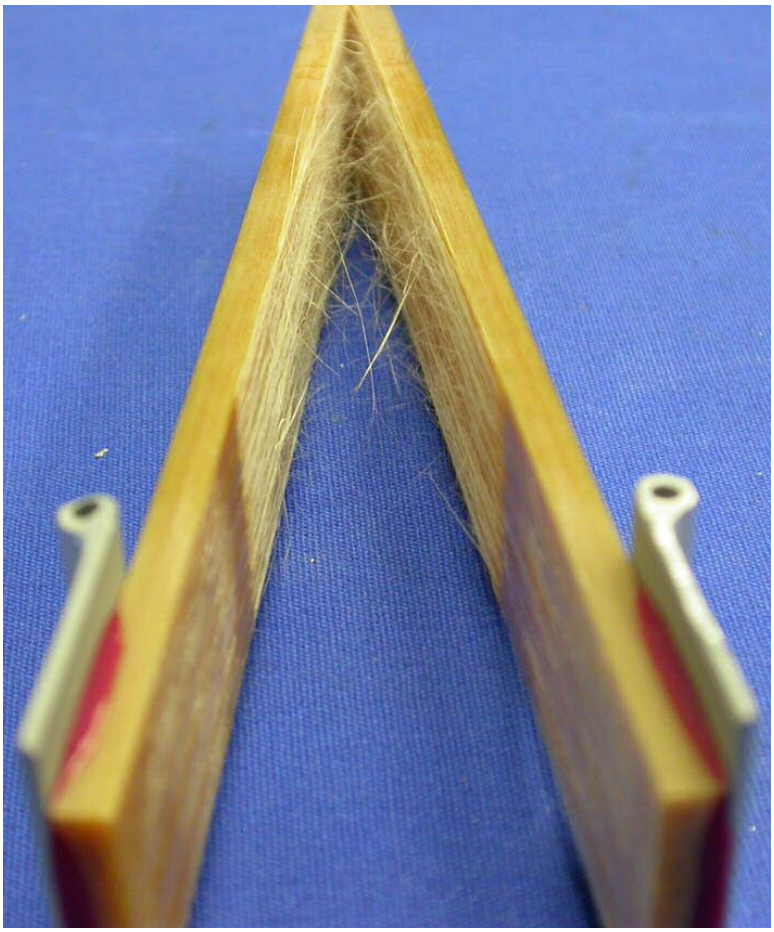

Figure 4.1: Example of typical fiber bridging for a fiberglass specimen.

Table 4.1: Fiberglass strain energy release rate data for Modes I and II.

Material Designation	**Material Description**	**Mode I Strain Energy, Onset, in-lb/in²**		**Mode II Strain Energy, in-lb/in²**	
		MBT	**Average**	**Individuals**	**Average**
A	Glass Tape, Epoxy1	1.110 1.260 1.352	1.24	5.16 4.83 5.43	5.14
B	Glass Roving, Epoxy1	1.277 1.360 1.383	1.34	5.37 5.32 4.79	5.16
C	Glass Tape, Epoxy2	2.308 2.186 2.266	2.25	8.91 8.42 8.27	8.54
D	Glass Roving, Epoxy2	2.296 2.277 2.157	2.24	10.35 9.47 9.62	9.81

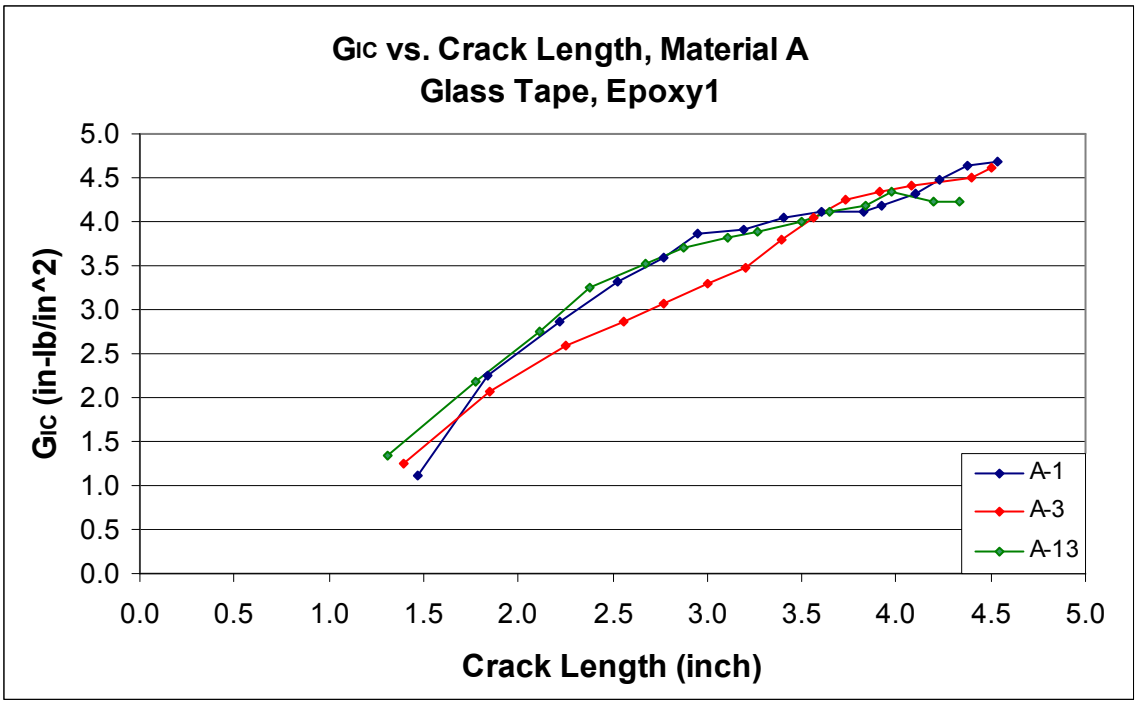

Figure 4.2: Strain energy release rate for Material A.

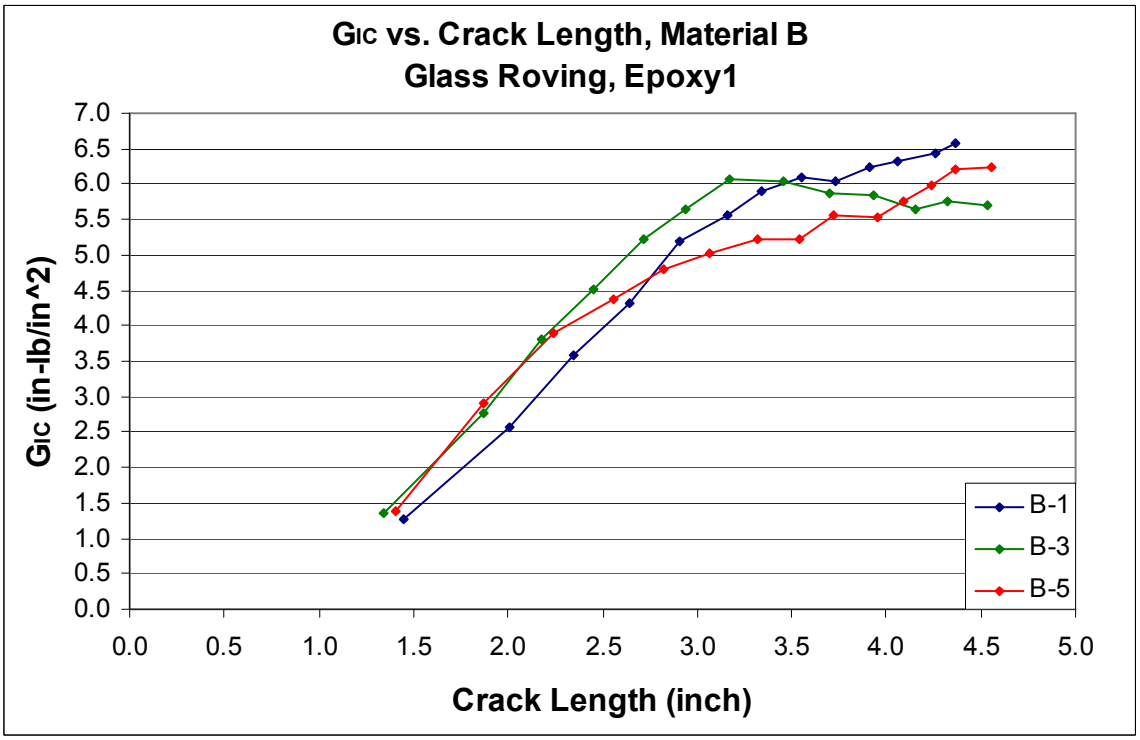

Figure 4.3: Strain energy release rate for Material B with increased fiber bridging for the roving specimen.

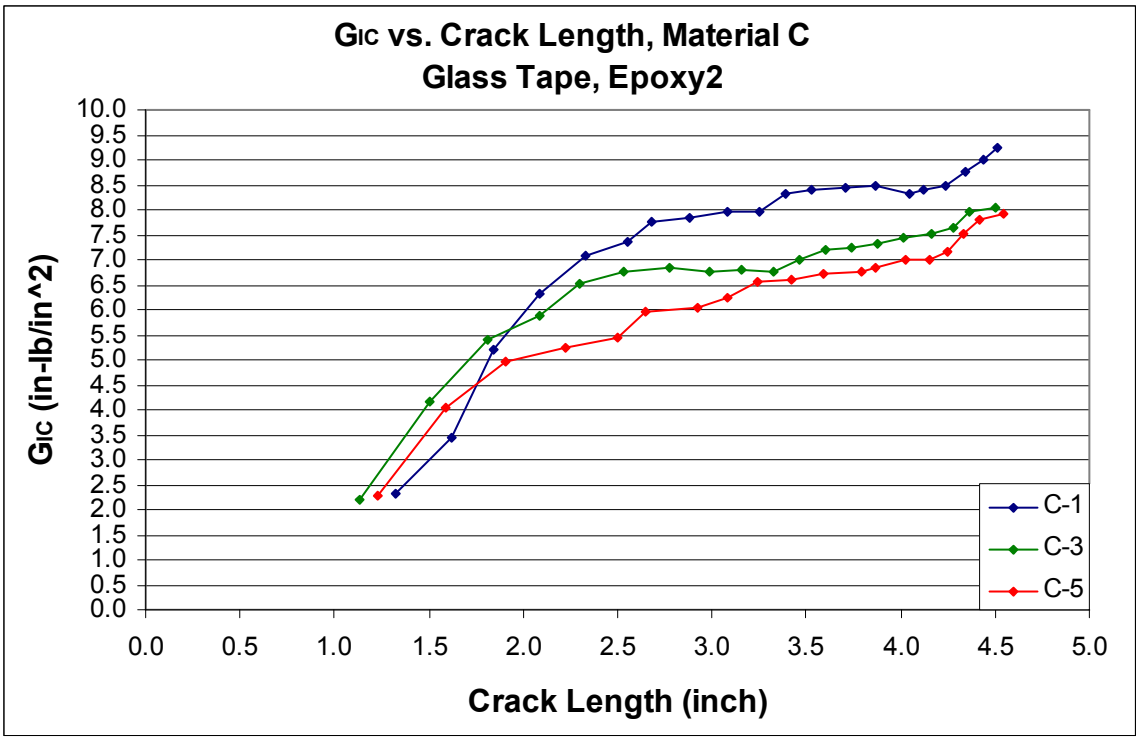

Figure 4.4: Strain energy release rate for Material C.

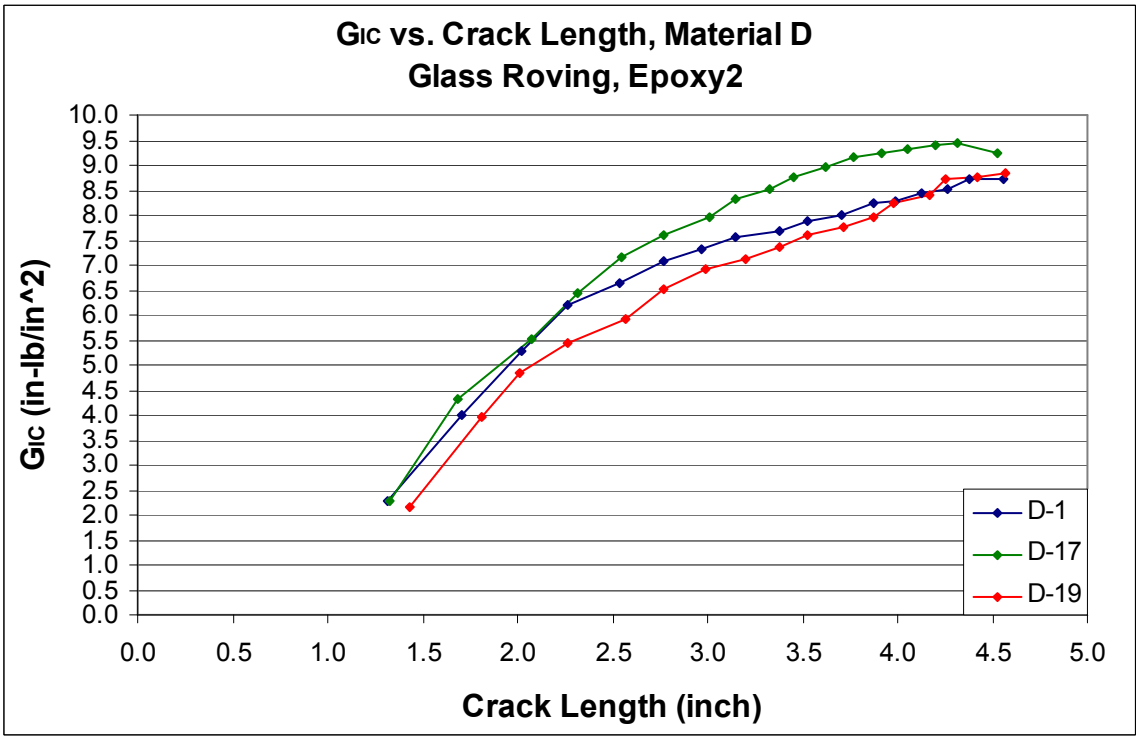

Figure 4.5: Strain energy release rate for Material D with increased fiber bridging for the roving specimen.

4.2 Carbon Fiber Strain Energy for Modes I and II

Since no carbon fiber materials had the same resin systems, direct comparisons of G_I of the laminate between varying carbon fibers can not be performed even though the carbon fibers used are have similar mechanical properties. Materials E and F equally had the lowest Mode I and II strain energy values for all carbon fiber specimens as shown in Table 4.2 and despite a greater required resin content than other specimens. Material E showed unstable crack growth near the end of the specimen's length.

The onset of G_I for Material I, only slit tape specimen, was nearly twice that of the more brittle resin systems of Materials E and F, but G_{II} was only 30% greater. It is difficult to explain only a slightly higher Mode II strain energy since the fracture morphology showed superior resin plastic deformation, resin/fiber adhesion, and micro-resin flow. A possible explanation could be the slit tape laminate form that could have not had transverse support under shear loading with large resin deformation. Slit tape is formed from slit unidirectional tape that is not composed of twisted fibers like roving. Fiber bridging in Material I was not observed.

Varying degrees of fiber bridging was observed in the Material F specimens due to larger voids (compared to fiberglass specimens of the same resin system) from volatiles during manufacture. However, Material G experienced significant and uniform fiber bridging as the crack grew, but the G_{II} value then decreased. Most other carbon fiber materials had constant strain energy with crack length. Material G morphology revealed sections of carbon fiber that separated during fiber bridging due to greater G_I values as shown in Table 4.2 and superior resin toughness as shown in Chapter 4. Material G also had a much higher Mode II strain energy compared to the more brittle

carbon fiber resin systems (approximately 2.5x greater). Morphology can easily show the mechanism for this increase due to groupings of severely deformed resin, more surface area, and mixed-mode and river patterns.

Material H had the highest measured Mode II strain energy due to similar morphology as Material G, but resin deformation continued after the fiber had separated from the resin, which was possible from the huge amount of resin deformation observed. From Mode I strain energy data, the resin system did not have superior strength over Material G, but was more ductile.

Table 4.2: Carbon fiber strain energy release rate data for Modes I and II.

Material Designation	**Material Description**	**Mode I Strain Energy, Onset, in-lb/in²**		**Mode II Strain Energy, in-lb/in²**	
		MBT	**Average**	**Individuals**	**Average**
E	Carbon1 Tape, Epoxy3	0.810 0.854 0.830	0.83	4.55 4.46 4.76	4.59
F	Carbon2 Tape, Epoxy1	0.812 0.831 0.821	0.82	4.98 4.27 4.31	4.52
G	Carbon4 Tape, Epoxy4	2.024 2.194 2.153	2.12	10.75 11.84 11.85	11.48
H	Carbon5 Tape, Epoxy5	1.220 1.617 1.355	1.40	11.36 12.48 12.55	12.13
I	Carbon3 Slit Tape, Epoxy2	1.537 1.442 1.473	1.48	6.07 5.84 5.79	5.90

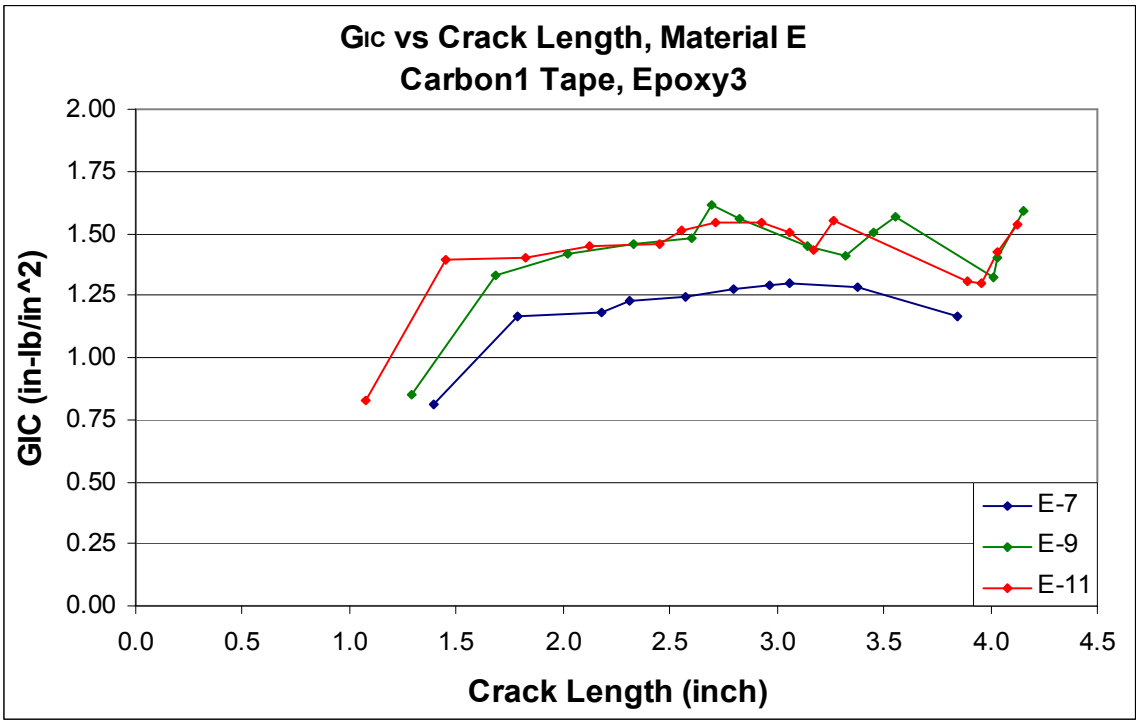

Figure 4.6: Strain energy release rate for Material E showing an increase of G_{Ic} when the delamination begins to develop then becomes constant.

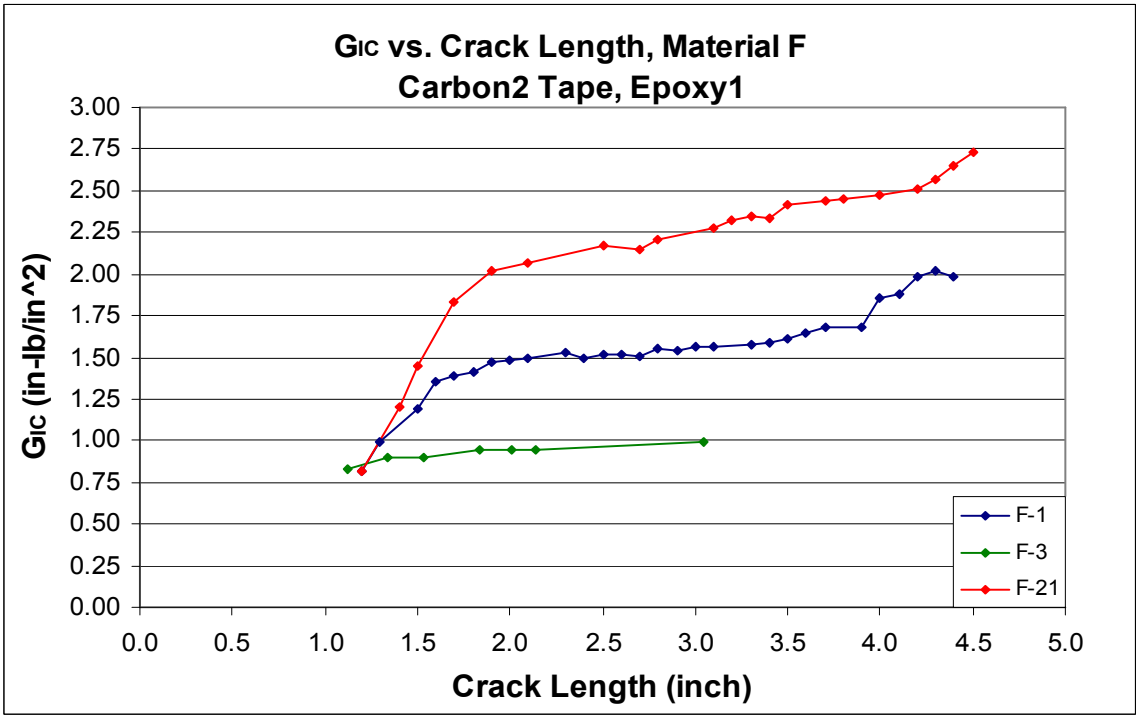

Figure 4.7: Strain energy release rate for Material F showing fiber bridging for at least one of the specimens.

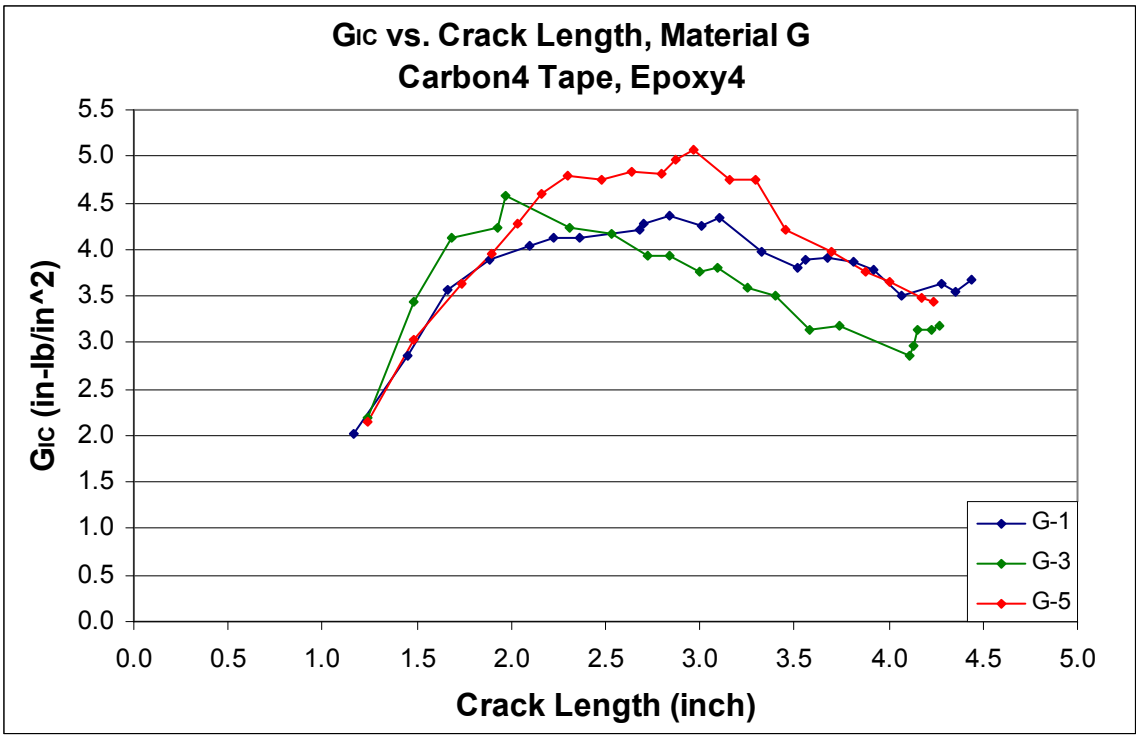

Figure 4.8: Strain energy release rate for Material G revealing an increase of G_{Ic} followed by a decrease.

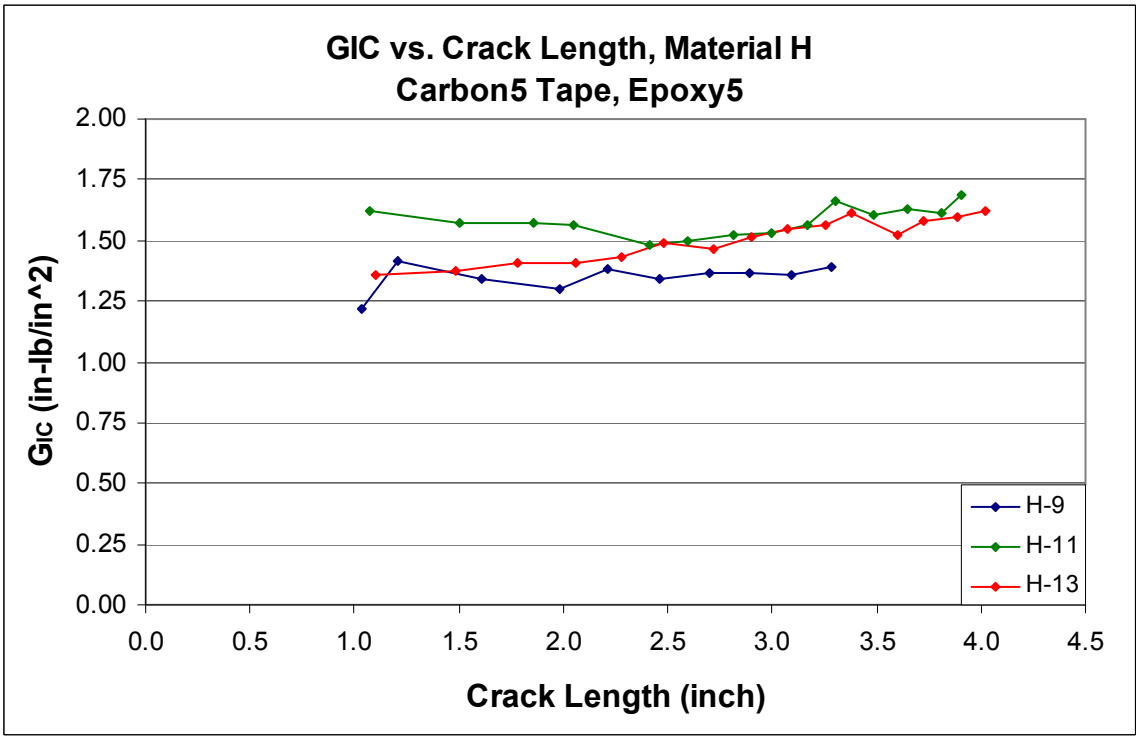

Figure 4.9: Constant strain energy release rate for Material H.

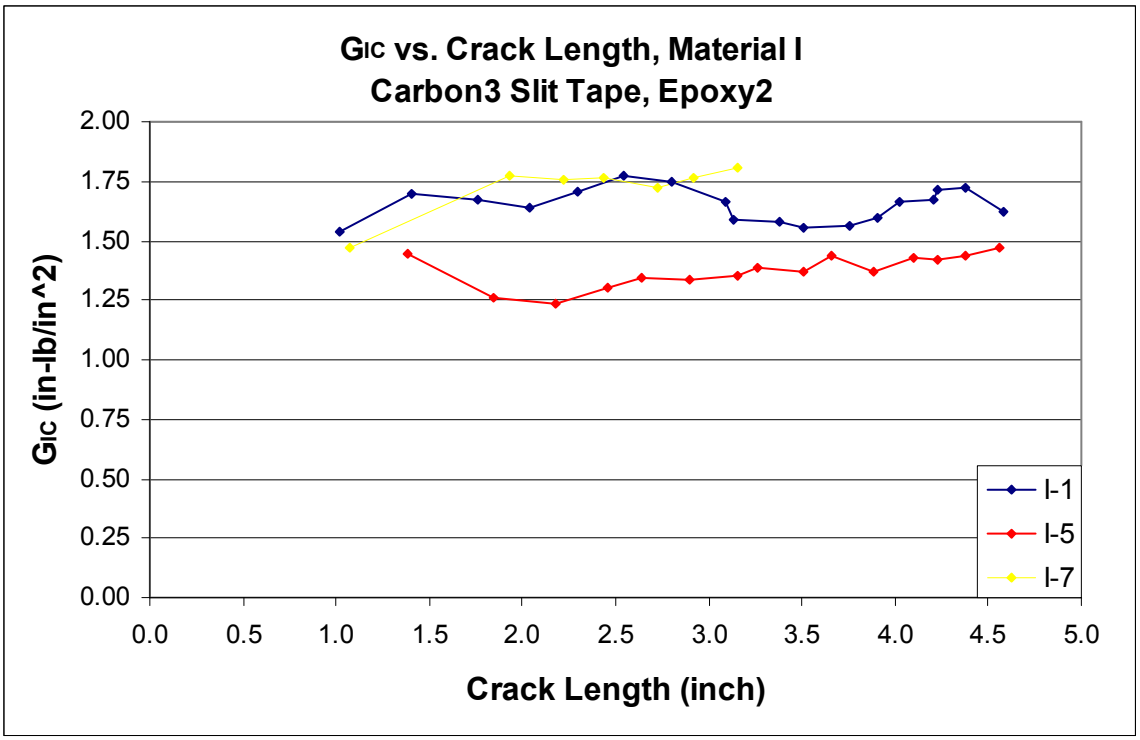

Figure 4.10: Constant strain energy release rate for Material I.

4.3 Resin Systems of Both Fiberglass and Carbon Fiber Specimens

A comparison between the brittle resin systems used in the fiberglass and carbon fiber specimens show a slightly higher Mode I and II strain energy values for fiber glass (approximately 55% and 15%, respectively) due to a lower laminate modulus and stiffness. The typical stiffness from fiberglass specimens is 7 Msi and compared to carbon fiber laminates of 20 Msi. Because of the lower modulus and stiffness, the glass fibers are allowed to bend while the resin system undergoes elastic and plastic deformation.

This is seen for the two same resin systems (Epoxy1 and Epoxy2) used in each the fiberglass and carbon fiber specimens Materials A, B, and F and Materials C, D and I. The tougher resin system, Epoxy2, showed a much greater increase in Modes I and II strain energy for fiberglass specimens (approximately 50% and 45%, respectively).

Epoxy1 fiberglass Mode I specimens had a much rougher resin fracture surface, whereas the carbon fiber specimens were extremely flat. Again, this is contributed to the lower modulus and stiffness of fiberglass laminates. Epoxy2 Mode I specimens also had a rougher surface and more pronounced micro-resin flow.

Mode II Epoxy1 fiberglass specimens experienced more resin deformation and more visible micro-resin flow as suspected. However, Epoxy2 specimens did not exhibit a significant difference in morphology.

CHAPTER 5

CONCLUSION

Several undisclosed fiberglass and carbon fiber laminates with toughened resin systems were tested and examined with the fracture surfaces using a SEM to document and correlate fracture morphology with the respective strain release energy. Modes I and II strain energy values were calculated for each of the nine laminates with varying types of processing forms such as roving, tape, and slit tape of glass and carbon fibers.

Overall, fiberglass laminates required greater strain energy for both Modes I and II crack progression over the carbon laminates, as expected. This was also confirmed by the significant amount of the fractured surface area and complex fracture features of the fiberglass laminates.

Mode I fiberglass specimens had a large amount of fiber bridging that carbon specimens did not exhibit. Of the fiberglass specimens, fiber bridging occurred more prevalently in the roving material than tape, because of overlapping, twisted prepreg bundles during manufacturing. However, the onset of strain energy was very similar for the roving and tape fiberglass and resin systems.

For the glass and carbon fiber laminates with the same resin systems, an increase in strain energy was observed for the fiberglass specimens due to higher strain and a lower modulus and stiffness.

REFERENCES

[1] Ed. Nicholas P. Cheremisinoff, Handbook of Ceramics and Composites, Vol. 2; Mechanical Properties and Specialty Applications. Marcel Dekker, Inc. New York 1992.

[2] A. C. Moloney, H. H. Kaiser, and H. R. Beer, *J. Mater. Sci.*, 22: 381 (1987).

[3] W. D. Bascom and D. L. Cottington, R. L. Jones, and P. Peyser, *J. Appl. Polym. Sci.*, 19: 2545 (1975).

[4] Russell, A. J. and Street, K. N., "Moisture and Temperature Effects on the Mixed-Mode Delamination Fracture of Unidirectional Graphite Epoxy," in Delamination and Debonding of Materials, ASTM STP 876, Oct. 1985, pp. 389-410.

[5] Prel, Y. J., Davies, P., Benzeggagh, M. and de Charentenay, F. X., "Mode I and Mode II Delamination of Thermosetting and Thermoplastic Composites," in Composite Materials: Fatigue and Fracture, Second Volume, ASTM STP 1012, April 1989, pp. 251-269.

[6] Reeder, J. R., "A Bilinear Failure Criterion for Mixed-Mode Delamination," in Composite Materials: Testing and Design, Eleventh Volume, ASTM STP 1206, Dec. 1993, pp. 303-322.

[7] D.J Wilkins, J.R. Eisenmann, R.A. Camin, W.S. Margolis, and R.A. Benson, "Characterizing Delamination Growth in Carbon/Epoxy", W.D. Bascom, "The Interlaminar Fracture of Organic-Matrix Woven Reinforced Composites", Vol. 11 1980, pp. 9.

[8] de Charentenay, F. X., Harry, J. M., Prel, Y. J., and Benzeggagh, M. L., "Characterizing the Effect of Delamination Defect by Mode I Delamination Test," in *The Effects of Defects in Composite Materials, ASTM STP 836*, D. J. Wilkins, Ed., American Society for Testing and Materials, 1984, pp. 84-103.

[9] Russell, A. J., "Factors Affecting the Opening Mode Delamination of Carbon Epoxy Laminates," DREP Materials Report 82-Q, Defense Research Establishment Pacific, Victoria, BC, Canada, 1982.

[10] Johnson, W. S., and Mangalgari, P. D., "Investigation of Fiber Bridging in Double Cantilever Beam Specimens," *Journal of Composite Technology and Research*, Vol. 9, Spring 1987, pp. 10-13.

[11] L. Arcan, M. Arcan, and Isaac M. Daniel, "SEM Fractography of Pure and Mixed-Mode Interlaminar Fractures in Graphite/Epoxy Composites," ASTM STP 948, 1987, pp. 41-67.

BIOGRAPHICAL INFORMATION

In 2003, Aaron Slager graduated from Iowa State University with a B.S degree in Materials Engineering. During his studies at ISU, Aaron was fortunate to work with Dr. David Jiles researching the Barkhausen effect and with Dr. Alan Russell on B2 ductile intermetallic compounds as well as the second-hardest material Al-Mg-B compounds with trace amounts of Si. Aaron co-authored two journals articles with one article published in *Nature Materials* titled "A Family of Ductile Intermetallic Compounds" and one published in *Acta Materialia* titled "Mechanical Properties of Single Crystal YAg".

In 2003, Aaron started work at Bell Helicopter Textron Inc. as a Failure Analysis Engineer and also cross-trained in the Non-Destructive Evaluation and Metallurgical Labs while pursuing his M.S. degree in Materials Science and Engineering.